Cloning, expression, purification and drug targeting of *Plasmodium falciparum* hypoxanthine guanine xanthine phosphoribosyltransferase (HGXPRT)

A thesis presented in fulfilment of the requirement for the degree of DOCTOR OF PHILOSOPHY

in the Division of Chemical Pathology

Faculty of Health Sciences

UNIVERSITY OF CAPE TOWN

25th November 2005

BONIFACE MBEWE

DECLARATION

Unless stated otherwise all work described in this PhD thesis was carried out in the Division of Chemical Pathology, Faculty of Health Sciences and the Department of Chemistry, Faculty of Science at the University of Cape Town by Boniface Mbewe under the joint supervision of Associate Professors David B. McIntosh and Kelly Chibale respectively.

Neither the substance nor any part of this thesis has been submitted in the past, or is being, or is to be submitted for a degree at this University or at any other university.

The University of Cape Town is hereby granted permission to reproduce whole or parts of this thesis for the purpose of research.

Signed by candidate Signature removed

Boniface Mbewe

25/11/2005

Date

ABSTRACT

The research concerns sub-cloning the gene for HGXPRT from *Plasmodium falciparum* from a vector with a His-tag facility to one without, expression of the protein in *E. coli*, and purification. On an analytical scale (40 ml culture), a purification procedure was developed that involves extraction of contaminating proteins by anion exchange chromatography (HGXPRT does not bind under the conditions used), followed by Reactive Red 120 agarose affinity chromatography. A single-manoeuvre preparative scale purification (1 L culture) was then achieved using a DE52 column in series with a Reactive Red 120 column to yield the required protein of >95% purity. The protein was inactive as isolated, but could be activated by incubation over 5 h at 4°C with Mg^{2+} + phosphoribosyl pyrophosphate (PRPP) or PRPP + hypoxanthine to yield a specific activity of 1-5 μmol/min/mg of protein. Free Reactive Red 120 is shown to be a fairly potent inhibitor of catalytic activity (K_i < 2 μM).

In previous work, the chalcone, (2*E*)-3-(4''-iodophenyl)-1-(2',4'6'-trihydroxyphenyl)prop-2-en-1-one or 4''-I-chalcone, had been found to specifically accelerate the catalytic turnover of HGXPRT from *Plasmodium falciparum* – it had no effect on the homologous enzymes from humans or *Toxoplasma gondii*. In the present study, nine analogues of this chalcone were synthesised, altering the positions and substituents on the two rings. The chalcones were synthesised by condensing appropriate acetophenones and halogenated benzaldehydes in a Claisen-Schmidt reaction. NMR, mass

spectrometry, IR spectrometry, and elemental analysis confirmed the desired products.

Out of the nine new chalcones synthesized only two accelerated catalytic turnover, and these only differed from the lead chalcone in the identity of the halogen. In ring A, changing the 2'- and 6'-OH groups to chloro, or removing the 4'- and 6'-OH groups, eliminated the accelerating effect, as did changing the position of the iodo substituent in ring B. It shows that the requirements for activation are extremely strict.

The chalcones that accelerate catalytic turnover were transformed into potent inhibitors when Ca^{2+} replaced Mg^{2+} as the divalent cation cofactor (K_d < 0.1 μM for 4''-I-chalcone). In addition, at least one of these chalcones (4''-I-chalcone) was able to replace PRPP in converting the isolated inactive enzyme into the active form, except that neither purine nor divalent cation was necessary. These effects of the halogenated chalcones suggest that they bind at the active site. A model for activation of inactive protein, and inhibition in the presence of Ca^{2+} is presented where the chalcones bind at the PRPP site with or without divalent cation. The model provides a rationale for the greater strength of the ternary complexation of HGXPRT/divalent cation/chalcone when the cation is Ca^{2+} compared with Mg^{2+}. If rate limitation is ascribed to nucleotide release (as in the human enzyme), then the chalcones may bind differently to accelerate turnover. It is also possible that another step is rate-limiting, and the PRPP site is vacant to allow the chalcone to bind and accelerate a slow conformational change.

The results and model suggests that these particular chalcones are good analogues of PRPP, the tri-hydroxyl aromatic portion with adjacent carbonyl and its symmetry and rotational mobility mimic PPi, the halogen and its unique bonding ability substituting for Pi, and the second aromatic ring overlapping with the ribose moiety. Alternative binding positions with the latter ring outside of the active site are also considered.

ACKNOWLEDGEMENTS

I would like to thank my supervisors Associate Professors David B. McIntosh and Kelly Chibale for the teaching and guidance on this PhD project. I wish to thank Dr. Jeanne Rousseau for the assistance with the molecular biology techniques. I am also grateful to Mrs. Joy-Anne Norman for help with developing the large-scale HGXPRT purification procedure. I also wish to thank Mr. Dave G. Woolley for assistance with many aspects of the project in the laboratory as well as the software applications.

I would also like to thank Mr. Chitalu C. Musonda for the tremendous help with the chemistry and interpretation of NMR spectra respectively.

I am grateful to all the people in both the Chemical Pathology and Medicinal Chemistry laboratories (UCT) for their friendship and willingness to help when I needed them.

I would like to express my sincere gratitude to the South African government through the National Research Foundation for funding most of this work and to the University of Cape Town for giving me an opportunity to undertake studies. I also wish to thank the University of Zambia for granting me study leave. Lastly, but not least, I wish to express my gratitude to my wife Esther and my daughter Mun'delanji for allowing me to be away from home during the entire PhD study period. May Jehovah God richly bless you all.

ABBREVIATIONS

Ac	acetate
AMP	adenosine 5'-monophosphate
Bn	benzyl
BSA	bovine serum albumin
CHES	(2-[N-cyclohexaylamino]ethanesulfonic acid)
cDNA	complementary deoxyribonucleic acid
Da	Dalton
δ_C	chemical shift (^{13}C NMR) in ppm
DCM	dichloromethane
δ_H	chemical shift (^{1}H NMR) in ppm
DE52	diethylaminoethyl cellulose (anion exchange resins)
DMSO	dimethylsulfoxide
DMF	*N*,*N*-dimethyformamide
DNaseI	deoxyribonuclease I
DTT	1,4-dithiothreitol
EDTA	ethylenediamine tetra-acetic acid
EGTA	Ethyleneglycol-bis-(β-aminoethyl ether) N,N,N',N'-tetra-acetic acid
EtOAc	ethylacetate
EPPS	N-(2-hydroxyethyl)piperazine-N'-(3-propanesulfonic acid)
GMP	guanosine 5'-monophosphate

HGXPRT	hypoxanthine-guanine-xanthine phosphoribosyltransferase
HG(X)PRT	hypoxanthine-guanine-(+/- xanthine) phosphoribosyltransferase
HGPRT	hypoxanthine-guanine phosphoribosyltransferase
H/GXPRT	hypoxanthine (or guanine-xanthine) phosphoribosyltransferase
his-tag	histidine tag or tail
Hx	hypoxanthine
IPTG	β-D-isopropyl-thiogalactopyranoside
IR	infrared
IMP	inosine 5'-monophosphate
LB	Luria-Bertani medium (Luria Broth)
MHz	megahertz
MeOH	methanol
MEM	methoxyethoxylmethoxyl
MEM-Cl	methoxyethoxylmethoxyl chloride
MES	(2-[N-morpholino]ethanesulfonic acid)
MOPS	(3-[N-morpholino]propanesulfonic acid)
mp	melting point
MS	mass spectrometry
MW	molecular weight
NMR	nuclear magnetic resonance
OD	optical density
Pi	inorganic phosphate

PIPES	piperazine-*N*,*N'*-bis-[2-ethanesulfonic acid]
PMSF	phenylmethanesulfonylfluoride
PPi	inorganic pyrophosphate
ppm	parts per million
PRPP	5-phospho-α-D-ribofuranosyl-1-pyrophosphate
PRT	phosphoribosyltransferase
RNaseA	ribonucleaseA
SDS-PAGE	sodium dodecyl sulphate polyacrylamide gel electrophoresis
TE	10 mM Tris-Cl, pH 8.0, 1 mM EDTA
THF	tetrahydrofuran
TLC	thin layer chromatography
TMS	tetramethyl silane
TNP-GMP	2',3'-O-(2,4,6-trinitrophenyl)-guanosine 5'-monophosphate
Tris-Cl	Tris(hydroxymethyl)aminomethane.HCl
U	enzyme units
ν_{max}	wave number
WHO	World Health Organisation
XMP	xanthosine 5'-monophosphate

TABLE OF CONTENTS

Chapter 1 BACKGROUND

1.1 Introduction

Malaria is a major world health problem that affects the tropical, sub-tropical and some temperate regions (Figure 1.1). In many instances, the countries in these regions are also the poorest in the world. This makes the fight against malaria very difficult in these countries. According to Roll Back Malaria, a United Nations publication, 40 % of the world population is at risk of malaria (http://www.who.int/inf-fs/en/InformationSheet01.pdf). Every year, 300 - 500 million people, mostly children and pregnant women, are infected by malaria (Greenwood and Mutabingwa, 2002; Miller *et al.*, 2002). As one review puts it, across the globe, a child dies of malaria in every 40 seconds (Sachs and Malaney, 2002). In all, up to 3 million people worldwide die of malaria every year (Butler, *et al.* 1997). Malaria affects Africa more than any other continent in the world. It is estimated that 90 % of the malaria deaths occur in sub-Saharan Africa (WHO/UNICEF, 2003; Greenwood and Mutabingwa, 2002). This is in spite of the fact that many of these malaria deaths can be prevented by early diagnosis and administration of appropriate treatment.

Malaria is transmitted by intracellular protozoan parasites of the genus *Plasmodium*. These parasites are carried by the female *Anopheles* mosquito especially *A. gambiae* and are passed from one person to another through mosquito bites. *A. gambiae* is particularly effective at transmitting malaria among humans because it preferentially feeds on humans and is long-lived.

There are four *Plasmodium* species that transmit malaria and these are *P. ovale*, *P. malariae*, *P. vivax*, and *P. falciparum*. Of these, *P. falciparum* is the most lethal and responsible for virtually all malaria deaths.

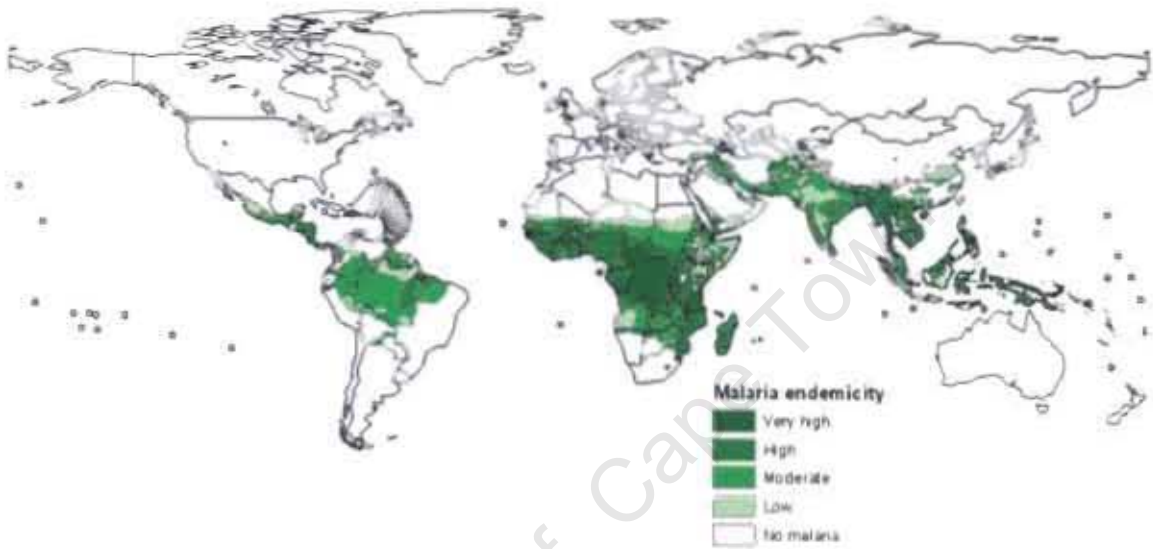

Figure 1.1 **Map of the world highlighting malaria infected countries** (Source: WHO, 2003 report).

1.2 Life cycle of *P. falciparum*

Figure 1.2 summarizes the life cycle of the malaria parasite as it occurs in the mosquito, and human hosts. For a comprehensive review, see Miller *et al.*, 2002. The life cycle of the malaria parasite can be said to start with an infected female *Anopheles* sp. mosquito injecting a primitive form of malaria

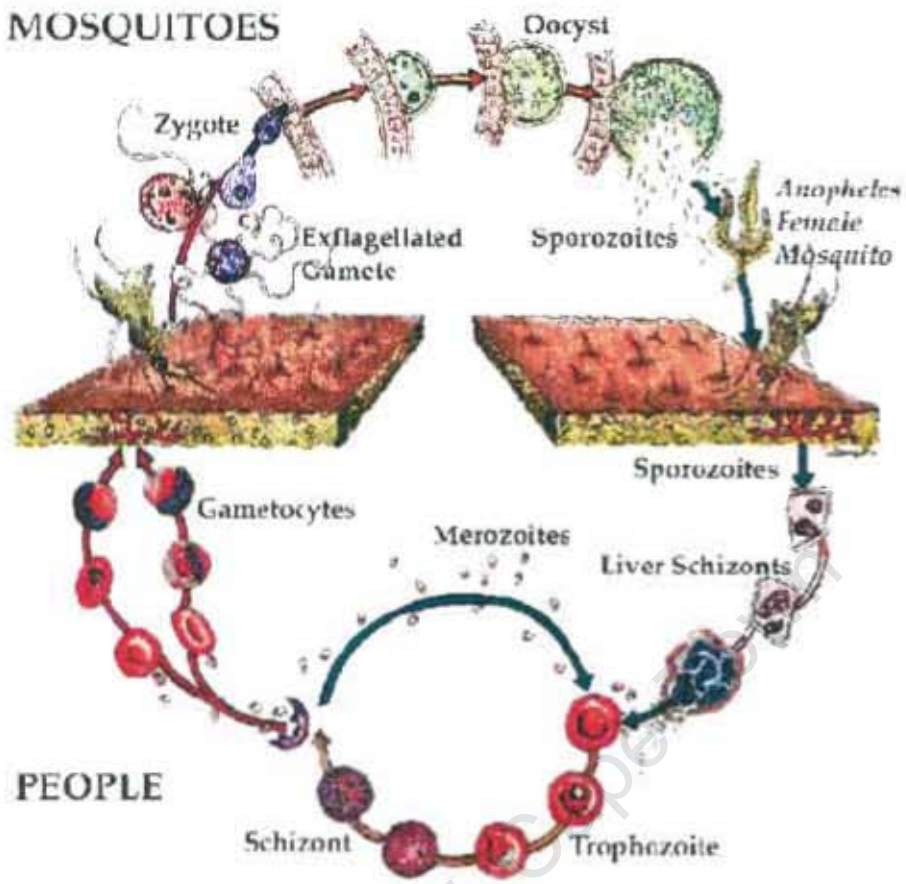

Figure 1.2 **The *Plasmodium* sp. life cycle** (see text for description). This Figure is taken from http://www.malariatest.com/cycle.html website.

parasites known as sporozoites into subcutaneous tissue, or less often, directly into the blood-stream where they are transported to the liver. Sporozoites are an infective form of the parasite found in the salivary glands of the mosquito. Once in the hepatocytes (parenchymal cells of the liver), the sporozoites undergo asexual multiplication generating thousands of liver merozoites, another form of the parasite. The infected hepatocytes eventually rupture resulting in the release of merozoites back into the blood stream. The merozoites in the blood then invade erythrocytes where they complete

another round of asexual multiplication that takes about 48 h. In the erythrocytes, the parasites first differentiate from ring stage into trophozoites that become schizonts. The schizonts eventually turn into red blood cell merozoites. Each infected erythrocyte can produce up to 20 additional merozoites. The fever associated with malaria is thought to be the result of the synchronous release of merozoites from red blood cells. In fact, malaria pathogenesis is associated only with the blood stage of the *Plasmodium* parasite (Egan, 2003). The production of merozoites in erythrocytes is accompanied by the degradation of haemoglobin by the parasite itself. Released merozoites can either infect fresh red blood cells and repeat the asexual reproduction cycle or develop into male and female gametocytes that are taken up by the *Anopheles* sp. mosquito host. In the mosquito, the parasite continues its multiplication following a sexual route that starts with the gametocytes fusing to form a zygote (Greenbaum *et al.*, 2002). Zygotes form oocysts in the wall of the mosquito stomach. The oocysts develop over a period of time and contain numerous sporozoites, ready to start the cycle all over again.

1.3 Malaria drug targets

1.3.1 The genome

The sequencing of the *P. falciparum* genome in 2002 has provided an unprecedented opportunity for exploring new drug targets (Gardner *et al.*, 2002). The genome contains about 5 300 protein-encoding genes and 60%

of these could not be assigned any function. This constitutes an enormous group of possibly unique malarial proteins that are potential drug targets. The parasite also has several other unique features such an apicoplast with its own genome of 30 genes, an unusual electron transport chain with critical ubiquinol cycling, a seemingly non-functional F_1F_0 ATP synthase, and possible reliance on a proton-translocating pyrophosphatase for developing an electrical potential across the plasma membrane.

The apicoplast probably arose by endosymbiosis, like mitochondria and chloroplasts, and imports most of the 551 enzymes for diverse functions. The organelle synthesizes fatty acids, isoprenoids, and haem, and is involved in DNA replication and repair, transcription and translation, protein import and turnover, and malaria parasite-specific metabolic pathways. Many of the enzymes comprising fatty acid synthesis, isoprenoid synthesis, and the latter metabolic group may be good drug targets. The protein import machinery is itself a potential drug target.

The parasite obtains its ATP from glycolysis - all the glycolytic enzymes are present, including two unusual phosphofructokinases, which are related to, or are, pyrophosphatases. A complete tricarboxylic acid cycle was identified, but with several deviant features, perhaps because it is mainly directed to the synthesis of succinyl CoA for haem biosynthesis.

All pathogenic protozoan parasites do not synthesize purines *de novo* and rely on the host for purine needs (Sherman, 1979). The genome contains

purine and nucleoside transporters, and the purine salvage enzymes hypoxanthine phosphoribosyltranferase (HPRT), which converts hypoxanthine, guanine, or xanthine into IMP, GMP, or XMP and purine nucleoside phosphorylase (PNP), which cleaves the glycosidic bond of inosine to produce hypoxanthine and ribose-1-phosphate, all of which are possible drug targets (see below).

During the intra-erythrocytic phase, the parasite exports several proteins to the cytosol of the erythrocyte and plasma membrane. This requires crossing of the parasitophorous vacuole surrounding the parasite. It is not clear how this is achieved, but the genome besides containing a classical secretory protein pathway and vesicle transport proteins, also harbours proteins that may provide a secondary route. These proteins are potential drug targets.

After invasion of the red blood cells by parasites the host cells become much more permeable to a variety of small molecular weight compounds, a process termed New Permeability Pathways (NPP); see Staines *et al.*, 2005 for a review. It is not clear whether these transport systems originate from the parasite or host, but they can be good drug targets. Compounds that target the NPP have been synthesized. For instance, phloridzin (Kutner *et al.*, 1987; Silfen *et al.*, 1988), and glibenclamide (Kirk *et al.*, 1993) target NPP and inhibit parasite growth in culture.

The malaria parasite exports some of its proteins to the erythrocyte membrane. These proteins are important virulence factors associated with the

manifestations of the disease. They could also help in the binding of the parasite to organs within the host. Some are also antigenic determinants of our immune system. There is a huge potential for identifying new determinants among the surface proteins and for developing vaccines.

1.3.2 Biological targets of:

1.3.2.1 Quinolines

Quinoline derivatives are the main drugs used against malaria. They are believed to inhibit haem detoxification.

During the intra-erythrocytic stage of the malaria parasite's life cycle, the host haemoglobin is a primary source of amino acids. Haemoglobin proteolysis occurs within the vacuole of the parasite, a lysosome-like organelle, and free haem [Fe(II)protoporphyrin IX] is produced, which is oxidised to haematin [HO-Fe(III)protoporphyrinIX], and is toxic. It can cause cell lysis and the generation of damaging reactive oxygen species (Wiser 2003). The parasite detoxifies haematin by forming haemazoin (malarial pigment), which has been characterized as a polymer of β-haematin (Slater *et al.*, 1991; Adams *et al.*, 1996). The latter is a dimer of haematin linked *via* two of the propionic acid groups and the Fe(III)s (Pagola *et al.*, 2000). The mechanism of haemazoin formation *in vivo* is controversial. Synthetic β-haematin formation occurs spontaneously in concentrated acetate (pH 4.5) and elevated temperatures (Egan *et al.*, 1994), but may be too slow to account for haemazoin formation

under physiological conditions. Its formation is possibly catalyzed or initiated either by histidine rich proteins, e.g. HRP-2 (Sullivan *et al.*, 1996; Schneider and Marletta, 2005), or through aggregation with lipids, e.g. linoleic acid (Fitch *et al.*, 1999 and 2000). The natural process may occur through a combination of methods, perhaps depending on *in vivo* conditions.

The quinoline antimalarials interfere with the process of haem detoxification. 4-aminoquinolines e.g. chloroquine, quinidine, halofantrine, desbutylhalofantrine, and mefloquine, inhibit the formation of synthetic crystalline β-haematin by associating with haematin (Egan *et al.*, 1999). Solvent and electrostatic factors play an important role in this interaction (Egan and Ncokazi, 2004). Substituents at position 7 (see Figure 1.3) influence the pK_a of the quinoline and tertiary nitrogens, thereby possibly affecting their accumulation within the acidic compartment of the food vacuole (Kaschula *et al.*, 2002). Quinoline and quinacrine derivatives also inhibit the binding of haem to HRP-2 (Choi *et al.*, 2002). It also seems that chloroquine

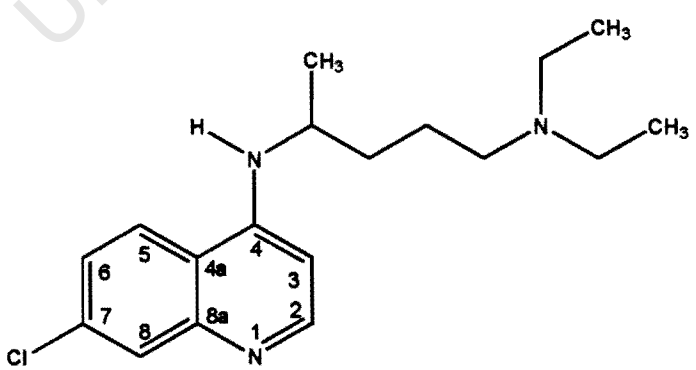

Figure 1.3 **Chloroquine and numbering of atoms in the ring system.**

inhibits the dimerisation of haematin mediated by lipids through increasing the proportion of lipids unable to promote the dimerisation process (Fitch *et al.*, 2003). Therefore it appears that these quinoline antimalarials inhibit all three of the recognized methods of haemazoin formation, pointing to them interacting with the haem or haematin rather than the end catalysts like protein or lipid. The inhibition of haemazoin formation results in the accumulation of toxic haematin thereby killing the parasite.

1.3.2.2 Artemisinin

Artemisinin and its derivatives are becoming an increasingly important treatment for malaria. They, alone or in combination with the more usual antimalarials like mefloquine, are now the first line drugs for the treatment of malaria in several African and Asian countries. Artemisinin is derived from the Chinese plant, *Artemisia annua*, and is present in a herbal tea, quighao, that has been used as an antidote for fever for several centuries, and for the treatment of malaria and haemorrhoids for 150 years. It is a sesquiterpenoid lactone with an endoperoxide bridge across the seven-membered ring (see Figure 1.4) and is rather insoluble in water and oil, but exists in more soluble forms such as artesunate and artelinate. Artemisinin is effective at low nanomolar concentrations, much lower than its cytotoxic effect, which is in the micromolar range (Woerdenbag *et al.*1993).

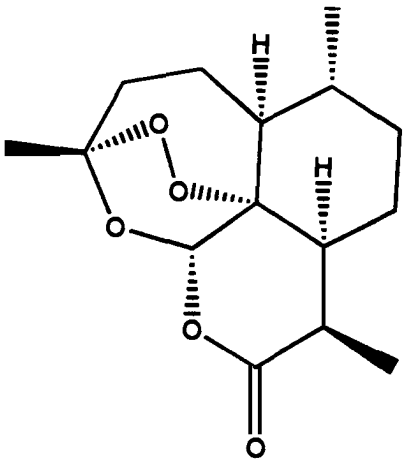

Figure 1.4 **Structure of artemisinin (or qinghaosu).**

These compounds are converted to dihydroartemisinin by haem, Fe(II)protoporphyrin IX, which produces toxic, carbon centred free radicals, which are proposed to alkylate critical parasite enzymes (Meshnick *et al.*, 1991; Posner and Oh, 1992). It is also plausible the artemisinin acts as a source of hydroperoxide that leads to the generation of hydroxyl radicals that hydroxylate parasite proteins and produce reactive oxygen species that have other deleterious effects (Posner *et al.*, 1995; Haynes *et al.*, 1999). The production of a wide range of destructive reactive species may make it difficult for the parasite to develop resistance, and none has been reported yet.

Recently, artemisinins have been found to inhibit a malarial Ca^{2+}-ATPase, *PfATP6* (Eckstein-Ludwig *et al.*, 2003). Inactivation of the pump and parasite death was antagonised by thapsigargin, a potent sesquiterpenoid lactone inhibitor of sarcoplasmic/endoplasmic Ca^{2+} pumps. The inactivation was

irreversible and catalyzed by Fe^{2+} suggesting covalent interaction *via* a reactive form of artemisinin. The protein could be the primary target of the activated artemisinins.

However, it has more recently been shown that Fe^{2+} is not essential for the antiplasmodial effects of artemisinin in parasite cultures (Parapini *et al.*, 2004). Growth of the cultures in CO rendered the Fe^{2+} unavailable for oxidative electron transfer and reduction of the trioxane ring and yet the effects of artemisinin actually occurred in a lower concentration range. These experiments also suggest that the oxidative mechanisms alluded to above play only a minor role.

Artemisinin seems also to exert an anti-inflammatory effect through inhibiting the inducible form of nitric oxide synthase (Aldieri *et al.*, 2003). This may help to alleviate the neurological complications of malaria.

One potential drawback to artemisinin may be its availability through the need to extract it from plants. A cheap, synthetic route to artemisinin or a derivative has taxed chemists for many years. One simple endoperoxide structure analogue (OZ 277), stabilized by an adamantane ring, has recently been synthesized and shown to be more potent than artemisinin and seemingly to possess few side effects, at least in animals (Vennerstrom *et al.*, 2004).

1.3.2.3 Antifolate agents

For a number of years a combination of pyrimethamine and sulfadoxine has been first line therapy in some African countries, such as Malawi and Kenya. These agents target enzymes in the folate pathway. Folate and its metabolites provide a number of cofactors necessary for the supply of one-carbon units. For example, 5,10-methylenetetrahydrofolate transfers a one-carbon unit to dUMP to yield dTMP, which goes into DNA, and to certain amino acids such as methionine. The pathway consists of five enzymes required for the synthesis of folate, and other enzymes interconvert the various folate forms (for review see Hyde 2005).

Pyrimethamine is a competitive inhibitor of dihydrofolate reductase. This enzyme reduces the 5, 6 - double bond in dihydrofolate to tetrahydofolate. The activity is actually located in one domain of a bi-functional enzyme (the other activity being thymidylate synthase) (Bzik *et al.*, 1987). The crystal structure of the dimer containing both activities has been elucidated with inhibitors bound at the active site (Yuvaniyama *et al.*, 2003).

The sulfonamide drugs (e.g. sulfadoxine and dapsone) are competitive inhibitors of dihydropteroate synthase, an enzyme which converts 6-hydroxylmethyl-7,8-dihydropterin pyrophosphate and ρ-aminobenzoic acid into 7,8-dihydropteroate. It is also a bi-functional protein, which also catalyses the preceding step in the pathway (Triglia and Cowman, 1994).

1.3.2.4 Some other drug targets

1.3.2.4.1 Proteases

Several parasite proteases are involved in the digestion of haemoglobin and they also participate in the invasion and release from the erythrocyte. Inhibitors, like peptidyl fluoromethyl ketone (Rockett *et al.*, 1990) and vinyl sulfone (Rosenthal *et al.*, 1996), are potent antimalarial agents in model systems.

Aspartyl proteases have two active site aspartic acid residues that activate a water molecule to catalyze the hydrolysis of peptide bonds. Two aspartyl proteases, plasmepsin I and II are implicated in the early degradation of haemoglobin (Gluzman *et al.*, 1994). They are synthesized as pro-enzymes and each contains a membrane-spanning section that probably anchors the protein to the membrane of the food vacuole before activation by another protease (Francis *et al.*, 1997). This is a very active field for drug targeting. Many of the drugs developed against the human immunodeficiency virus aspartic protease may be effective antimalarials (Skinner-Adams *et al.*, 2004; Abdel-Rahman *et al.*, 2004). However, disruption of expression of these genes yields viable parasites, although with slower growth characteristics, even though they remain sensitive to protease inhibitors, suggesting other aspartyl proteases may be more critical than plasmepsin I and II (Liu *et al.*, 2005).

The best-characterized proteases are the cysteine proteases, which have a critical catalytic cysteine residue at the active site. Falcipain 1, 2, and 3 are expressed during the intra-erythrocytic phase of the life cycle and the latter two degrade haemoglobin at acidic pH (Shenai *et al.*, 2000; Sijwali *et al.*, 2001). Both are targeted to the acidic food vacuole, and falcipain 2 also exists outside perhaps to participate in the degradation of proteins of the erythrocyte cytoskeleton during rupture (Dahl and Rosenthal, 2005; Dua *et al.*, 2001). Many inhibitors of cysteine proteases exist and are being explored as antimalarials (Chibale and Musonda, 2003).

A novel approach is the development of "double drugs" in which single molecules contain protease inhibitor and quinoline moieties. Thus, both processes, namely haemoglobin degradation and haemozoin formation may be inhibited. Thiosemicarbazones conjugated to a 4-aminoquinoline moiety *via* an isatin scaffold showed good activity against parasite growth *in vitro*. The thiosemicarbazone contained electrophilic imine and thiol carbonyl groups that could covalently derivatise the reactive cysteine (Chiyanzu *et al.*, 2005).

1.3.2.4.2 Purine salvage targeting agents

As indicated earlier, pathogenic protozoan parasites, including *P. falciparum*, lack the ability to synthesize purines *de novo* and rely on the host to supply the bases for purine nucleotides that are essential for energy needs and DNA and RNA synthesis. Sequencing the malarial genome has confirmed that the

parasite lacks the synthetic enzymes (Gardner *et al.*, 2002). The major purine base salvaged is hypoxanthine. It comes principally from inosine *via* adenosine using the enzymes adenosine deaminase and purine nucleoside phosphorylase, respectively. Smaller amounts of the bases themselves, namely, hypoxanthine, xanthine, and guanine cross the parasite membrane as well, perhaps by a different transporter. Hypoxanthine, xanthine, and guanine are converted to IMP, XMP, and GMP respectively by the enzyme hypoxanthine xanthine guanine phosphoribosyl transferase (HXGPRT). The malaria parasite seems to be unique among protozoan parasites in lacking adenosine kinase (deduced from the genome sequence), which could otherwise provide an alternative source of AMP from adenosine. All of the former enzymes, as well as two nucleoside/purine base transporters (evident in the genome), are likely to be good drug targets. Removal of medium hypoxanthine by xanthine oxidase inhibits the growth of malaria parasites in culture, indicating the parasite's reliance on their salvaged pool of hypoxanthine (Berman and Human, 1990; Berman *et al.*, 1991). A summary of the central role of HXGPRT in purine salvage is shown in Fig. 1.5.

Two nucleoside/purine base transporters occur in the malaria genome (Gardner *et al.*, 2002). One has been characterized and found to transport adenosine and adenine, as well as the other bases guanine and hypoxanthine (Carter *et al.*, 2000; Parker *et al.*, 2000). The first soluble enzyme in the pathway is adenosine deaminase and it seems to differ from the human form because selective inhibitors have been found (Daddona *et al.*, 1984; Brown *et al.*, 1999).

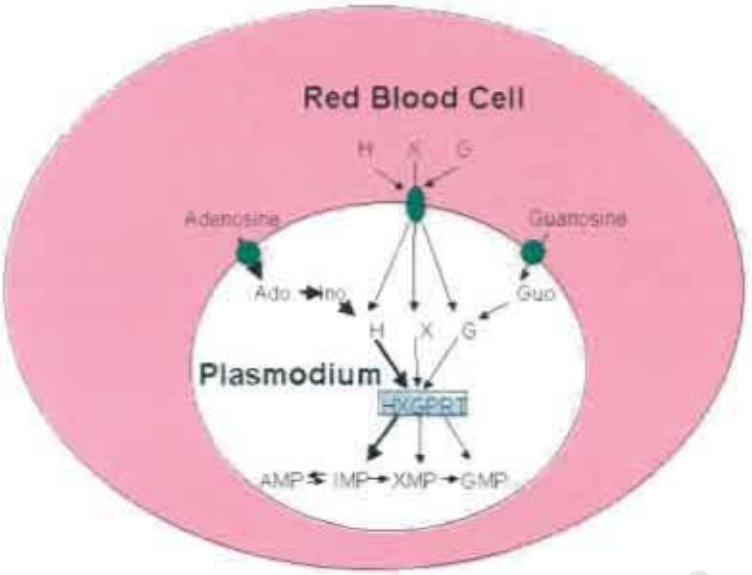

Figure 1.5 **Pathways for purine salvage in *P. falciparum*** The main route is indicated in bold arrows (H = hypoxanthine, X = xanthine, G = guanine, Ado = adenosine, Ino = inosine, and Guo = Guanosine).

As mentioned, purine nucleotide phosphorylase (PNP) provides the main source of hypoxanthine in parasites by converting inosine to hypoxanthine and ribose-1-phosphate. The importance of this pathway is demonstrated by the inhibition of this enzyme by immucillins, purine nucleoside analogues containing a 1-(9-deazapurin-9-yl)-1,4-dideoxy-4-iminoribitol moiety, which mimic the enzyme's transition state through protonation of the imino nitrogen and resulting positive charge (Kicska *et al.*, 2002). The inhibitor kills parasites in culture with an IC_{50} value of 35 nM. Growth limitation is reversed by hypoxanthine but not inosine, showing the block is at the level of PNP. The human erythrocyte PNP exhibits a higher affinity for the analogue compared

with that of the parasite, and parasite death only occurs at higher concentrations where both enzymes are inhibited, suggesting that adenosine and not hypoxanthine provides the main pool for purines coming from the erythrocyte. A crystal structure of malarial PNP with bound ImmucillinH (an immucillin with substituent features of hypoxanthine) and sulphate identified a solvent filled cavity close to the 5'-OH, which led to the discovery of 5'-methylthio-immucillinH as a potent and selective inhibitor of the malarial enzyme (Shi *et al.*, 2004). The parent compound, 5'-methylthio-inosine, is a substrate of the enzyme and a parasite metabolite (Ting *et al.*, 2005).

Several other potent inhibitors of the human enzyme had previously been found, including acyclovir diphosphate (Ki ~ 10 nM) with an acyclic ethylene linkage between the phosphate and the guanine (Tuttle and Krenitsky, 1984).

HXGPRT has long been recognized as a possible drug target against malaria and other parasitic protozoans since the early work of Sherman and others (Sherman, 1979; Ullman and Carter, 1995). The malarial enzyme, like that of other protozoan parasites, is highly homologous to the human enzyme, and the active site residues are virtually identical. However, it does differ in exhibiting lower K_m values for the substrates and showing activity with xanthine (Queen *et al.*, 1988; Heroux *et al.*, 1999b; Keough *et al.*, 1999). Mutant, inactive, forms of human HGPRT or its absence leads to Lesch-Nyhan syndrome, a disease identified by hyperuricemia and neural problems. Partial deficiencies result in gouty arthritis. The malarial enzyme is the subject of this thesis and will be introduced in detail later.

1.3.3 Drug resistance

Chloroquine has been a safe and effective treatment against malaria for several decades. However, resistance to this drug appeared 50 years ago, first in South East Asia, South America, East Africa, and thence to the rest of the continent. Antifolate drugs came into existence as effective agents against chloroquine-resistant parasites. However, resistance to these soon appeared, and now combination therapies are becoming common. Artemisinin has provided new hope, especially in combination with other antimalarials.

The problem of resistance is highlighted by a recent news article in *NewAfrican* (March 2004, no. 427), in which WHO is accused of "medical malpractice" by encouraging the use of chloroquine and antifolates. The article suggests that artemisinin-class combination therapy would be more effective, although the cost is approximately 10-fold higher.

Chloroquine resistance has been linked to mutations in a digestive vacuole transporter termed "chloroquine resistance transporter" *pfcrt* (Fidock *et al.*, 2000). This is a 424 amino acid protein with 10 predicted transmembrane helices and lys76 to thr in the first transmembrane helix is the principal mutation conferring resistance. This mutation is accompanied by an arg220 to ser mutation in most resistance organisms. The mechanism of resistance by this protein is unclear. Possibly the most feasible is that it normally functions as an amino acid (or other metabolite) symporter with H^+ and that

the positive charge on lys76 inhibits its interaction with the protonated and charged chloroquine in the digestive vacuole. The mutated protein, without the charge, allows interaction and passive downhill efflux of the protonated drug, thereby lowering its concentration in the vacuole (Bray *et al.*, 2005).

A homologue of the mammalian multidrug resistance P-glycoprotein, *pfmdr1*, is also implicated in chloroquine resistance (Foote *et al.*, 1989). It is a typical ABC transporter with two ATP binding domains and two membrane domains. Mutations in this gene occur in many, but not all, of the resistant parasites (Foote *et al.*, 1990). Insertions of the mutations in the wild type gene affected sensitivity to several quinolines (Reed *et al.*, 2000). It appears to play a role in modulating resistance (Duraisingh and Cowman 2005). It is not clear how mutations to the drug pump could affect the accumulation of chloroquine, but perhaps the protein normally helps to actively pump the drug into the vacuole and the mutations inhibit this.

Resistance to the antifolate combination of pyrimethamine and sulfadoxine, similar to that to chloroquine, is growing in Asia and Africa. Resistance to pyrimethamine is due to point mutations in the reductase gene, mainly ser108 to asn, that lower the affinity of the enzyme for the inhibitor without affecting activity (Cowman *et al.*, 1988; Peterson *et al.*, 1988; Sirawaraporn *et al.*, 1990). Other mutations, like those at positions 16, 51 or 59, in combination with the one at 108, exacerbate the resistance. Resistance to sulfadoxine requires mutation/s in the synthase gene, mainly ala437 to gly, but also at

positions 436, 540, 581, and 683, which again inhibits binding of the drug to the enzyme (Triglia *et al.*, 1997; Basco *et al.*, 2000).

Atomic structures of both mutated and wild-type reductase enzymes with bound substrates or inhibitors shows that the resistance mutations sterically prevent rigid antifolates like pyrimethamine and cycloguanil from binding (Yuvaniyama *et al.*, 2003; Yuthavong *et al.*, 2005). The structures have guided synthesis of more potent antifolates that bind to the resistant forms as well.

1.4 The purine salvage enzyme HG(X)PRT

1.4.1 HG(X)PRT reaction mechanism

The reaction of HG(X)PRT is shown in Figure 1.6. 5-phospho-α-D-ribofuranosyl-1-pyrophosphate (PRPP) reacts with hypoxanthine, guanine or xanthine (in parasite enzymes) to form IMP, GMP or XMP respectively and pyrophosphate (PPi). Mg^{2+} is required, probably in the form Mg_2PRPP (Salerno and Giacomello, 1980), and, as we will see below, the requirement for two Mg^{2+} is borne out by the crystals structures. Early kinetic studies, mostly carried out on the human erythrocyte enzyme, have indicated that the forward reaction is ordered, with PRPP binding first followed by the purine to yield a ternary enzyme-substrate complex followed by ordered product release (Henderson *et al.*, 1968). Later work cast some doubt on the ordered

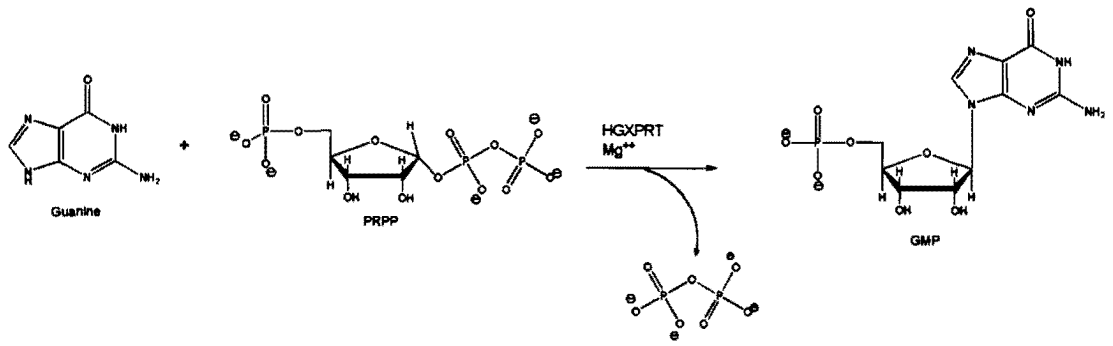

Figure 1.6 **The HG(X)PRT reaction**. In this example, guanine (purine) is converted to guanosine 5'-monophosphate (GMP) by linking it to PRPP in the presence of magnesium ions.

release of products as random binding of IMP and PPi in the reverse reaction (termed pyrophosphorolysis) followed by ordered release of first hypoxanthine and then PRPP was found (Giacomello and Salerno, 1978). Isotope exchange with IMP-GMP and guanine stimulation IMP pyrophosphorolysis suggested slow release of PRPP again indicating ordered binding/release of substrates (Salerno and Giacomello, 1979). A more recent detailed study, of the human enzyme, combining pre-steady state and steady state kinetic measurements, has found the ordered binding of substrates and products in the forward direction (Xu *et al.*, 1997). PRPP binds tightly (K_d = 1.3 μM) first and needs Mg^{2+}. The base binds second with a similar affinity (K_d ~ 2 μM). The purine did not bind to the apoenzyme. IMP, but not PPi, competed with PRPP binding, from which a K_d of 53 μM was extracted, and showing that the affinity for PPi is very low. In the reverse direction IMP binds first and PPi

second. Enzymes from other species, such as *E. coli*, *Plasmodium*, *Tritrichomonas foetus* have similar K_m values for substrates (Liu and Milman, 1983, Xu *et al.*, 1997; Keough *et al.*, 1999; Munagala *et al.*, 1998).

There is evidence for both dissociative S_N1- and associative S_N2-type chemical reactions (see reaction pathways below). A two-step S_N1-type transfer comes out of kinetic isotope effects with orotate-PRT, which points to the activation of PRPP through PPi loss and the formation of a distinct oxacarbenium-like transition state (see scheme 1.1, Goitein *et al.*, 1978). A later study on the same enzyme confirmed that the transition state had distinct oxacarbenium character on the ribose and substantial negative charge on the orotate (Tao *et al.*, 1996). This mechanism is supported by the slow, but extremely tight, binding of stable nucleotide analogues of the proposed transition state, the phosphorylated immucillins (e.g. ImmucillinHP), in a complex with PPi and Mg^{2+} (Li *et al.*, 1999). In these analogues the O4' oxygen of the ribose moiety is replaced by N and the N9 of the purine is C instead of N (see structures in Figure 1.7). N7 in the deazapurine ring is protonated.

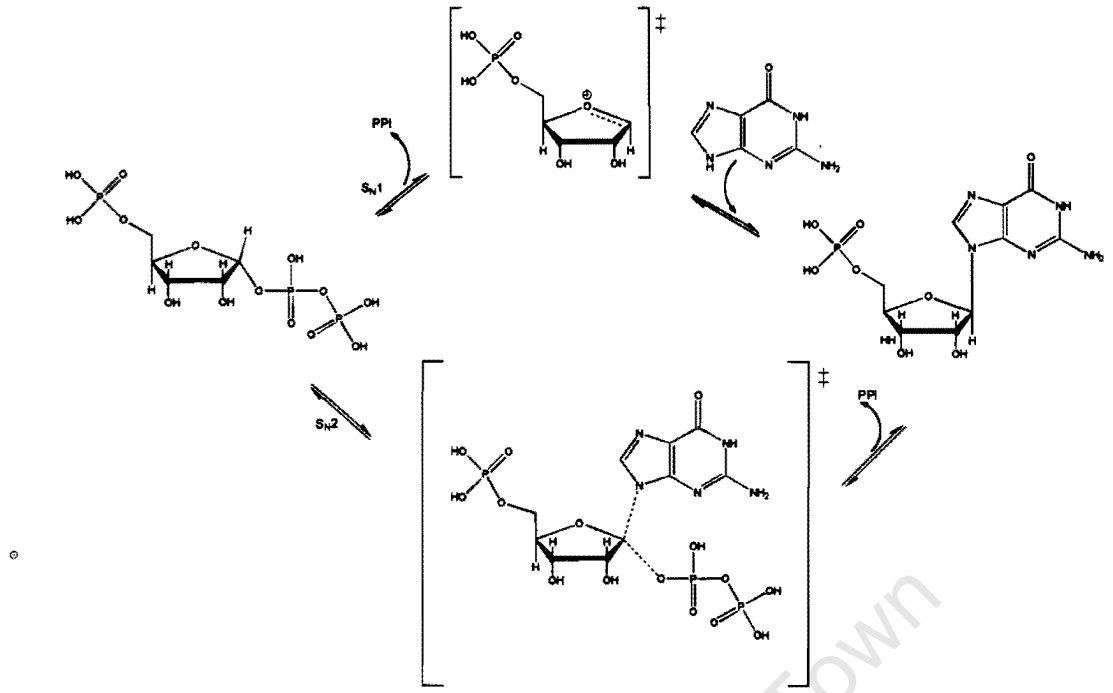

Scheme 1.1 **S_N1 and S_N2 reaction pathway**. The S_N1 pathway is shown in an extreme version where the oxacarbenium ion is generated as a distinct species following PPi dissociation. In the S_N2 reaction, bond formation and breaking occur simultaneously (dotted lines).

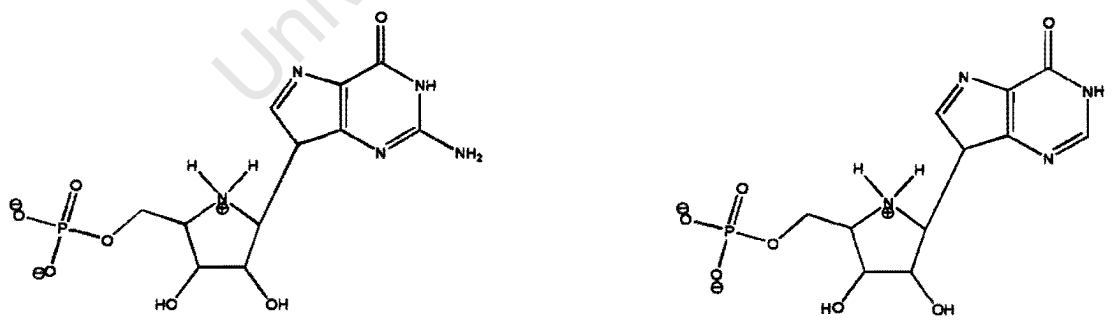

ImmucillinGP **ImmucillinHP**

Figure 1.7 **Structures of nucleotide analogues that mimic the transition state and bind at the active site of HG(X)PRT enzymes** (Li *et al.*, 1999).

The iminoribitol moiety has a pKa of 6.7, which means that it is largely protonated at pH 7, and positively charged, mimicking the oxacarbenium state. Later, when the structures are considered, it will be seen that there could be the need for significant movement of the C1' ribose from the reacting O of the pyrophosphate to the N9 of the purine, implying that a stable oxacarbenium intermediate must form transiently, and therefore an S_N1 type reaction is indicated (Shi *et al.*, 1999a). Evidence of an associative S_N2 mechanism is indirect, and derives from analysis of crystal structures of the closed active site with PRPP and an analogue of hypoxanthine, which is considered to represent a stage just prior to the transition state, and yet there was no evidence of activation of the PRPP to an oxacarbenium form (Focia *et al.*, 1998).

There is also no obvious means of stabilizing the activated oxacarbenium cation intermediate with nearby polar amino acid residues, making it difficult to understand why the transition state mimics bind so tightly. It has been suggested that this may derive rather from an altered ribose configuration and H-bonding to N7 (Craig and Eakin, 2000). Also, the presence of a significant number of trapped water molecules in the closed active site conformation seems to mitigate against stabilization of a reactive intermediate (Heroux *et al.*, 2000).

1.4.2 Structure of HGPRTs

The HGPRTs belong to a larger group of PRTs that share a common reaction mechanism and a characteristic structural fold. Over 40 crystal structures have been determined for a variety of PRTs incorporating 16 different proteins (for review see Sinha and Smith, 2001). The PRTs can be identified by a sequence motif incorporating 4 hydrophobic amino acids, a glutamate and aspartate involved in binding the ribose hydroxyls, and 7 variable amino acids including glycine and threonine, which form the 5' phosphate binding loop.

Sequences from 5 HGPRTs are aligned in Figure 1.8. The identifying sequence motif is in β-strand 6 and Loop III. Other conserved amino acids are indicated. In particular, Loop I contains a leu-lys-gly motif that is involved in significant structural changes to bind the pyrophosphate of PRPP. There is a highly conserved ser-tyr motif in loop II, which overlay PRPP and the purine base and occludes the catalytic site. In Loop III' there are conserved lys and arg amino acid residues, which interact with the purine and fixes the loop onto Loop III underneath. Towards the end of the protein is conserved β-strand 9, which forms a cap over the base. Further on in the sequence is a highly conserved asp (Loop IV) that ligates one of the Mg^{2+} and the pyrophosphate.

Looking at the tertiary structure, the PRTs have a core domain consisting of a 5-7 β-stranded sheet lodged in between 3 main α-helices (light blue and dark blue respectively, Figure 1.9). There is also a hood domain arising from the N-

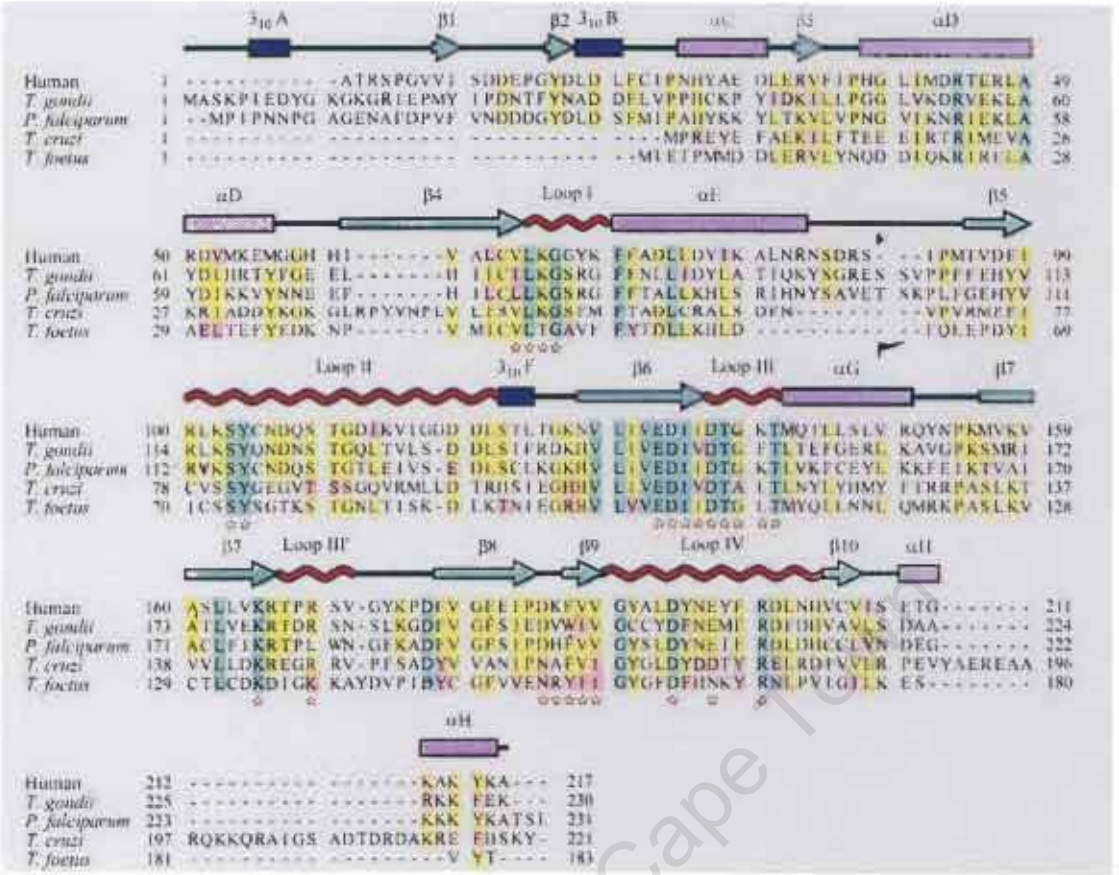

Figure 1.8 **Sequence alignments of PRTs from human, *T. gondii*, *P. falciparum*, *T. cruzi* and *T. foetus*.** Green shaded residues are absolutely conserved across the PRTs while those in yellow are conservatively substituted. Active site residues have gold stars under them. The 2^0 structural elements of the *T. gondii* HGXPRT are placed above the sequence alignment. This Figure was taken directly from Heroux *et al.* (1999a).

and C-terminal ends consisting of one helix and several small strands. The hood can be a small unit such as that of *E. coli* HGXPRT with 29 amino acids or it can be extremely large as that of *Giardia lamblia* that has 97 residues (Vos *et al.*, 1997; Shi *et al.*, 2000). The active site is formed on one end of the

central sheet and is surrounded by several loops and the hood domain that enclose it during catalysis.

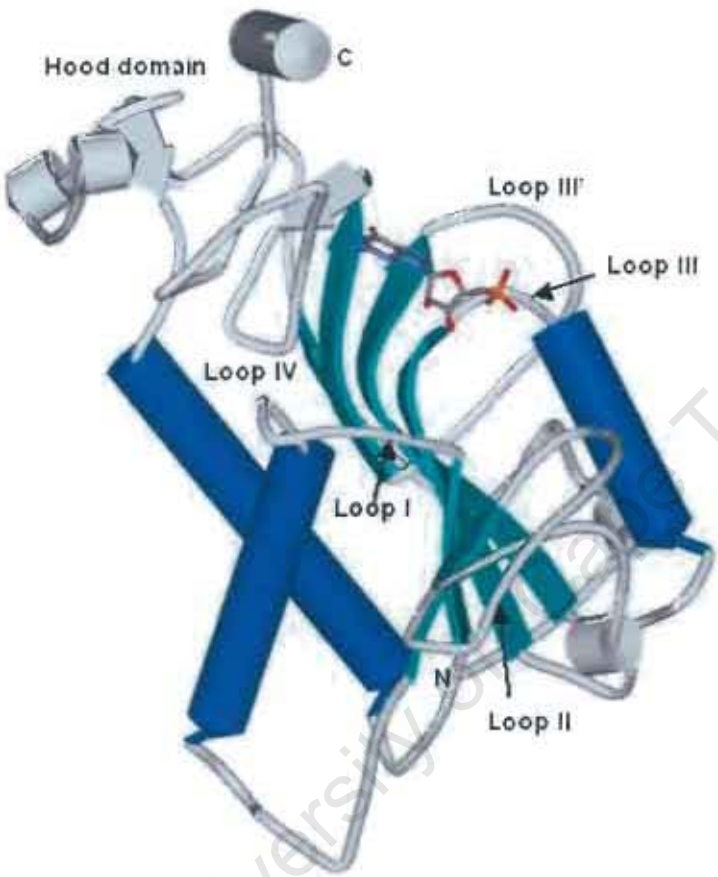

Figure 1.9 **The PRT fold**. The protein is HGPRT from *T. gondii*, with GMP at the active site (Heroux *et al.*, 1999a).

Several atomic structures with one or two substrates or products have been elucidated. The following analysis is based on the *T. gondii* structures, mainly based on the work of Heroux and colleagues (Heroux *et al.*, 1999b). Crystal structures from other species show the mechanism is applicable to the other

PRTs in the family. The apoenzyme has an open active site with surrounding Loops I, II, III, III' and IV fairly well apart (Figure 1.10, Schumacher *et al.*, 1996). Loop I possesses a critical lys79, which is oriented outwards in this

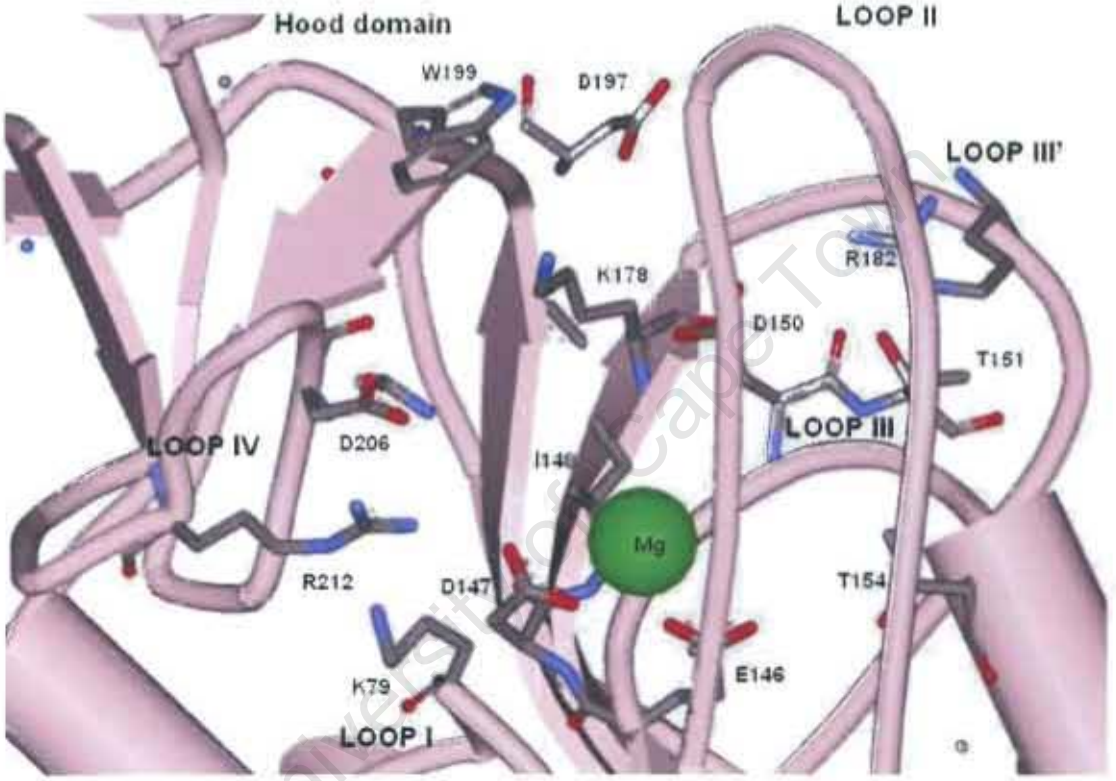

Figure 1.10 **Active site residues in HGPRT$_{apo}$ from *T. gondii*** (Schumacher *et al.*, 1996). Residues 116-118 are missing in Loop II (often referred to as the flexible or catalytic loop), including ser117 and tyr118, which overlay the nucleotide in the transition state.

structure and has a *trans* peptide bond with leu78 (see later for significance). Loop II is pointing out of the active site and, in the subunit shown, part of the

loop was disordered including the conserved ser-tyr motif and is omitted from the structure.

Loop III is somewhat disordered with the thr151 and thr154 side chains not in an optimal position for interacting with the 5' phosphate of PRPP. In Loop III' arg182 is pulled well back away from asp150 and asp197. Loop IV has asp206 and arg212 turned in and poised to bind Mg^{2+} and the pyrophosphate moiety of PRPP.

The Hood domain is angled back and trp199 (Hood domain) and ile148 (Core domain) are 14.5 Å apart. These residues will eventually clamp the purine ring between them and in this structure are too far apart for this purpose. The crystal structures show Mg^{2+} bound to glu146 and asp147. The crystals were grown in 200 mM $MgCl_2$ and its presence may be artifactual. We will see below that this is not the true position of either of the two Mg^{2+}. The side chains of the two acidic residues are pointing upwards, in a position suitable to bind the ribose hydroxyls of PRPP.

Thus, in general, the apoenzyme is set up to bind the pyrophosphate and ribose moieties of PRPP. Loop III needs to be adjusted and the Hood domain is too far away to bind purine. Binding of Mg_2PRPP will bring Loops I, III, and IV together, but still leaving the Hood domain well back to allow the entry of the purine. The ternary complex with PRPP and an analogue of guanine, 9-deazaguanine, is shown in Figure 1.11. It represents a complex just before the transition state and the active site is closed, in particular Loop II, with

tyr118, is folded over the catalytic site and Loop III' has been drawn in by arg182 and is clamped by asp150 and asp197 (obscured in Figure 1.11). Deletion of a large section of Loop II, including the tyrosine, slows enzyme turnover 2-3 orders of magnitude (Lee *et al.*, 2001). The ternary structure shows that PRPP is bound directly to protein through at least 6 hydrogen bonds. The peptide bond between ser78 and lys79 is now in a strained *cis* conformation, which allows the main chain amide to interact with the pyrophosphate moiety. The ribose ring is contorted and adopts a C2'-endo pucker, rather than the usual C3'-endo in solution. Two Mg^{2+} are present on either side of the pyrophosphate moiety; and only one is in direct contact with the protein (at asp206). This latter Mg^{2+} is also coordinated to 3 water molecules and 2 oxygens of the pyrophosphate of PRPP. The other is coordinated to 2 water molecules, the 2 hydroxyls of the ribose, and 2 oxygens atoms of the pyrophosphate, in particular, one that is directly linked to the scissile bond to C1' of the ribose. The purine is lodged between try199 and ile148 and bonded to the main chain carbonyl of asp206 and side chain of lys178. Asp150 is thought to be the catalytic acid/base that accepts a proton from N7 of the purine in order to increase the nucleophilicity of N9 (Xu and Grubmeyer, 1998). Closure of Loop II has brought tyr118 over the ribose moiety and the oxygen interacts with the 5' phosphate group. It is likely that folding of this loop over the active site is the last event before catalysis. The crystal structure of the ternary bi-product complex shows the situation immediately after the transition state (Heroux *et al.*, 1999b). Here Loop II and Loop III' were not discerned, pointing to their flexibility and open state. Hence it appears that release of products occurs by these two loops dissociating first,

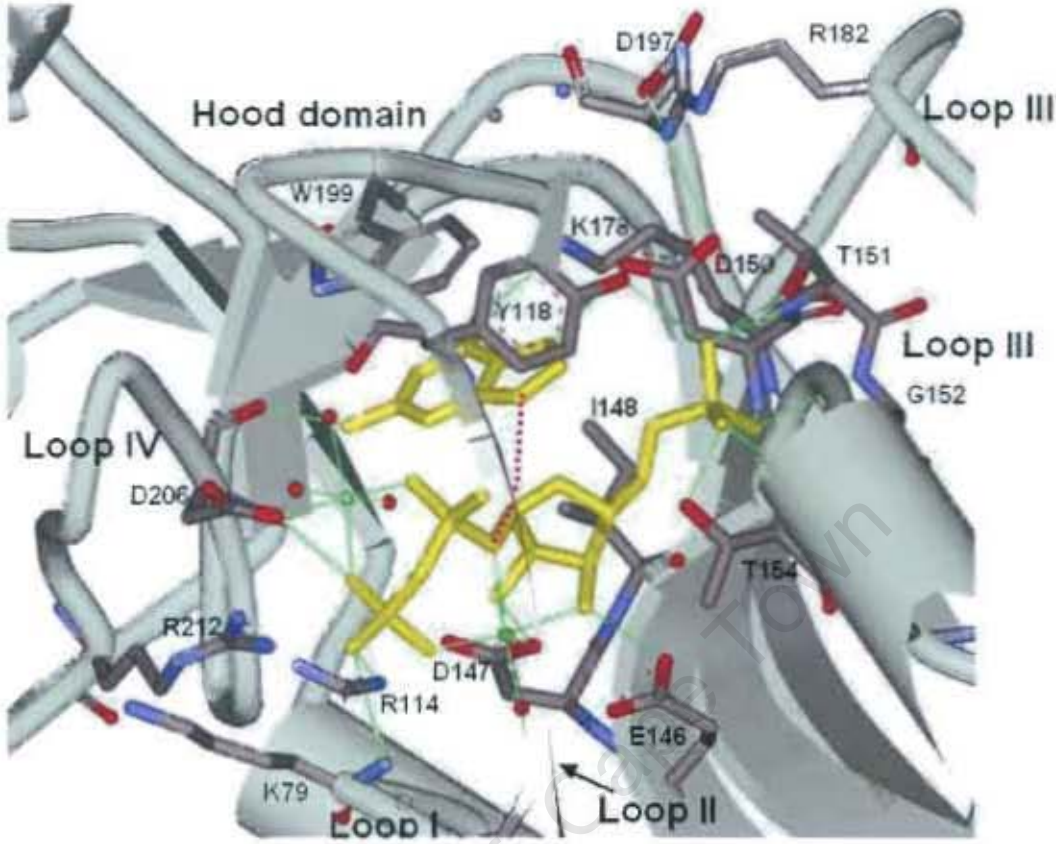

Figure 1.11 **Active site residues in HGPRT$_{PRPP + deazaguanine}$ from *T. gondii*** (Heroux *et al.*, 2000). The PRPP and deazaguanine are in yellow and the Mg^{2+} in green. Bonds of 3 Å or less are shown in green lines.

followed by Loops I and IV allowing the exit of PPi. These events would permit the release of Loop III and the Hood domain in order for the nucleotide to dissociate.

Aside from the loop changes, there are 3 (the last being only a strong possibility) other significant changes in this bi-product complex. The first is that the peptide bond between ser78 and lys79, which is still in cis

configuration, must loosen the interaction of the amide with the pyrophosphate and probably aid its release. The second is that the coordination of Mg^{2+} with the 2 ribose hydroxyls is broken and replaced by water molecules. Thirdly, and possibly related to the latter, the ribose of the nucleotide configuration has relaxed back to the normal C2'-exo form. Thus the interaction of the protein with the products is less than that seen with the bi-substrate complex, the one product is in a lower energy state, and the Mg^{2+} link to the ribose has been severed, favouring spontaneous and separate dissociation of first the PPi and then the nucleotide.

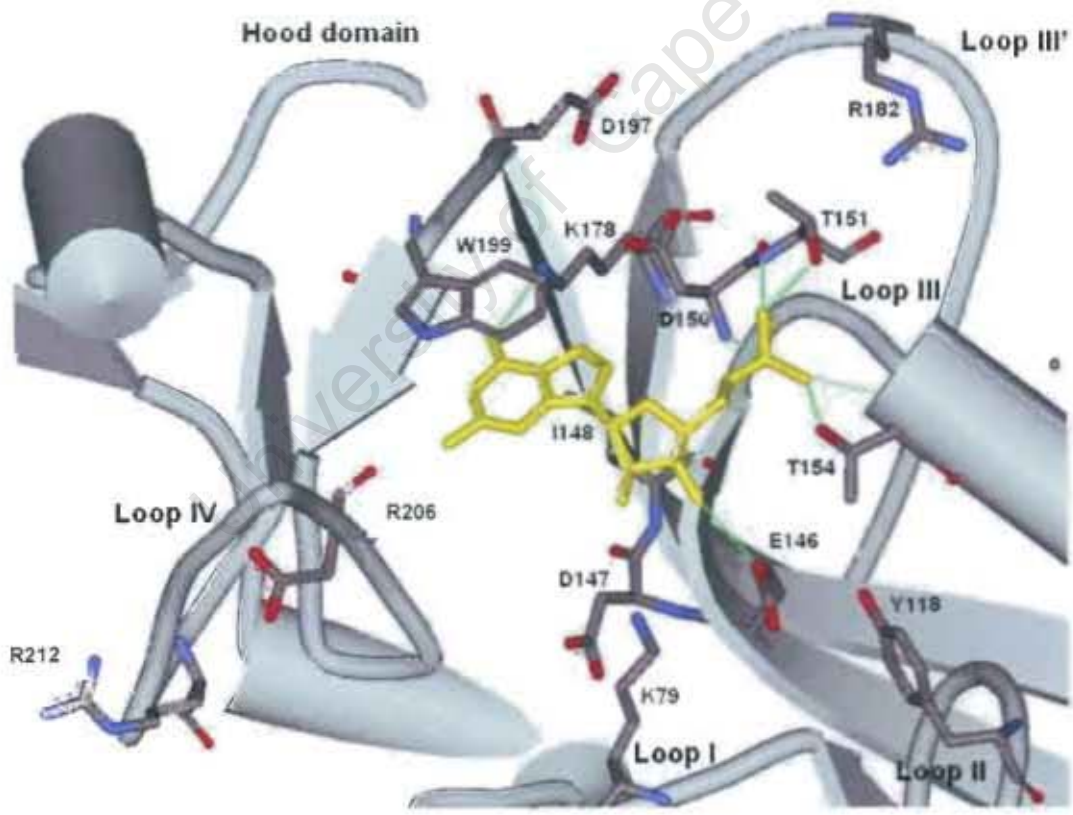

Figure 1.12 **Active site residues of $HGPRT_{GMP}$ from *T. gondii*** (Heroux *et al.*, 1999a). GMP is shown in yellow

The departure of Mg^{2+} and PPi promotes relatively large structural changes involving Loops I, III', and IV (Figure 1.12, Heroux *et al.*, 1999a). Loop II remains outside of the catalytic site. In Loop I, the side chain of lys79 moves into the space previously occupied by PPi. This movement brings a positive charge alongside asp147, and may facilitate the bending of this side chain downwards, releasing the interaction with the O2' of the ribose. Loop III' has moved back and arg182 is no longer associated with asp150 and asp197. Loop IV has also receded and residues asp 206 and arg212 are turned out of the catalytic site.

In order for GMP to be released, these changes must permit the Hood domain to tilt backwards opening the trp and ile clamp on the purine ring and loosen the grip Loop III has on the 5' phosphate. Departure of nucleotide must promote further changes that bring the protein back to the apoenzyme seen in Figure 1.10 to complete the cycle.

1.4.3 HGXPRT from *P. falciparum*

Malaria HGXPRT consists of 231 amino acids per subunit with a calculated MW of 26 232 Da. Analytical ultracentrifugation suggests that the enzyme is tetrameric and dimeric at low and high ionic strength respectively (Keough *et al* 1999). It is only active at low ionic strength, which contrasts with the human enzyme, which is insensitive to ionic strength. The malaria HGXPRT is 44 % homologous to that of the human HGPRT enzyme (Shi *et al.*, 1999b). The former, like most protozoan parasite HGPRTs, has broader substrate

specificity compared with the human and is able to use xanthine, as well as hypoxanthine and guanine (Queen *et al.*, 1988).

Malaria HGXPRT is unstable and purification directly from parasites yields enzyme with very low activity (Queen *et al.*, 1988). The enzyme has been successfully expressed recombinantly in *E. coli* (Shahabuddin and Scaife, 1990; Keough *et al.*, 1998; Keough *et al.*, 1999). The specific activity of the pure enzyme was 3 - 8 µmoles GMP/min/mg of protein with guanine as substrate at pH 8.5, 25 ^{0}C, which is several times less than that of the human equivalent enzyme. The enzyme was stabilized by hypoxanthine and PRPP, and inactive protein could be reactivated by these substrates.

It has been difficult to obtain crystals of the enzyme, due most probably to its instability. Only one crystal structure exists and it was obtained with the transition state mimic, ImmucillinHP (Figure 1.7), PPi, and Mg^{2+} (Shi *et al.*, 1999b). The protein crystallises as a tetramer with 3 unique interfaces. Two of them are shown Figure 1.13. The figure also indicates how the active sites are largely, but not entirely (see extreme left hand subunit), away from the interfaces. Each subunit of the malaria HGXPRT is folded into a single domain structure consisting of 6 α-helices and 11 β-stranded sheet. In each subunit of the malaria enzyme, residues 46 - 149 make up the core region while residues 1 - 46 and 195 - 231 form a hood region. The protein fold, shown in Figure 1.14, is very similar to what we have seen for *T. gondii* (compare with Figure 1.9).

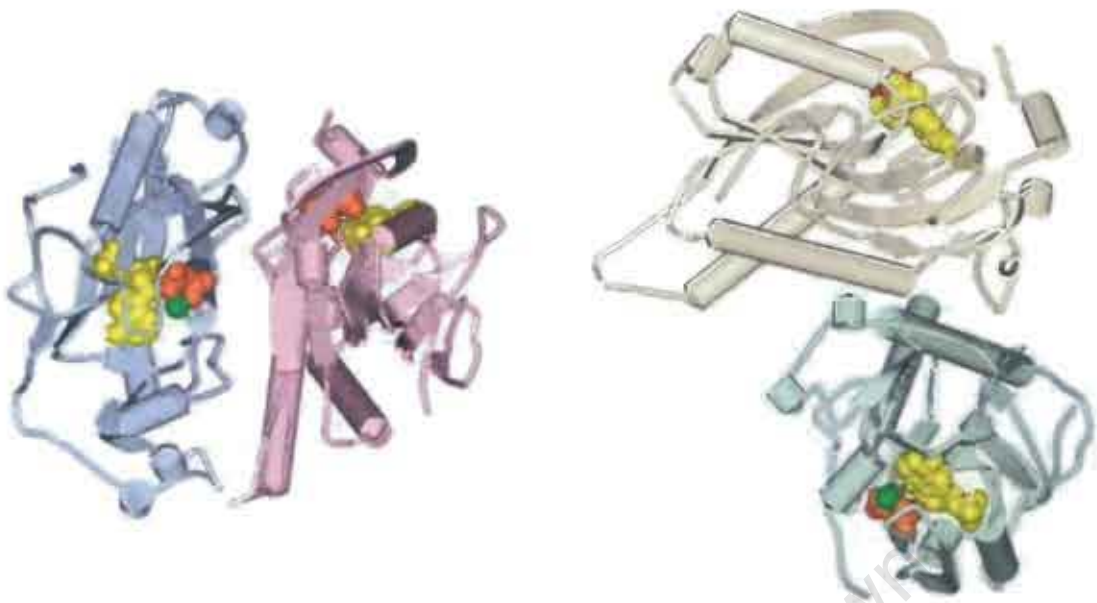

Figure 1.13 **The four subunits of HGXPRT from *P. falciparum*** ImmucillinHP, PPi and Mg^{2+} are shown in yellow, orange, and green respectively (Shi *et al.*, 1999b).

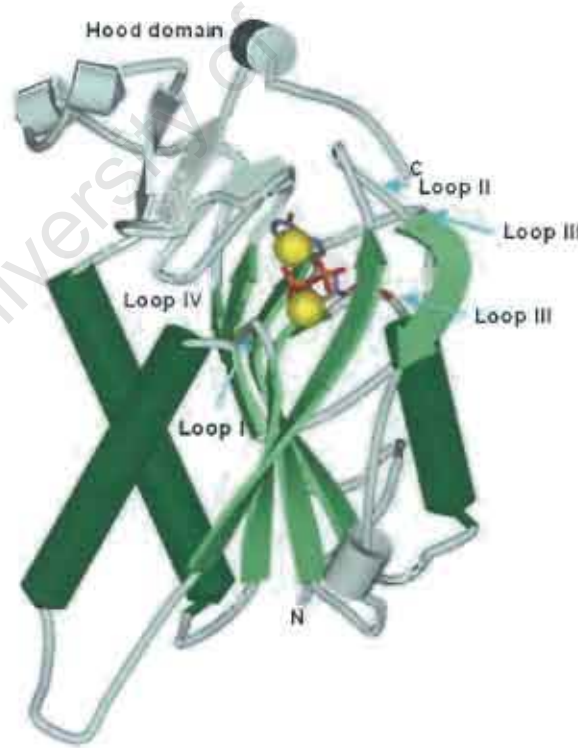

Figure 1.14 **Protein fold of HGXPRT from *P. Falciparum*** The core sheet is shown in light green and the 3 main helices in dark green. The active site contains ImmucillinHP (stick form), PPi (stick form), and 2 Mg^{2+} (yellow balls). Structure from Shi *et al.*, 1999b.

As before, the hood is made up of amino acids that are located on the N- and C- termini of the polypeptide. The core sheet contains an extra β-strand because Loop II is folded over the catalytic site.

The crystal structure of malarial HGXPRT in the transition state adds to our understanding of the chemical interconversion (Figure 1.15).

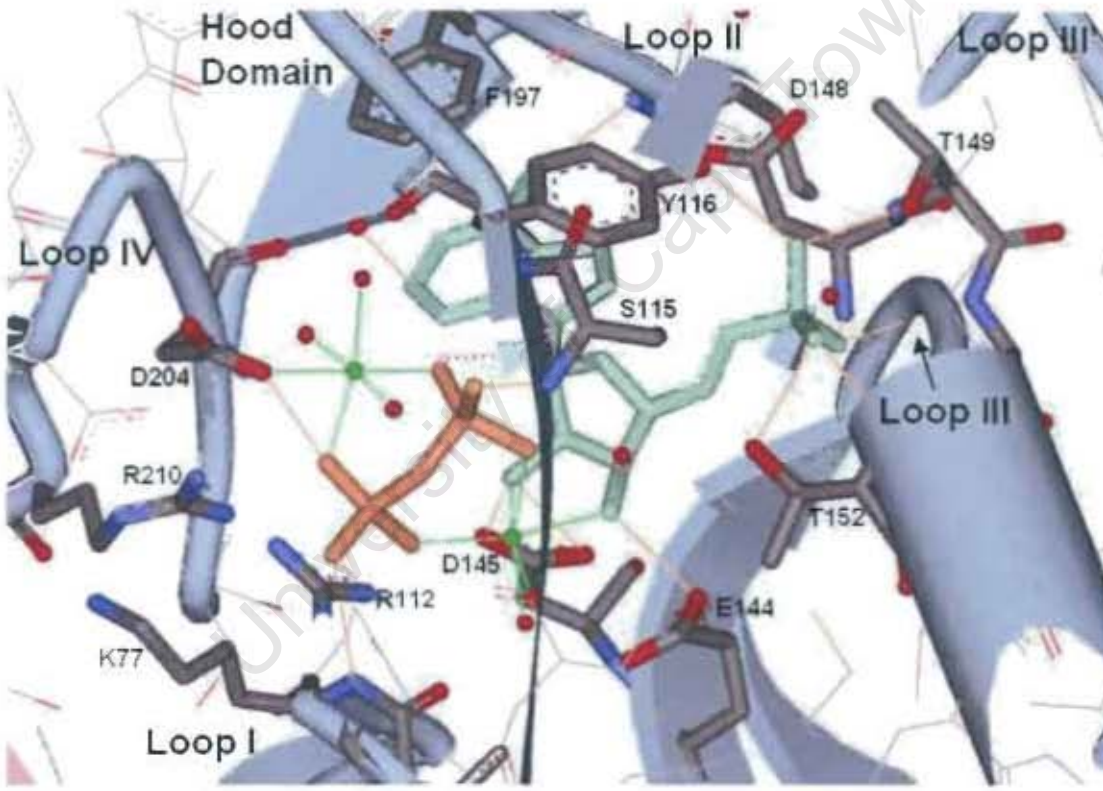

Figure 1.15 **Active site of HGXPRT from *P. falciparum* in the transition state with bound ImmucillinHP (light green), PPi (orange), and 2 Mg^{2+} (green).** The bonds involved in the chemical transfer are shown in dotted pink. Hydrogen bonds to the substrates/analogues are shown in orange, and those coordinating the two Mg^{2+} are in green. Structure from Shi *et al.*, 1999b.

Firstly, the substrate mimic, with oxacarbenium ion character and distorted iminoribitol ring, binds slowly but extremely tightly suggesting that these features of the mimic are found in the transition state (Li *et al.*, 1999). We have seen before in the bi-substrate complex from *T. gondii* how one Mg^{2+} is coordinated to the ribose hydroxyls, evidently withdrawing electrons from the furanose ring. Further, the latter was distorted to favour carbenium ion formation (3-exo to 3-endo). The O5' was strained to interact with the O4' oxygen. These features are retained in the transition state structure, but in addition tyr116 is flattened over the N4', which may provide additional stabilization through cation-aromatic interactions.

Now we see a more extensive hydrogen-bonding network anchoring the substrates compared with the bi-substrate ternary complex. In particular, arg210 ligates PPi and additional bonding is seen around the 5' phosphate. Thus, in the actual reaction, the purine, ribose hydroxyls, and 5' phosphate moieties and the PPi are tightly held in position. Within these constraints it may be possible that the furanose ring is twisted further to allow the C1' atom to move in the required direction to aid the reaction.

An NMR study of purine nucleoside phosphorylase from *Mycobacterium tuberculosis* and HGPRT from *T. foetis* established that the ImmucillinHP bound as the neutral N4' form and was protonated in the development of the transition state (Sauve *et al.*, 2003). The C1' atom also developed sp^2 hybridization character. The phosphoryl groups decreased their pK_as (fully

ionized), thereby contributing to an enhanced electrostatic stabilization of the cationic transition state.

1.5 Chalcones

Chalcones are compounds that are made of two aromatic rings (generally referred to as rings A and B) joined by a propenone linker. (2*E*)-Chalcone shown in Figure 1.16 below is the simplest chalcone.

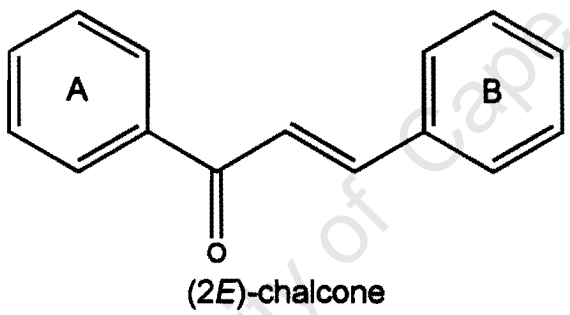

(2*E*)-chalcone

Figure 1.16 **Structure of the simplest chalcone.**

Chalcones are found in many higher plants (for example, Star and Mabry, 1971; Stevens *et al.*, 2000). They have been demonstrated to have a wide range of biological activity including anti-bacterial and anti-fungal (Lin *et al.*, 2002; Nielsen *et al.*, 2004; Nielsen *et al.*, 2005; Satyanarana and Rao, 1993; Jayasinghe, *et al.* 2004). They have also been shown to have anticancer (Satyanarana and Rao, 1993; Shibata, 1994; Ducki *et al.*, 1998; Rao *et al.*, 2004) as well as anti-inflammatory (Meng *et al.*, 2004) activities. Hydroxylated

chalcones inhibit tyrosinase, an enzyme involved in melanin biosynthesis (Nerya *et al.,* 2004). Halogenated chalcones bind with high affinity to multidrug resistance P-glycoprotein, which is overexpressed in cancer cells (Bois *et al.*, 1998). The most potent of these, 2',4',6'-trihydroxy-4-iodochalcone [also referred to in this thesis as (2*E*)-3-(4"-iodophenyl)-1-(2',4',6'-trihydroxyphenyl)prop-2-en-1-one], is our lead compound for accelerating the catalytic turnover of malarial HGXPRT (see below).

The first chalcone to be reported to have antiprotozoan activity is licochalcone A (Chen *et al,* 1994). Licochalcone A (see Figure 1.17 below) was isolated from Chinese licorice roots and was demonstrated to have antimalarial activity against *P. falciparum* and *P. yoelii.* Later it was shown to inhibit parasite respiratory chain of *Leishmania major* and *L. donovani*, and seemed to target fumarate reductase (Chen *et al.*, 2001). Li *et al.*, (1995) found that 1-(2,5-dichlorophenyl)-3-(4-quinolinyl)-2-propen-1-one (Figure 1.17) out of a library of chalcones, has high activity against chloroquine resistant and sensitive strains of *P. falciparum*. This chalcone was proposed to interact with a cysteine protease. 2,4-dimethoxy-4'butoxychalcone (Figure 1.17) has potent activity against human malaria parasite *P. falciparum in vitro* and murine malaria parasites *P. berghei* and *P. yoelii in vivo* (Chen *et al.*, 1997). The target enzyme is unknown. Alkoxylated and hydroxylated chalcones have been reported to have antiplasmodial activities, and ring B was the more critical one, and size and hydrophobicity of the substituents were correlated with potency (Liu *et al.,* 2001). These chalcones have since been demonstrated to target New Permeability Pathways, because they inhibit

sorbitol-induced lysis of parasitized red blood cells (Go *et al.*, 2004, see section 1.3.1). Methoxy or dimethoxy substituents in ring B were important determinants for activity. Substituting ring A or ring B with ferrocene, a grouping with antimalarial activity for unclear reasons, did not destroy, but could not augment the antimalarial effects (Wu *et al.*, 2002).

Some quinolinyl chalcones were synthesized as possible falcipain inhibitors and antimalarials, but there was no correlation between the two activities and the target enzyme appears not to be the protease (Dominguez *et al.*, 2001). Natural product prenylated chalcones also exhibit antimalarial activity (Narender *et al.*, 2005).

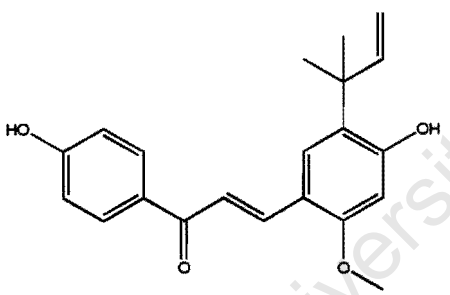

licochalcone A

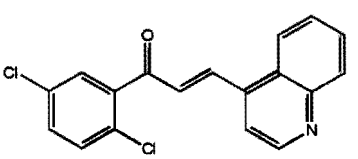

1-(2,5-dichlorophenyl)-3-(4-quinolinyl)-2-propen-1-one

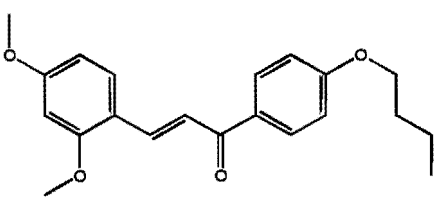

2,4-dimethoxy-4'butoxychalcone (2,4-mbc)

Figure 1.17 **Structures of chalcones with anti-malarial activity** (Chen *et al.*, 1994; Li *et al*,., 1995; Chen *et al.*, 1997).

Besides there being a large number of natural chalcones, chemists find them useful because they are readily synthesized and substituents on the phenyl rings can result in a large diversity of compounds. This facilitates structure/activity relationships with a target protein.

1.6 Overview of the chemistry involved in the synthesis of chalcones

1.6.1 Claisen-Schmidt reaction

The key organic chemistry reaction used in this PhD project is the Claisen-Schmidt reaction also referred to as mixed aldol condensation reaction. This reaction is one in which an aldehyde and a ketone are joined together to form an α,β-unsaturated compound. Claisen-Schmidt reactions are generally performed in polar solvents like methanol or ethanol in the presence of an alkaline catalyst such as NaOH or KOH. Alternative catalysts for this reaction have been developed (see Go *et al.*, 2005 for a review). For instance, a solid catalyst prepared by adding sodium nitrate to natural phosphate at 900 ^{0}C can be used in the synthesis of chalcones. Other catalysts that can be used include calcium hydrotalcites.

Although chalcones can be synthesized at low (25 ^{0}C) or slightly elevated (60 - 70 ^{0}C) temperature, other methods that employ different forms of energy like ultrasound or microwave, have been employed.

As mentioned earlier, Claisen-Schmidt reactions are generally base catalysed (see mechanism in Figure 1.18) but as can be seen in Figure 1.19, acids can

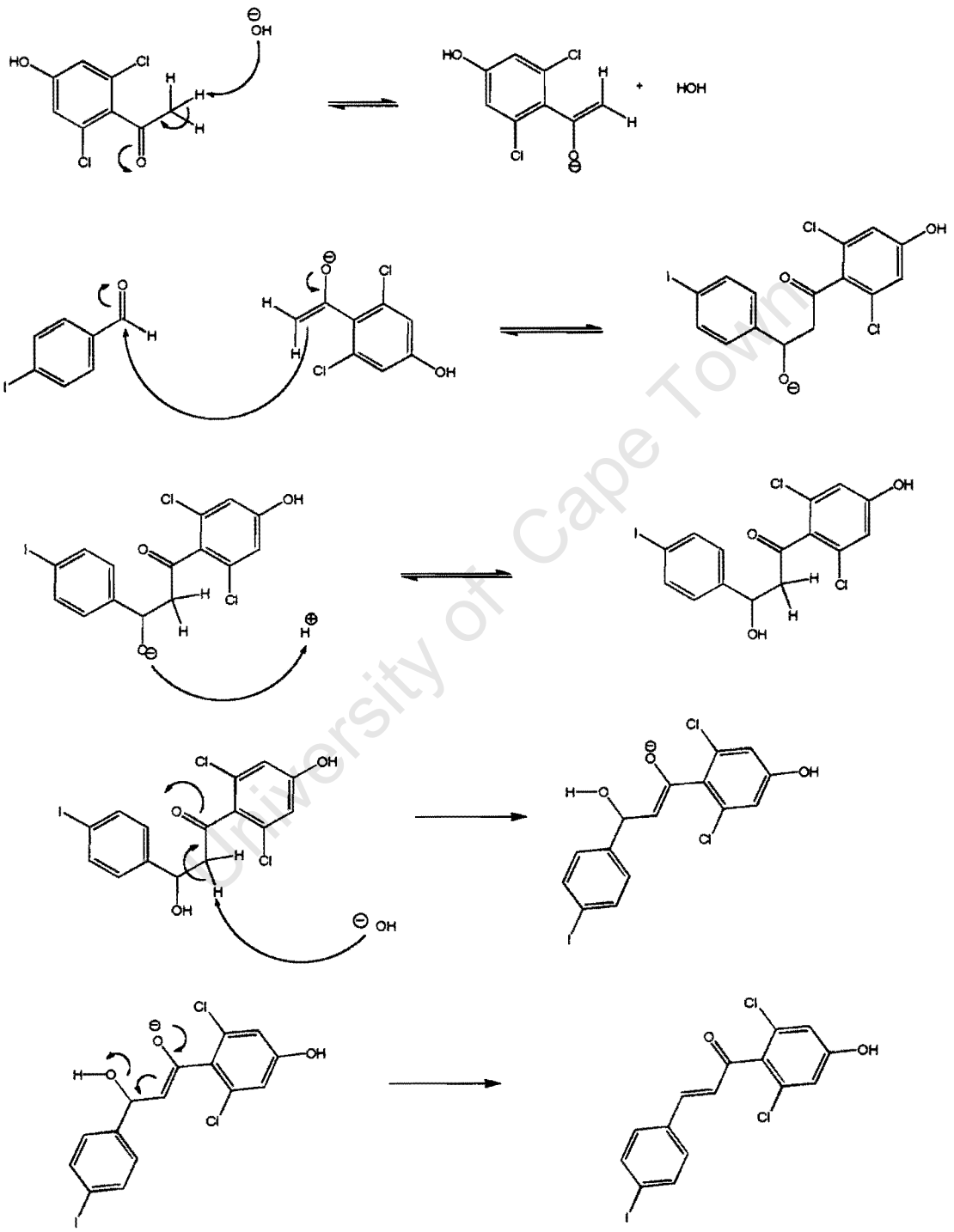

Figure 1.18 **Mechanism of base (OH^-) catalysed Claisen-Schmidt condensation** (adapted from http://www.cem.msu.edu/~reusch/VirtualText/aldket2.htm).

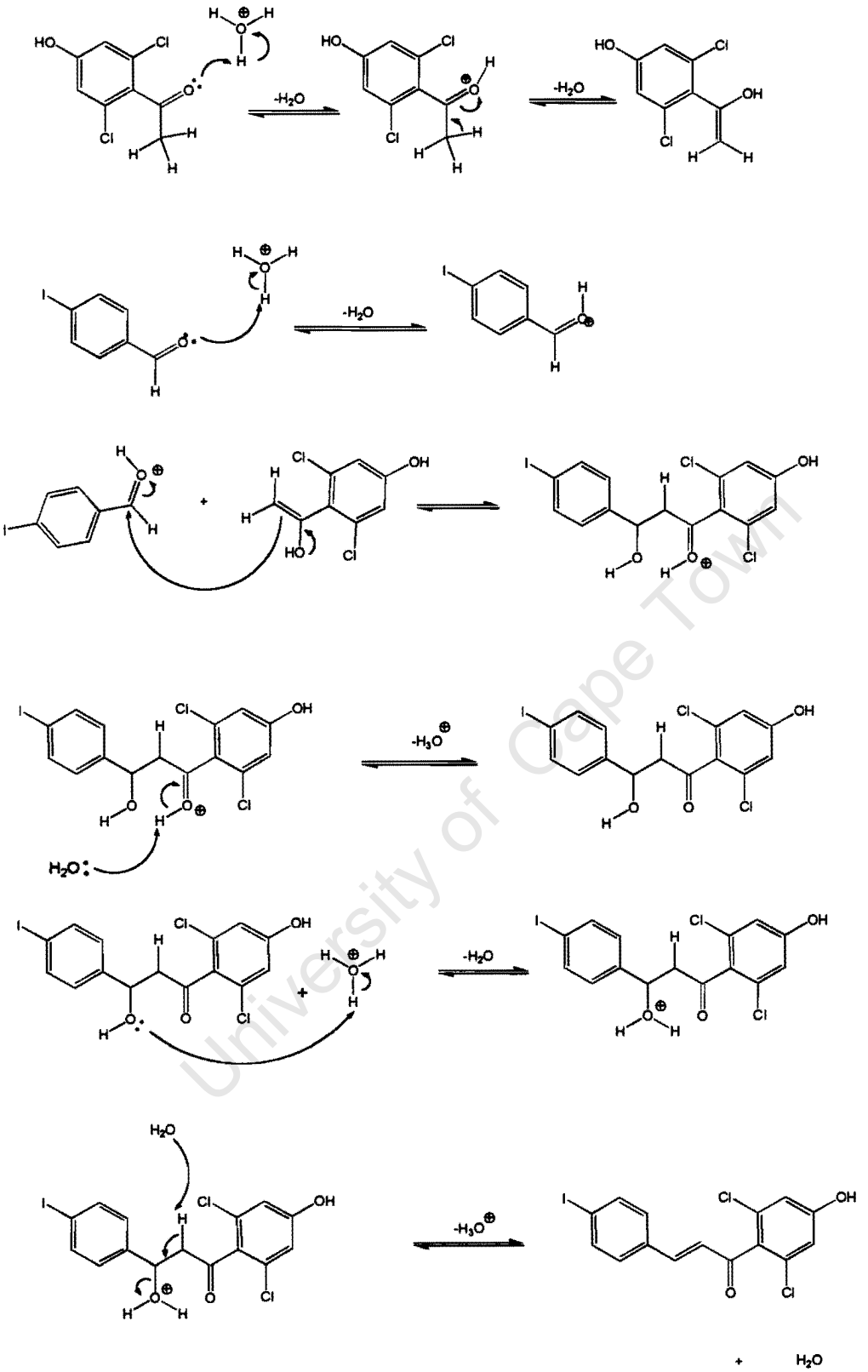

Scheme 1.19 **Mechanism of acid (H^+) catalysed Claisen-Schmidt condensation reaction** (adapted from http://www.cem.msu.edu/~reusch/VirtualText/aldket2.htm).

also be used to catalyse these reactions. In both cases the ketone reacts with either OH^- or H_3O^+ to form a reactive ionic species that fuses with an aldehyde. The resultant product of the fusion undergoes elimination ($E1_{CB}$) to give the final Claisen-Schmidt product. The catalyst (OH^-, or H_3O^+) is also regenerated. The types of substrates involved usually determine the specific reaction conditions for any given Claisen-Schmidt reaction. While a weak base (for base catalysed reactions) such as $Ba(OH)_2$ may be adequate for the reaction to proceed, a strong one maybe necessary in another. In general, when a base is too strong, a Cannizzaro reaction becomes competitive. A Cannizzaro reaction is one in which a benzaldehyde is reduced to a primary alcohol.

1.6.2 Target compounds (chalcones) for this project

The chalcones (or general class of) targeted for synthesis in order to achieve the second aim of the project (see section section 1.7) are shown in Figure 1.20. Type A and B were synthesized directly from commercially available starting materials (appropriately substituted acetophenones and benzaldehydes). As such only the Claisen-Schmidt reaction was needed to synthesize these target chalcones. Figure 1.21 shows a retrosynthetic scheme that was followed to obtain these compounds. Type C required an acetophenone that could not be obtained from commercial sources. Figure 1.22 shows a retrosynthetic scheme followed in order to synthesize this particular chalcone. As can be seen, this chalcone required an acetophenone that is not commercially available. It had to be synthesized in a number of

steps (1st, Reimer-Tiemann, 2nd, Grignard, and 3rd, oxidation reactions, see section 1.6.2.1 for details) from 3,5-dichlorophenol.

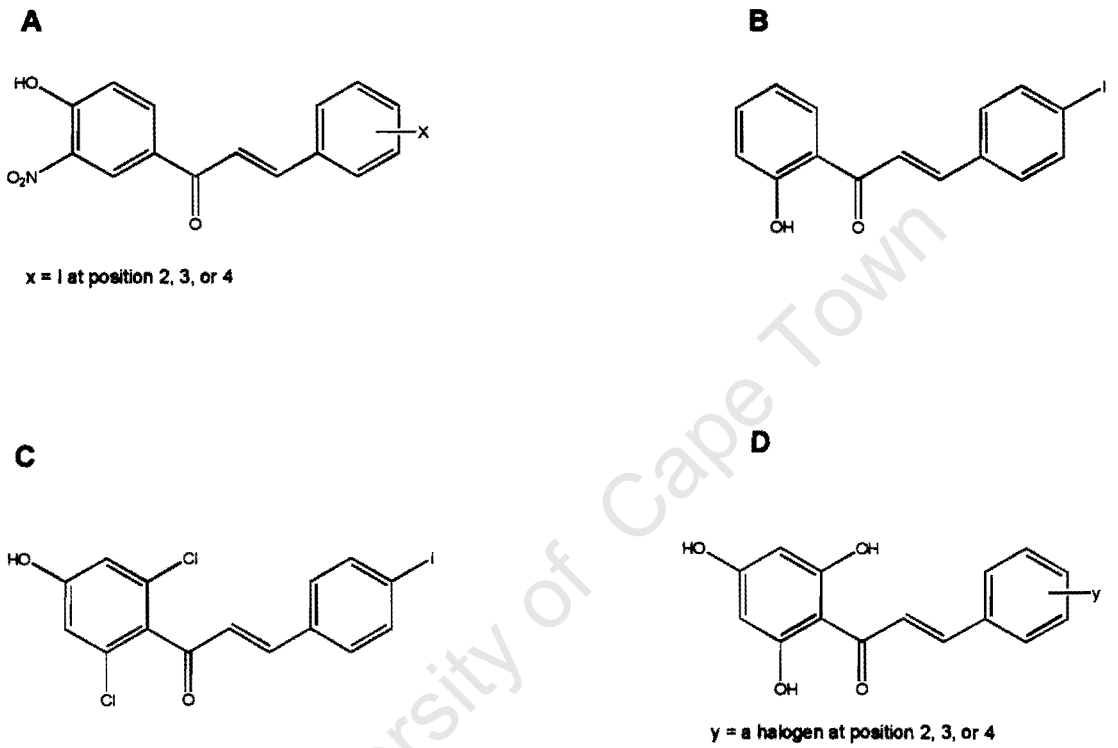

Figure 1.20 **Chalcones (or class of chalcones) targeted for synthesis.**

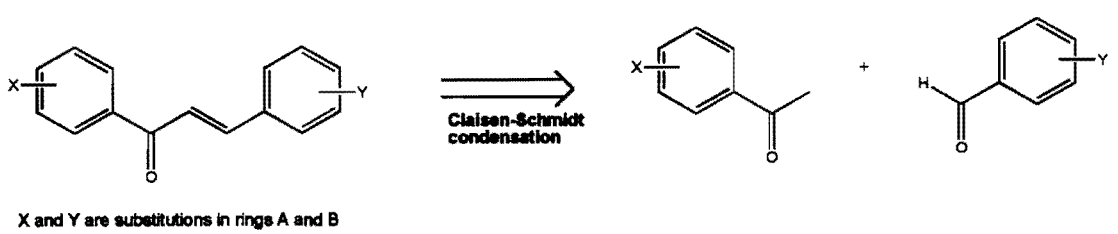

Figure 1.21 **Retrosynthetic scheme for target compounds of type A and B.**

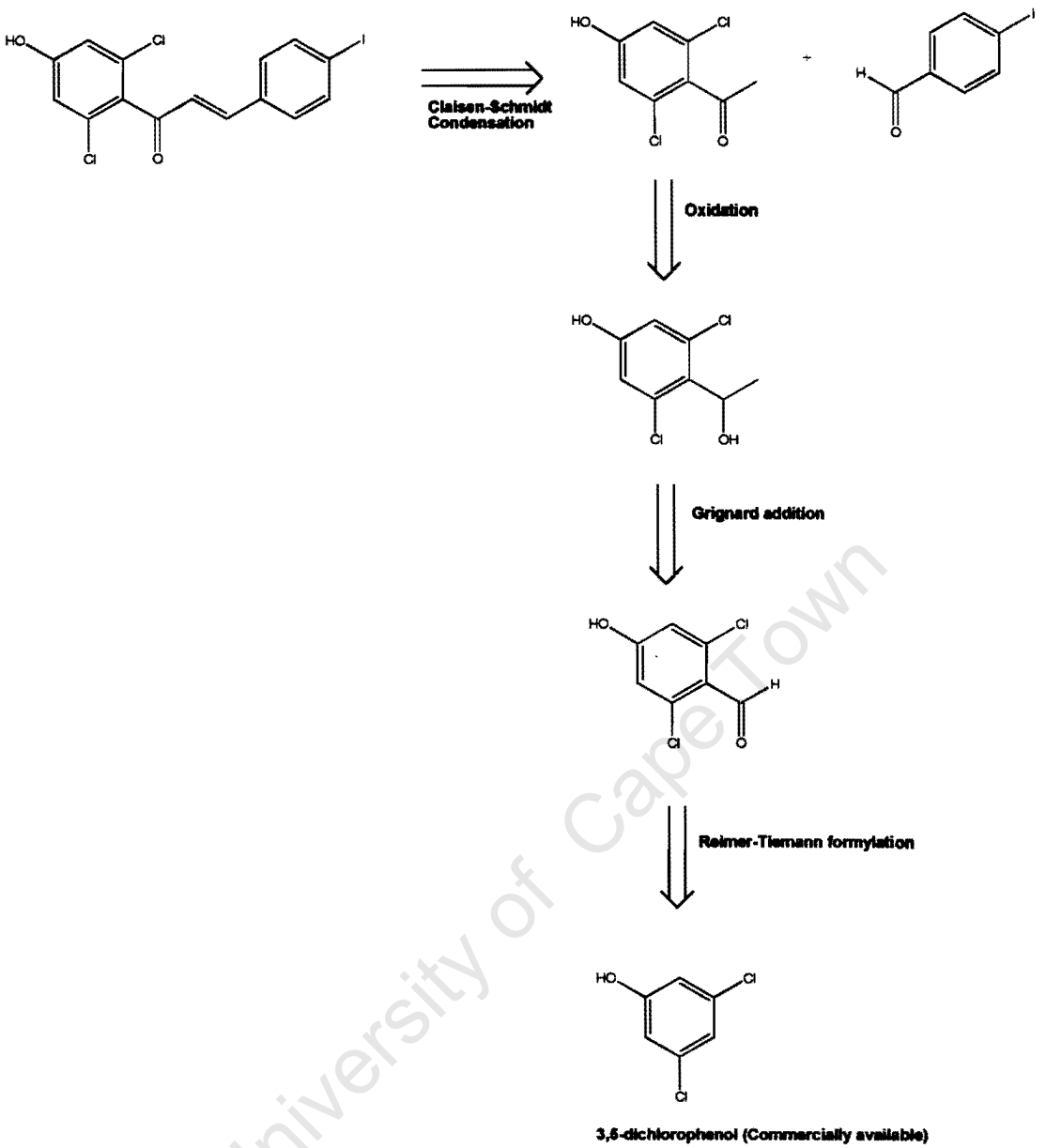

Figure 1.22 **Retrosynthetic scheme for target compound type C.**

1.6.2.1 Riemer -Tiemann reaction

This reaction is used to add a carbon atom to a phenol moiety. The C-atom (oxidatively added) is obtained from chloroform under basic conditions. The

specific protocol that utilises the Reimer-Tiemann reaction employed in this project is that developed by Knuutinen and Kolemainen (1983). Figure 1.23 shows a reaction in which a C-atom is oxidatively added to 3,5-dichlorophenol.

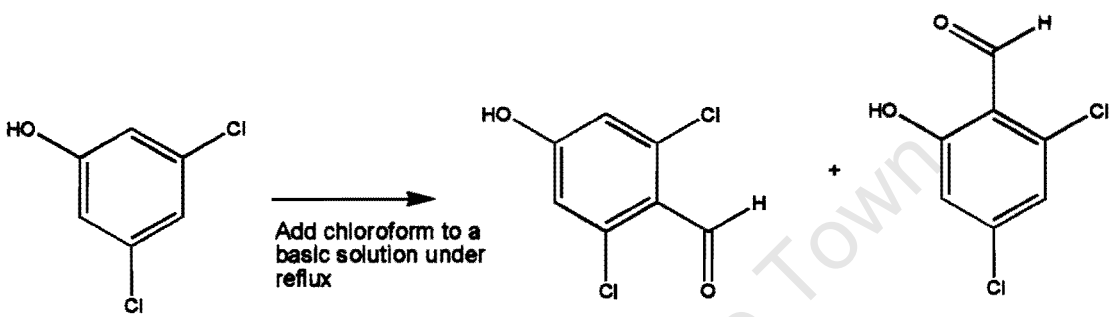

Figure 1.23 **Reimer-Tiemann oxidative addition of a C-atom to 3,5-dichlorophenol** (Knuutinen and Kolehmainen, 1983).

The major product in this reaction is one in which the C-atom is oxidatively added to the *para* position relative to the hydroxyl group. Figure 1.24 shows a proposed mechanism by which the C-atom is oxidatively added to 3,5-dichlorophenol. An electron deficient carbene is generated from chloroform in the alkaline (OH^-) solvent. The OH^- ion also abstracts a proton from the hydroxyl group of 3,5-dichlorophenol to generate a phenoxide species. This ionic species then reacts with the electron-deficient carbene to generate an intermediate that rearranges (with the participation of water) to form an aldehyde.

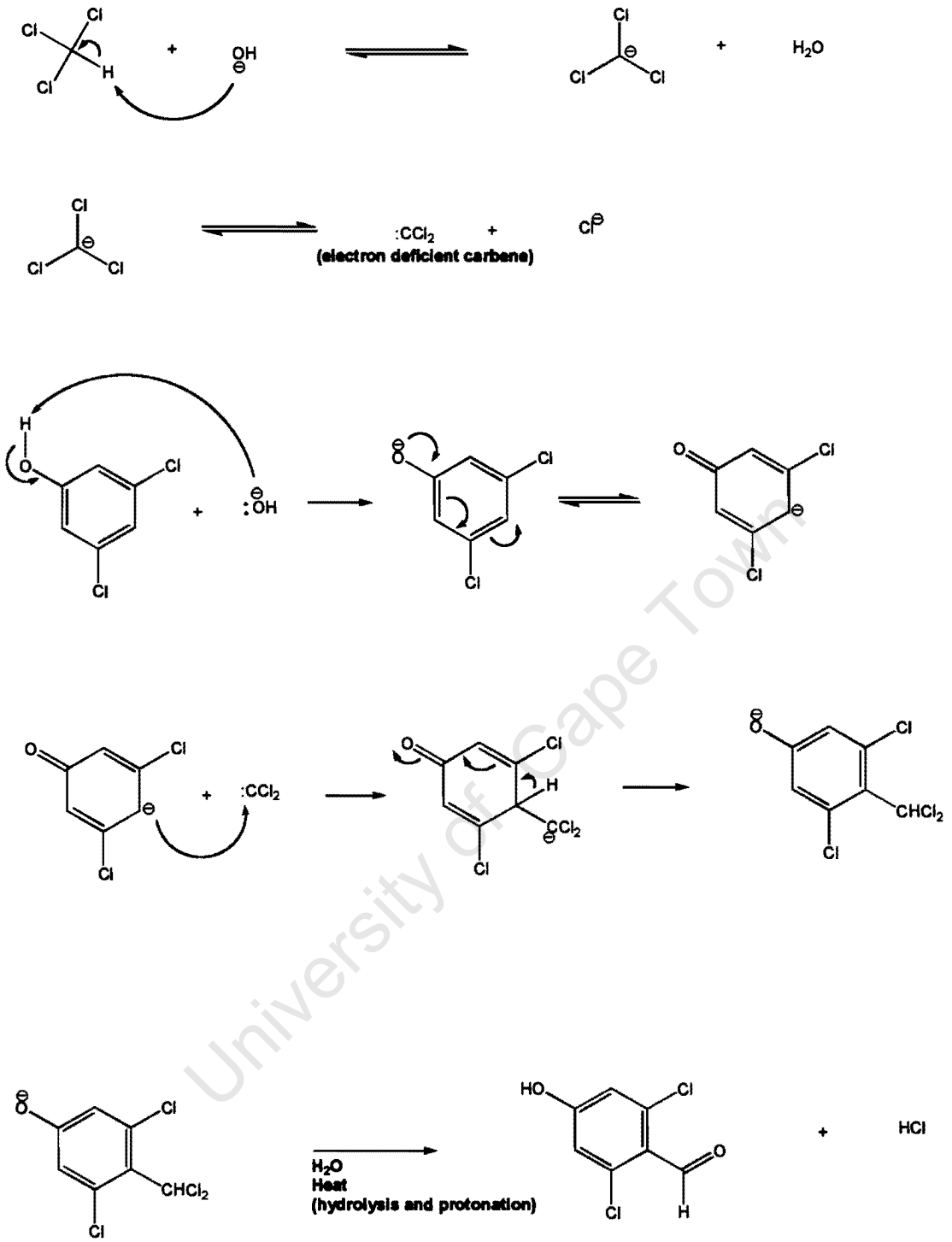

Figure 1.24 **Reaction mechanism for the Reimer-Tiemann reaction** (adapted from http://clem.mscd.edu/~wiederm/oc2ppt/aminesphenols.ppt).

A major diadvantage of this reaction is that yields are poor. Typical yields are in the range of 5 - 15 % (Knuutinen and Kolehmainen, 1983). This becomes a significant drawback when large quantities of product are required such as those needed in multi-step reactions where this is a step employed in the initial stage. An alternative method for oxidative addition of carbon units is one developed by von Hirscheydt and Voss (2004). This is claimed to be a better product yielding reaction than the Reimer-Tiemann reaction. Figure 1.25 highlights the main features of the improved method for addition of C-atoms to dichlorinated phenyl (or phenolic) compounds. Unfortunately, this method was only published towards the end of 2004 when we were winding up the chemical synthesis segment of the project.

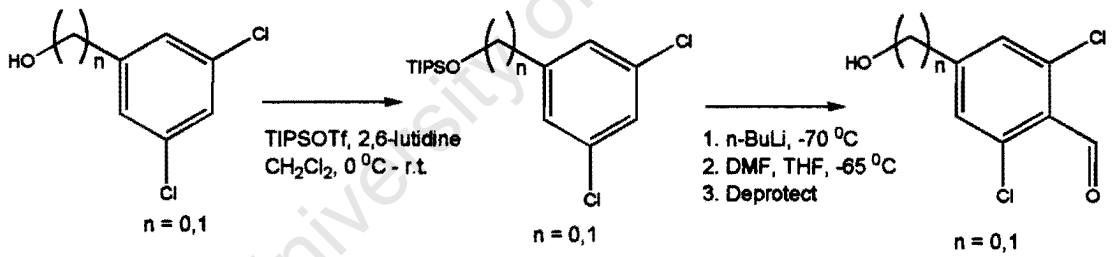

Figure 1.25 **Oxidative addition of a C-atom to phenyl group** (taken directly from von Hirscheydt and Voss, 2004).

1.6.2.2 Grignard reaction

Grignard reactions are employed in instances were a nucleophilic C-unit (alkyl or aryl) is to be added to a carbonyl C-atom of an aldehyde (or ketone). Victor

Grignard developed this reaction in 1898. In general, an aldehyde is dissolved in cold THF at (- 20 ^{0}C or below) in the complete absence of water and oxygen. A Grignard reagent (an organomagnesium halide such as methylmagnesium bromide) is then slowly added to the reaction mixture. The reaction is quenched with the addition of either acid or saturated ammonium chloride. The acid (or ammonium chloride) hydrolyses the O-Mg bond in the R-O-Mg-X intermediate (where R is an alkyl or aryl group and X is a halide). Figure 1.26 below shows the mechanistic details of the reaction between an aldehyde and a Grignard reagent (methylmagnesium bromide). If the aldehyde (or ketone) has a -OH or -SH group, excess Grignard reagent must be added to the reaction mix because Grignard reagents are known to react with such chemical entities.

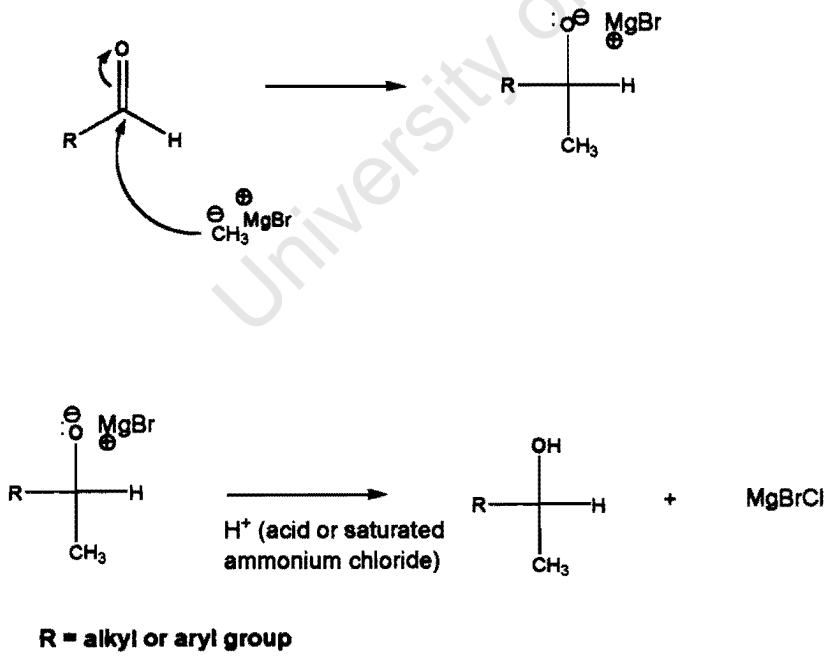

Figure 1.26 **Mechanism of a Grignard reaction** (adapted from http://www.organic-chemistry.org/namedreactions/grignard-reaction.shtm)

Grignard reagents may be synthesized on demand if they are not available from commercial sources. Figure 1.27 below shows an outline for the synthesis of Grignard reagents. It should be noted here that organolithiums (R-Li, where R is an alkyl or aryl group) could be used if a particular Grignard reagent is not available. Organolithiums are carbon nucleophiles similar to Grignard reagents.

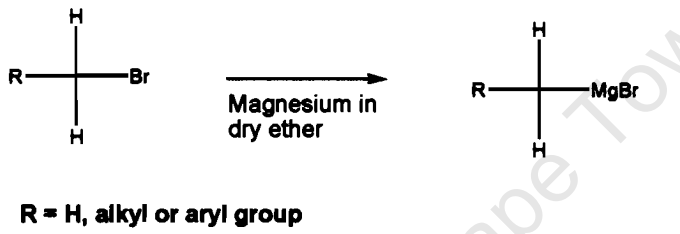

Figure 1.27 **Preparation of a Grignard reagent such as methylmagnesium bromide**.

1.6.2.3 Oxidation of secondary alcohols

Oxidation of a primary alcohol yields an aldehyde while a secondary alcohol leads to formation of a ketone. Tertiary alcohols do not undergo any form of oxidation. Aldehydes are prone to further oxidation (yielding carboxylic acids). Oxidation of alcohols can be achieved by use of a wide range of reagents. These reagents may be placed into two broad categories, aqueous and anhydrous oxidants. Aqueous oxidants include chromic acid, permanganate, chromate and dichromate salts while pyridinium dichromate (PDC) and pyridinium chlorochromate (PCC) are examples of anhydrous oxidants. PDC

and PCC (see structures in Figure 1.28 below) are also referred to as Collins reagents.

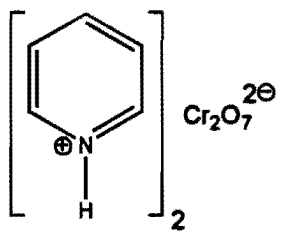

Pyridinium dichromate (PDC)

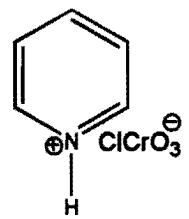

pyridinium chlorochromate (PCC)

Figure. 1.28 **Structures of PDC and PCC.**

Choice of oxidant depends on the type of alcohol to be oxidized. Cost and availability are other factors to be considered when choosing an oxidant for a particular alcohol. The alcohol formed from the Grignard reaction in our case (see Results) was not water-soluble hence choice of oxidant was between PDC and PCC. As the alcohol generated in the Grignard reaction was a secondary alcohol, the expected and desired oxidation product was a ketone. PDC was already available in our laboratory and has been used with a lot of success, hence it was the choice as the oxidant for our alcohol.

Sodium hypochlorite (NaOCl) in acetic acid is another oxidizing agent that may be used in the conversion of alcohols to ketones (Stevens *et al.*, 1980). This reagent has several key advantages including speed, high yields and

environmentally more friendly waste products than those associated with manganese and chromium reagents (Stevens *et al.*, 1980).

1.6.2.5 Protection of hydroxyl groups

Target compounds D (Figure 1.10) followed a retrosynthetic scheme shown in Figure 1.29. For the synthesis of these chalcones containing three hydroxyl (-

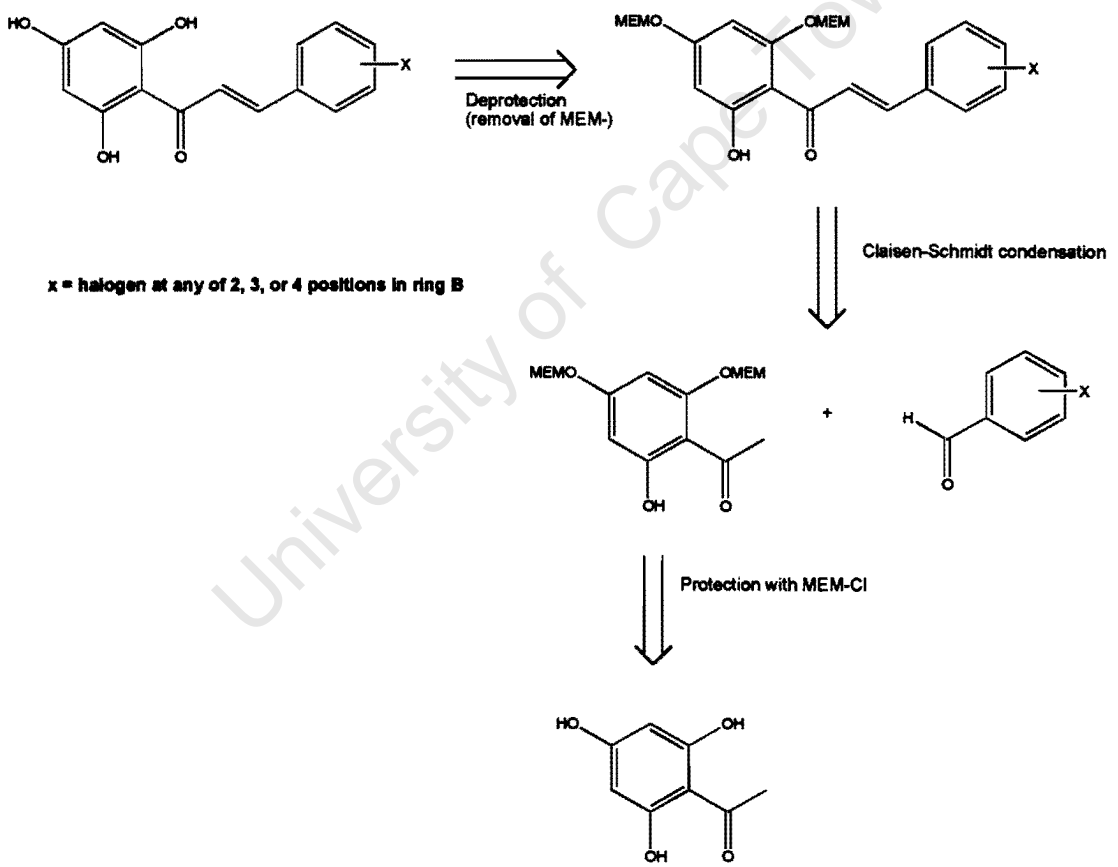

Figure 1.29 **Retrosynthetic scheme for the synthesis of chalcones (type D) containing trihydroxyl groups in ring A.**

OH) groups in ring A at positions 2',4',6'- of the phenyl ring, it is necessary to mask at least two of the three -OH groups. This is done in order to increase the yield of the final chalcones obtained (Bois *et al.*, 1999). Protection renders the hydroxyl (or any reactive) group in a molecule temporarily inactive (Greene and Wuts, 1999). There are several protecting groups that can be used in masking hydroxyl groups (see Greene and Wuts, 1999 for a review). Perhaps one of the most common chemical entities is a methyl group. Hydroxyl groups are converted to methyl ethers. Methyl ethers are quite easily formed by reacting the hydroxyl-containing compound with methyl iodide in the presence of sodium hydride in DCM or THF. They may be removed by use of iodomethylsilane in quinoline. Methoxymethyl (MOM), methylthiomethyl (MTM), benzyloxymethyl (BOM), tetrahydropyranyl (THP), ethoxyethyl (EE), benzyl (R-Obn), *t*-butyldimethylsilyl (TBDMS), and ethoxymethyl (MEME) ethers are a few examples of an almost endless list of -OH protecting groups that can be employed. This project employed the MEM (methoxyethoxylmethoxyl) group to successfully diprotect 2',4',6'-trihydroxyacetophenone. MEM ethers are generally stable in base and mild acid conditions. Stability in base is particularly important as the formation of chalcones was done under basic conditions. MEM protection may be carried out in a solution of the hydroxylated substrate in the presence of methoxyethoxymethyl chloride, sodium hydride and THF. Figure 1.30 shows a proposed mechanism for the formation of a MEM ether *via* the reaction of MEM-Cl with a hydroxylated compound. Perhaps a key feature of this reaction mechanism is the formation of a reactive oxacarbenium (also known as oxocarbenium) ion. The by-product of this step is HCl that is mopped up by a

base (usually K_2CO_3). The oxacarbenium ion is a good electrophile that is readily attacked by the alcohol to form the desired protected alcohol. Removal of the MEM group can be achieved by the use of Lewis acids such as $ZnBr_2$, and $TiCl_4$. It can also be achieved by refluxing in diethyl ether containing hydrochloric acid (Bois *et al.*, 1998).

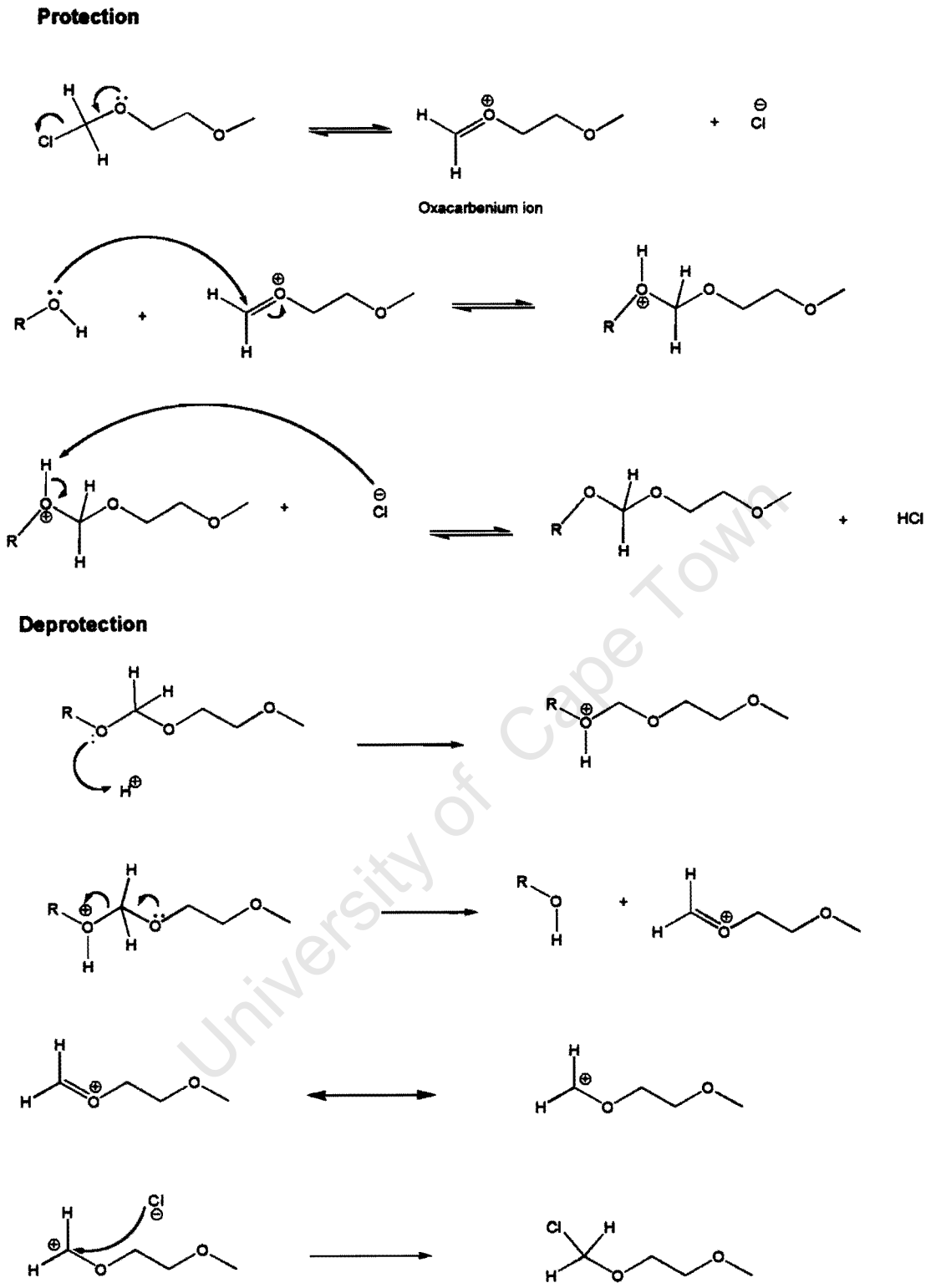

Figure 1.30 **Probable mechanism for the protection and de-protection of hydroxylated compound with MEM-chloride.**

1.7 Rationale and aims of the present study

This laboratory (PhD thesis, Phehane, 2002) had found that 4"-I-chalcone is a specific accelerator of catalytic turnover of malaria HGXPRT (see chemical structures in Figure 1.31). This compound had no effect on human or *T. gondii* enzymes. In contrast to the latter two recombinant proteins, it was also found that the isolated malarial enzyme was partially active, if stabilized by PRPP during cell lysis, and could be further activated by substrates following isolation. During enzyme assay at low protein concentrations, the protein inactivated within a few minutes.

The proteins were expressed in *E. coli* using a pET system that employed a histidine tail (his-tag) on the N-terminal end. Phehane (2002) suggested that the instability of the malaria enzyme might be attributed, in part, to the presence of the his-tag.

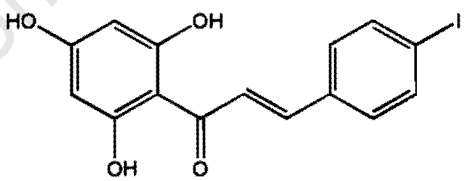

4"-I-Chalcone

Figure 1.31 **Chemical structure of 4"-I-chalcone (Phehane, 2002).**

AIM 1. The first objective of this project was to clone, express and develop a purification procedure for the malaria HGXPRT without a his-tag.

In the previous work, the accelerating chalcone was found by screening a library of 38 flavonoids and chalcones (see de Wet *et al.*, 2001 for list). None of the others showed any inhibitory or accelerating effects, including 4"-F-chalcone and 4"-OH-chalcone, suggesting rather specific requirements for binding and activation.

As far as we are aware, this is the first time that an accelerator of catalytic turnover has been found for any of the PRT family. It could provide insights into the limiting reaction during catalysis of the malarial enzyme and may reveal an effector site that may be exploited for drug targeting.

Aim 2. The second objective was to synthesise a number of related chalcones for structure/activity relationship studies.

Chapter 2 MATERIALS AND METHODS

2.1 Materials

E. coli XL 1 blue cells (purchased from Stratagene) were a gift from Prof. Eric H. Harley in the Department of Chemical Pathology, University of Cape Town, Faculty of Medicine, while competent *E. coli* BL21(DE3)pLysS cells also from Stratagene, were kindly provided by Associate Prof. Daan Steenkamp also of the same Department. Bacto-agar and agarose were purchased from B & M Scientific, while Tryptone powder and Yeast extract were from Merck. Ampicillin, and DTT were purchased from Boerhinger Mannheim GmbH. Lysozyme, PIPES, PPi, water soluble reactive dyes (Reactive Red 120 and Reactive Blue 2), agarose bound Reactive Red 120, IPTG, RNase, PRPP, PMSF, dialysis tubing, and silica were obtained from Sigma. Recombinant pET-15b containing *P. falciparum* HGXPRT cDNA was obtained as a gift from Drs. D. Borhani and G. Vasanthakumar of Southern Research Institute (SRI) in Birmingham, Alabama (USA), while pET-17b was also a gift from Prof. David Pugh of the University of Western Cape, South Africa. SDS was purchased from Bio-Rad. Restriction enzyme kits [*Nde* I and *Bam* HI along with their buffers and acetylated BSA], lambda DNA and a 1kb DNA ladder were purchased from Promega. The QIAEX II Agarose Gel extraction kit (from Qiagen), and T4 DNA ligation kit (from USB Corporation) were kindly provided by Dr. Jeanne Rousseau of our Department while Fast-Link™ DNA ligation Kit was purchased from Epicentre Technologies. Protein SDS-PAGE standards were bought from Pharmacia. DNaseI was bought from Roche Molecular

Biochemicals and β-mercaptoethanol from Riedel-De Haenag (Seelze-Hannover). DE52 was purchased from Whatman, while Centricon and Sep-Pak cartridges were obtained from Millipore Corporation. All the other reagents were either analytical or biochemical grade.

2.2 Methods in cloning, expression, purification and activation

The gene for malaria HGXPRT was obtained as an insert in pET-15b (with his-tag) and needed to be placed in pET-17b (without his-tag). The sequence of the gene in pET-15b was thoroughly checked and shown to be correct (Phehane, 2002). To achieve the insert transfer, both plasmids had to be cloned in competent *E. coli* cells, the gene excised with restriction enzymes *Nde* I and *Bam* HI, and ligated into similar sites in the other plasmid.

2.2.1 Preparation of competent *E. coli* XL1 blue cells using $CaCl_2$

E. coli XL1 blue cells are a mutant strain that is recombination (*recA*) and endonuclease (*endA1*) deficient. Thus cloned DNA is not cleaved. Furthermore, the quality of the plasmid is improved because being endonuclease deficient ensures insert stability (Stratagene Instruction Manual, 2002).

Competent *E. coli* XL1 blue cells were prepared according to the $CaCl_2$ method described by Seidman, *et al.* (1997). XL1 blue cells (10 µL) were spread on Luria agar plates (10 g/L tryptone powder, 5 g/L Yeast extract, 5

g/L NaCl, 1 mM NaOH, 15 g/L agar) without antibiotic and grown overnight at 37 ^{0}C. A single colony was then picked and inoculated in sterile 50 mL LB (10 g/L Tryptone powder, 5 g/L Yeast extract, 5 g/L NaCl; pH 7.2 - 7.4) and grown overnight at 37 ^{0}C with shaking set at 250 rpm. This culture (4 mL) was then inoculated into LB (400 mL) in a sterile 2-litre flask with shaking set at 250 rpm. When the OD_{590nm} of the cell culture had reached 0.4 units, the cells were aliquoted into 50 mL pre-chilled sterile polypropylene tubes and incubated on ice for 10 min after which the cells were centrifuged at 3 000 rpm (allowing the centrifuge to decelerate without applying brakes). The pellet obtained after discarding the supernatant was then suspended in 10 mL ice-cold 60 mM $CaCl_2$ solution (containing 15 % (v/v) glycerol and 10 mM PIPES, pH 7 and sterilized by autoclaving). The cells were then centrifuged for 5 min at 1 000 x g at 4 ^{0}C. The supernatant was discarded and the cells were re-suspended in 2 mL ice-cold 60 mM $CaCl_2$ solution, stored in 250 µL aliquots, frozen immediately in liquid nitrogen, and stored at - 80 ^{0}C.

2.2.2 Transformation of *E. coli* XL1 blue cells with pET-17b and pET-15b (containing malaria HGXPRT cDNA)

Recombinant pET-15b (3 µL), pET-17b plasmid (3 µL) [or pUC 18 used for checking transformation efficiency] was added to competent XL1 blue cells (50 µL) in separate eppendorf tubes. The resulting mixtures were then placed on ice for 10 min followed by heat-shock at 42 ^{0}C for 2 min after which the tubes were immediately placed back on ice for 2 min to minimize damage to *E. coli* cells. Sterile 2X TY medium [16 g/L Tryptone powder, 10 g/L Yeast

Extract, 5 g/L NaCl] (950 µL) without antibiotic was added to each of the mixtures and incubated at 37 ^{0}C for 1 h. The cells were then centrifuged at low speed for 1 min and the resulting pellet suspended in residue medium. The suspended cells (10 µL) were then plated on sterile LB plates supplemented with ampicillin (100 µg/mL) and incubated at 37 ^{0}C for 16 h.

2.2.3 Generation of plasmid preparations (recombinant pET-15b and pET-17b with no insert)

Two methods were tried:

The *Rapid alkaline extraction of plasmid DNA* method (with modifications) was used to generate plasmid preparations (Birnboim and Doly, 1979). In this method, 100 mL sterile LB supplemented with ampicillin (100 µg/mL) was inoculated with a single colony of *E. coli* XL1 blue cells containing plasmid DNA (either pET-17b or recombinant pET-15b) and grown overnight at 37 ^{0}C until OD_{600nm} of between 0.6 and 1.0 units was attained. The cells (4 to 6 mL) were then spun at maximum speed for 1 min on a bench centrifuge at room temperature. The cell pellet was re-suspended in a sterile solution of 10 % glucose, 25 mM Tris/HCl, pH 8, 10 mM EDTA, 10 µg/mL DNAse-free RNAse A (obtained by boiling for 15 min) and a small amount of lysozyme. The re-suspended cells were then allowed to stand at room temperature for 5 min. A freshly prepared lysis solution (0.2 N NaOH and 1% (w/v) SDS) was then added to the re-suspended cells and the resulting solution was mixed thoroughly by inverting the tubes several times until the re-suspension was

clear after which the tubes were incubated at room temperature for 5 min. 5 M potassium acetate, pH 4.8 was then added to the cell lysis mixture to precipitate the dodecyl detergent. This mixture was vortexed for 2 s to ensure complete mixing. The tubes were placed on ice for 30 min after which they were spun for 5 min at maximum speed on a bench centrifuge. The supernatant was carefully transferred into fresh tubes and spun again for 5 min to ensure complete removal of all solids. Plasmid DNA was then precipitated with 100 % isopropanol and washed with ice-cold 80 % (v/v) ethanol. After spinning, the plasmid DNA pellet was dissolved in 20 μL sterile deionised water or 10 mM Tris/HCl, pH 8 and 1 mM EDTA (TE buffer). The DNA was analysed on agarose gel electrophoresis in the presence of ethidium bromide and visualised under a UV light.

Plasmid preparations were also made using an alternative alkaline method developed by Brown (1997). In this method, plasmid DNA extraction is done using silica powder. In the first step, the cell pellet obtained after centrifugation of a cell culture is re-suspended in 50 mM Tris/HCl, pH 8 and 10 mM EDTA containing 50 μg/mL RNase A. The rest of the steps are the same as those in the *Rapid alkaline plasmid extraction* method described above, except after the potassium acetate neutralisation step, the supernatant is mixed with a silica suspension, incubated on ice for 5 min and then centrifuged at maximum speed in a bench centrifuge for 1 min. The supernatant is discarded and the pellet washed with a 50 mM NaCl, 10 mM Tris/HCl, pH 7.5, and 2.5 mM EDTA solution in 50 % (v/v) ethanol. The wash solution is then removed by centrifugation at maximum speed for 1 min

followed by aspiration of supernatant. The pellet is then re-suspended in TE buffer and incubated at 55 ^{0}C for 2 min.

2.2.4 Restriction digestion of pET-15b and pET-17b and ligation

2-4 μL of pET-15b (with insert) or pET-17b (without insert) plasmid preparations were digested with 10 U (enzyme units) of each of *Bam* HI and *Nde* I in presence of the manufacturer's (Promega) 1X Multicore buffer with 2 μg BSA at 37 ^{0}C for 16 h. Control digestions were performed with lambda DNA.

The pET-15b and pET-17b digests were electrophoresed on 0.8 % agarose gel. The band for the insert and opened pET-17b plasmid were excised and the DNA purified by a Qiagen QIAEX II agarose gel extraction kit according to the manufacturer's instructions.

The ligation of the malaria HGXPRT cDNA into pET-17b was carried out using the USB Corporation or Fast-Link™ DNA ligation kits according to the manufacturer's instructions.

The ligation product (recombinant pET-17b) was amplified by transforming into *E. coli* XL1 blue cells using the same protocol described in section 2.2.2.

A plasmid prep was carried out as described is section 2.2.3, and the presence of the insert verified by restriction digestion and agarose gel electrophoresis.

2.2.5 Transformation of competent *E. coli* BL21(DE3)pLysS cells with pET-17b

The empty pET-17b plasmid and that containing malaria HGXPRT cDNA were transformed into the expression strain *E. coli* BL21(DE3)pLysS following a procedure described earlier in section 2.2.2. Glycerol stocks of the transformed BL21(DE3)pLysS cells were prepared according to instructions given in the pET system manual (Novagen, 2002).

2.2.6 Induction of protein expression by IPTG

Two LB plates supplemented with ampicillin (100 μg/mL) and chloramphenicol (34 μg/mL) were streaked with a glycerol stock of BL21(DE3)LysS that had been transformed with recombinant pET-17b and pET-17b without insert. These plates were then incubated at 37 ^{0}C for 16 h. A colony from each plate was inoculated into separate LB media supplemented with ampicillin (100 μg/mL), chloramphenicol (34 μg/ml), and 10 mM sodium phosphate. These were then incubated at 37 ^{0}C until OD_{600nm} 0.4 - 0.6 was attained. At this point, IPTG (0.4 mM) was added to the cell cultures to induce recombinant protein expression.

The expression was monitored by taking 500 μL aliquots at 0 min, 30 min, 1 h, 3 h, and 5 h. The samples were spun at 9 000 rpm for 5 min at room temperature to pellet the cells. 50 μL water and 50 μL 2x solubilization buffer (125 mM Tris/HCl, pH 6.8, 10 % glycerol, 0.1 mg bromophenol blue, 4 % SDS, 300 mM β-mercaptoethanol) was then added to each pellet followed by vortexing after which, they were heated at 70 ^{0}C for 15 min. Each sample (10 μL) was then loaded onto 15 % SDS-PAGE and analysed according to the method of Laemmli (1970).

2.2.7 Cell lysis

The standard method adopted for lysis of *E. coli* cells was the following:
The cell pellet obtained as described in 2.2.6 was placed at - 80 ^{0}C overnight, then thawed, and suspended in 50 mM Tris-Cl, pH 8.0, 25 mM NaCl, 2 mM EDTA, 1 mM PMSF, and 1 mM DTT, in a volume that was 1/10 of the cell culture. The viscous cell paste was then treated with DNAse I (20 μg/mL) in presence of 10 mM $MgCl_2$ for 20 min at room temperature, followed by centrifugation at 21 000 x g for 20 min at 4 ^{0}C to yield a crude pellet and supernatant.

In preliminary experiments, the effects of added lysozyme, salt, $MgCl_2$, and extra freezing and thawing were assessed.

2.2.8 HGXPRT purification

For purification on a small scale, typically 40 mL sodium phosphate buffered LB media supplemented with ampicillin (100 μg/mL) and chloramphenicol (34 μg/mL) would be inoculated with BL21(DE3)pLysS containing recombinant pET-17b and incubated at 37 ^{0}C for about 16 h. When OD_{600nm} 0.4 - 0.6 was attained, IPTG (0.4 mM) was added, and the expression of the malaria enzyme was conducted at 37 ^{0}C for 3 h in a shaking incubator (200 rpm). The cells were then aliquoted into 50 mL fractions and centrifuged at 8 000 rpm for 10 min at 4 ^{0}C. The pellets obtained were either used immediately or frozen at - 80 ^{0}C and used later.

2.2.9 Ion exchange chromatography

The behaviour of the crude supernatant containing malaria HGXPRT on cation and anion exchange resins was investigated on a small analytical scale through the use of Sep-Pak cartridges. The cartridge was prepared by passing through 1 - 2 mL of lysis buffer followed by the supernatant (typically 4 mL). It was washed with 1 - 2 mL buffer, which was added to the flow-through, and the retained proteins eluted with 1 mL 1 M NaCl. In some experiments, the pH of the applied supernatant was adjusted.

Using the Sep-Paks, it was established that HGXPRT did not bind to an anion exchange resin under the conditions used, but provided significant purification

by removing many proteins that did bind, similar to the results obtained by Keough *et al.*, 1999.

Larger-scale anion exchange chromatography was performed on a 2 x 6 cm column with DE52 resin. The resin was washed with water, placed in the column, and 10 mL lysis buffer passed through. The supernatant (100 mL) was applied to the column and the flow-through (containing HGXPRT) collected by gravity. The column was washed with more lysis buffer, and bound proteins (not HGXPRT) eluted with 1 M NaCl.

2.2.10 Reactive Red 120 chromatography

Small-scale Reactive Red 120 chromatography was performed with a column of 0.5 x 1 cm resin. The resin was prepared by washing with water. The sample was passed through, followed by 0.5 - 1 mL 50 mM Tris-Cl, pH 8 buffer containing 1 mM of each of DTT and PMSF, and then 0.5 - 1 mL 50 mM Tris-Cl, pH 8.9, 200 mM NaCl, 1 mM DTT and 1 mM PMSF. HGXPRT was eluted with 1 mL aliquots of 50 mM Tris-Cl, pH 8.9, 50 mM PPi, 1 mM PMSF, and 1 mM DTT.

Larger-scale experiments (100 mL supernatant) were performed with a column of 2 x 15 cm resin, and the volumes of the washes and elutions were adjusted accordingly.

The fractions collected at various stages in the purification were analysed on 15 % SDS-PAGE according to the method of Laemmli (1970).

Once the properties of the anion exchange (not binding HGXPRT) and Reactive Red 120 (binding HGXPRT) columns had been elucidated, the two steps were combined, and the columns placed in tandem, with the anion exchange on top of the Reactive Red 120. All procedures were performed either on ice or carried out at 4 ^{0}C. The supernatant (100 mL) was run through both columns overnight by gravity, the columns washed with a small volume of lysis buffer, and separated. The Reactive Red 120 column was washed with 50 mL 10 mM sodium phosphate buffer, pH 7.0, 200 mM NaCl, and the column developed with 8 mL 50 mM sodium phosphate buffer, pH 7.0, 50 mM PPi, 1 mM DTT, and 1 mM PMSF (eluate usually discarded). HGXPRT was eluted with a further 15 mL the phosphate/PPi buffer. The eluate was dialyzed against 10 mM sodium phosphate buffer, pH 7.0, overnight. The sample was then lyophilised to dryness, dissolved in 1 - 3 mL ice-cold water, re-dialyzed, filtered through a 0.45 μM filter and frozen at - 80 °C. The DE52 resin was discarded, but the Reactive Red 120 resin was washed with 1 M NaCl, and stored. It was washed with water before reusing.

2.2.11 Activity of malaria HGXPRT enzyme

Enzyme assays were carried out following the spectrophotometric method described by Keough *et al.*, (1987) on an Agilent 8453 Chemstation Spectrophotometer. The assay depends on the difference spectra of base and

nucleotide and was performed automatically by the instrument. A typical assay was conducted at room temperature (~20 ^{0}C) in 100 mM Tris-Cl, pH 8.5 (or pH 7.45 for xanthine), 110 mM $MgCl_2$ (or 12 mM $MgCl_2$ for xanthine), 60 μM purine base (314 μM for xanthine), and 1 mM PRPP. The reaction was initiated by the addition of an aliquot of enzyme, generally in the range 5-20 μg protein/ml, i.e. 1/100 dilution of purified preparation. The increase in absorbance was monitored at 245 nm, 257 nm, and 255 nm for the conversion of guanine, hypoxanthine and xanthine to their respectively nucleotides (at pH 8.5, the difference extinction coefficients [Δε] are 5817, 2283, and 4685 $M^{-1}cm^{-1}$ respectively while at pH 7.4 the Δε used in the conversion of xanthine to XMP was 3794 $M^{-1}cm^{-1}$). The initial rate was generally monitored over 15 s, and was calculated automatically by the instrument.

In some experiments the pH, $MgCl_2$, and purine concentrations were varied, and the effect of different chalcones was measured.

2.2.12 Protein assay

The dye-binding assay of Bio-Rad was performed as described in the manufacturer's booklet.

2.2.13 Activation of malaria HGXPRT

It will be seen in the Results section that malaria HGXPRT needed to be activated before any activity could be detectable (Keough *et al.*, 1999). The general procedure used to activate the enzyme was to add 1 mM PRPP and 60 μM hypoxanthine and incubate on ice or 4 ^{0}C for 16 h. Various other agents and conditions were tested as described in Results.

2.3 Chemical Synthesis

2.3.1 General information

NMR spectroscopy, Elemental Analysis, and FT-IR spectrophotometry are core service facilities in our Chemistry Department, and the Mass Spectrometry was a service provided by the Pharmacology Department.

All compounds synthesized were subjected to ^{1}H NMR (new chalcones were subjected to both ^{1}H and ^{13}C) analysis. The NMR analysis was carried out at ambient temperature using either Varian Mercury (300 MHz) or Varian Unity spectrometer (400 MHz). TMS was used as internal standard. Therefore, chemical shifts (δ in ppm) recorded are reported relative to TMS (δ = 0.0 ppm).

A Reicher-Jung thermovar (temperature range 0 - 350 ^{0}C) apparatus was used to determine melting points of the new chalcones synthesized. Since cover slips were used, the melting points obtained are uncorrected.

All the new chalcones synthesized were also subjected to Mass Spectrometric analysis on an API 2000 (from Applied Biosystems) VG micromass 16F machine at 70 eV with 4 kV as accelerating voltage.

Elemental analysis was also performed to establish the purity of the new compounds. It was carried out on a Fisons EA 1108 CHNS-O instrument

Infrared spectra of new compounds were recorded either in solution using chloroform on NaCl disks or as compressed solids (KBr pellets) on a Perkin Elmer spectrum FT-IR spectrophotometer.

The numbering system used in this thesis is as shown in Figure 2.4 below.

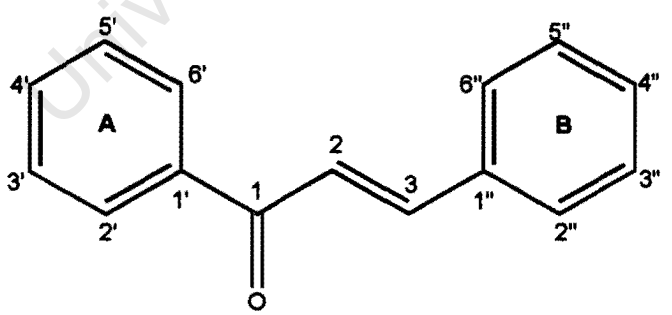

Figure 2.4 **Numbering of chalcones.**

Single ring systems are numbered according to the parent functional group.

2.3.2 Synthesis of chalcones with varying substitutions in rings A and B

2.3.2.0 Materials

Acetophenone, acetonitrile, methoxyethoxylmethyl chloride (MEM-chloride), 2-hydroxyacetophenone, 4-bromobenzaldehyde, 2-nitroacetophenone, 3,5-dichorophenol, 3,5-difluorophenol, 1-(2',4',6'-trihydroxyphenyl)ethanone monohydrate, 2-iodobenzaldehyde, 3-iodobenzaldehyde, 4-iodobenzaldehyde, 4-chlorobenzaldehyde, 1,4-dioxane, pyridinium dichromate, tetrahydrofuran, methylmagnesium bromide as well as deuterated NMR solvents (chloroform-d_3, acetonitrile-d_6, acetone-d_6 and dimethylsulfoxide-d_6) were purchased from Aldrich while 4-hydroxy-3-nitroacetophenone was purchased from Fluka. They were all used as received. Silica gel thin layer chromatography (TLC) plates and silica gel for preparative TLC were obtained from Merck while Celite filter gel was purchased from SAARCHEM (Pty). The rest of the chemicals were analytical reagent grade.

2.3.2.1 Synthesis of (2*E*)-1-(2',6'-dichloro-4'-hydroxyphenyl)-3-(4"-iodophenyl)prop-2-en-1-one

2.3.2.1.1 Method

Synthesis of (2*E*)-1-(2',6'-dichloro-4'-hydroxyphenyl)-3-(4"-iodophenyl)prop-2-en-1-one was done in four steps:

Step 1: Synthesis of 2,6-dichloro-4-hydroxybenzaldehyde

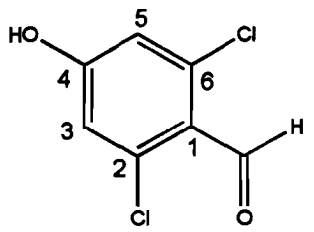

2,6-dichloro-4-hydroxybenzaldehyde

To a 10 mL water mixture of Na_2CO_3 (18.9 mmol), $Ca(OH)_2$ (23.6 mmol), and 3,5-dichlorophenol (5.5 mmol), chloroform (4.4 mmol) was added drop-wise. The temperature of the mixture was then raised to 70 ^{0}C at which point it was refluxed for 2 h. The reaction mixture was cooled to room temperature and the pH reduced to 2 with concentrated HCl. The product of the reaction in the mixture was then extracted into diethyl ether. The diethyl ether extract was then dried by use of anhydrous magnesium sulphate. Excess diethyl ether was removed under reduced pressure. The concentrated crude mixture was placed on silica gel column chromatography and the product isolated by use

of 20 % EtOAc in hexane. The solvent was removed by use of reduced pressure and the product dried on a vacuum pump.

A key ^{1}H NMR spectroscopic indicator for confirmation of the synthesis of 2,6-dichloro-4-hydroxybenzyaldehyde is the presence of a singlet resulting from the single proton in the region of 9 to 10 ppm due to -CHO. It is a new atom in the molecule (absent in the starting material) and so its detection is a positive indicator that the reaction has taken place.

The hydroxyl proton was not detected in the DMSO-d_6 NMR solvent used.

Further confirmation for the synthesis of 2,6-dichloro-4-hydroxybenzyaldehyde is in the ^{13}C NMR data, where detection of a carbonyl group at 195 ppm is a positive indicator.

Step 2: Synthesis of 3,5-dichloro4-(1-hydroxyethyl)phenol

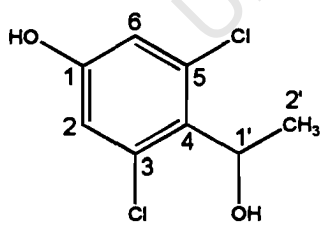

3,5-dichloro-4-(1'-hydroxyethyl)phenol

2,6-dichloro-4-hydroxybenzaldehyde [0.2 g, (1.05 mmol)] was dissolved in ice-cold 6 mL anhydrous THF under a stream of nitrogen and cooled to about 0 ^{0}C in an ice-water bath. 0.9 mL (2.70 mmol) of a solution of 3.0 M

methylmagnesium bromide in diethyl ether was then added to the aldehyde solution drop-wise also under a stream of nitrogen. The resulting mixture was then allowed to warm to ambient temperature where upon it was stirred for 2 h. 1 mL saturated ammonium chloride solution was then added to the reaction mixture to quench the reaction. The reaction mix was then extracted into 50 mL diethyl ether. The extract obtained was washed consecutively with an equal volume (50 mL) of saturated ammonium chloride and brine. It was then dried with anhydrous magnesium sulphate and concentrated under reduced pressure. The concentrated crude product was then purified on a silica gel column [10 % (v/v) MeOH in DCM]. The product was analysed on silica gel TLC (20 % MeOH in DCM) and the relevant fractions were pooled together and the solvent was removed under reduced pressure. The solid product obtained was dried on a vacuum pump.

The detection of protons in the methyl group (doublet that integrates for 3 protons around 2 ppm) and the proton attached to the C-atom linked to secondary alcohol (quartet that integrates for 1 proton at 6 ppm) are positive markers for confirmation of synthesis of 3,5-dichloro-4-(1'-hydroxy-ethyl)phenol. Both these sets of protons are absent in the starting material (2,6-dichloro-4-hydroxybenzyaldehyde).

Step 3: Synthesis of 1-(2',6'-dichloro-4'-hydroxyphenyl)ethanone

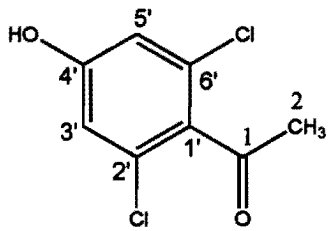

1-(2',6'-dichloro-4'-hydroxyphenyl)ethanone

Pyridinium dichromate 1.361 g (3.62 mmol) was suspended in 9 mL anhydrous dioxane. To this suspension, 0.24 g (1.166 mmol) 3,5-dichloro-4-(1'-hydroxy-ethyl)-phenol was added and the reaction mix stirred for 3 days. The reaction mix was filtered through Celite and the residue washed with DCM. The filtrate was washed with an equal volume of 10 % (v/v) HCl followed by another wash with distilled water. After separating the aqueous phase from the organic phase (DCM), excess DCM was removed under reduced pressure. The concentrated filtrate was then purified on silica gel preparative thin layer chromatography using 30 % (v/v) EtOAc in hexane as mobile solvent. The product was then extracted from silica gel into 100 % EtOAc. EtOAc was removed under reduced pressure and the product dried.

In ^{1}H NMR, the presence of a singlet at ~ 3 ppm that integrates for 3 protons ($-CH_3$) is the key signal for positive confirmation for the synthesis of 1-(2',6'-dichloro-4'-hydroxyphenyl)ethanone. This signal is absent in the starting material.

Step 4: Synthesis of (2*E*)-1-(2',6'-dichloro-4'-hydroxylphenyl)-3-(4"-iodophenyl)prop-2-ene-1-one

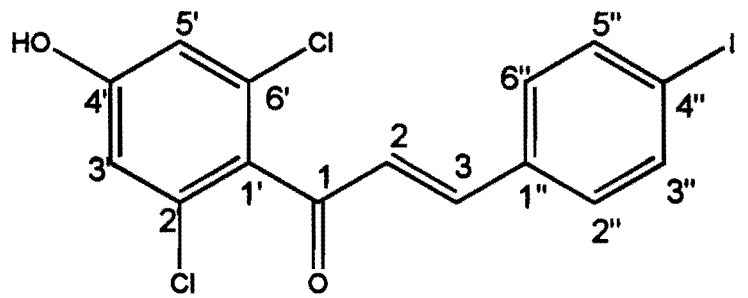

(2*E*)-1-(2',6'-dichloro-4'-hydroxyphenyl)-3-(4"-iodophenyl)prop-2-en-1-one
BM 01

(2*E*)-1-(2',6'-dichloro-4'-hydroxylphenyl)-3-(4"-iodophenyl)prop-2-ene-1-one (**BM 01**) chalcone was synthesized using a method developed by Mukherjee *et al* (2001). This method is a variation of the Claisen-Schmidt method (see Chapter 1). Approximately 20 mg (0.098 mmol) of 1-(2,6-dichloro-4-hydrophenyl)ethanone was dissolved in 1.45 mL absolute ethanol. To this solution, 16 mg (0.0836 mmol) $Ba(OH)_2.H_2O$ was added, followed by 24.7 mg (0.107 mmol) 4-iodobenzylaldehyde. The reaction mix was then refluxed for 4 h (monitored on silica gel TLC using 10 - 30 % (v/v) EtOAc in hexane with and without anisaldehyde staining). When the reaction was deemed to be complete, the reaction mixture was washed with 3 mL 5 % (v/v) HCl followed by extraction into 50 mL neat EtOAc. Excess EtOAc was then removed under reduced pressure. Finally, the product was purified on silica oxide prep TLC using 15 % (v/v) EtOAc in hexane as mobile solvent. It was then dried.

Confirmation for the synthesis of (2*E*)-1-(2',6'-dichlorophenyl)-3-(4'-iodophenyl)prop-2-en-1-one, and chalcones in general (this is applicable to all chalcones whose synthesis is reported sections 2.3.2.2, 2.3.2.3, and 2.3.2.4), is the detection of two doublets (in ^{1}H NMR) with large coupling constants. These doublets are for two new protons across a trans double bond (also new). They generally appear in the region 6 - 9 ppm and the coupling constant is the neighbourhood of 15 - 17 MHz.

As mentioned earlier all new chalcones were subjected to full characterization and **BM 01** being one such chalcone, complete analysis (NMR, IR, Mass Spectra, MP, and elemenatal analysis) was performed.

2.3.2.2 Synthesis of monohydroxylated chalcone (2*E*)-1-(2'-hydroxyphenyl)-3-(4"-iodophenyl)prop-2-en-1-one

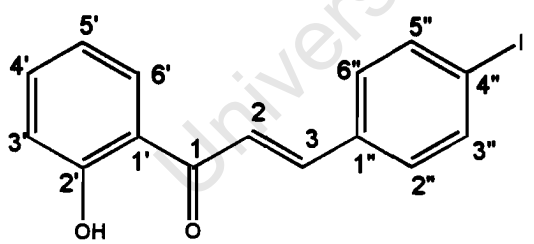

(2*E*)-1-(2'-hydroxyphenyl)-3-(4"-iodophenyl)prop-2-en-1-one
BM 02

2.3.2.2.1 Method

The method employed for the synthesis of (2*E*)-1-(2'-hydroxyphenyl)-3-(4"-iodophenyl)prop-2-en-1-one (**BM 02**) is same as that for synthesis of **BM 01**

except potassium hydroxide and methanol were employed instead of barium hydroxide and ethanol respectively.

For spectroscopic indicators for **BM 02**, please refer to section 2.3.2.1 (as described for **BM 01**).

2.3.2.3 Synthesis of chalcones containing both a nitro group as well as a hydroxyl group in ring A

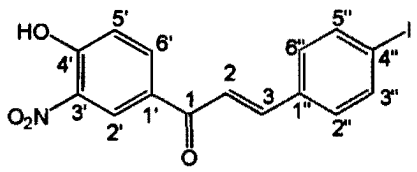

(2*E*)-1-(4'-hydroxy-3'-nitrophenyl)-3-(4"-iodophenyl)prop-2-en-1-one
BM 03

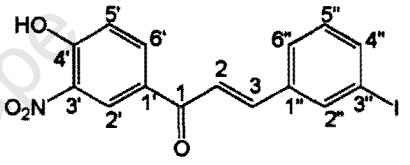

(2*E*)-1-(4'-hydroxy-3'-nitrophenyl)-3-(3"-iodophenyl)prop-2-en-1-one
BM 04

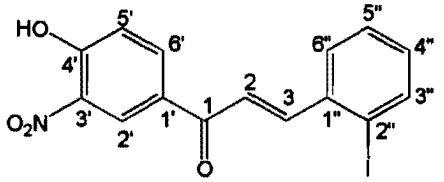

(2*E*)-1-(4'-hydroxy-3'-nitrophenyl)-3-(2"-iodophenyl)prop-2-en-1-one
BM 05

2.3.2.3.1 Method

The method used is as described in 2.3.2.2 above without any modification. As this set of chalcones (**BM 03**, **BM 04**, and **BM 05**) is being reported for the first time, full characterisation was carried out [same as was done for **BM 01**].

For key spectroscopic indicators, please refer to 2.3.2.1 (as described for **BM 01**).

2.3.2.4 Synthesis of chalcones containing trihydroxyl groups on ring A

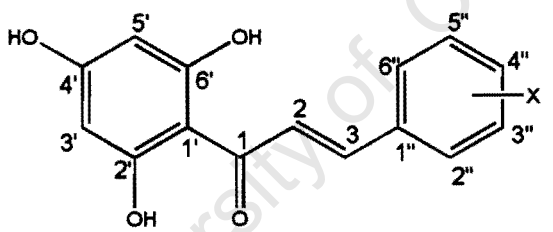

Figure 2.1 **2',4',6'-trihydroxylated chalcone** (x represents a halogen at any of the 5 available positions in ring B)

2.3.2.4.1 Method

Synthesis of chalcones containing three hydroxyl groups in ring A, that is, 2',4',6'-positions (see Figure 2.1 above), was carried out in three steps:

Step 1 Protection of hydroxyl groups using MEM-Cl

The method employed to protect two of the three -OH groups is that developed by Clark *et al.* (2004). In this method, 2.06 equivalents of K_2CO_3 was placed in 10 mL DMF. The mixture was stirred at room temperature for 30 min at which point 1 equivalent of 2',4',6'-trihydroxyacetophenone was added followed by 2.04 equivalents of MEM-Cl. The reaction mix was allowed to stir at room temperature for 16 h after which water (3x the volume of DMF) was added to quench the reaction. The organic portion was then extracted into EtOAc. It was washed several times with water, dried and purified on silica gel column using 20 % (v/v) EtOAc in hexane.

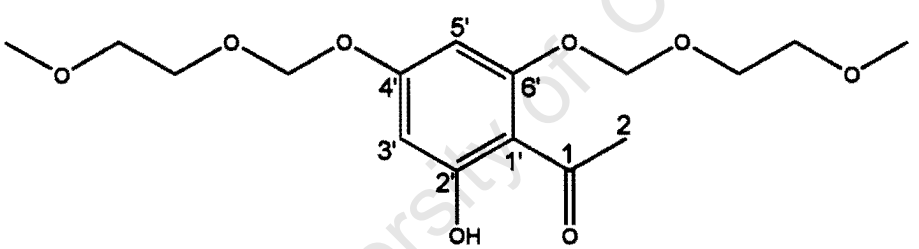

1-(2'-hydroxy-4',6'-bis[(2-methoxyethoxy)methoxy]phenyl)ethanone

There are 2 key ^{1}H NMR spectroscopic indicators that may be used to confirm the successful synthesis of diMEM protected 2,4,6-trihydroxylacetophenone {1-(2'-hydroxy-4'6'bis[(2-methoxylethoxy)methoxy]phenyl)ethanone}, (see structure above), and they are:

a) disappearance of a broad singlet between 4 and 10 ppm that integrates for 2 protons in -OH groups (H-4' and H-6'), and
b) appearance of a singlet ~ 6 ppm that integrates for 4 protons (Bn-OCH_2O-)

Step 2 Synthesis of diMEM-protected chalcones

Chalcones with varying substitutions in ring B were synthesized following a method used by Bois *et al* (1998). In this method, typically 0.145 mmol of the diMEM-protected acetophenone and 0.15 mmol of a halogenated benzaldehyde were placed in 30 mL of methanol. 1.2 mL aqueous 50 % (v/v) KOH was added and the reaction mix refluxed at 70 ^{0}C for 2 - 3 h [the progress of the reaction was monitored by silica TLC using 50 % (v/v) EtOAc in hexane]. When the reaction was deemed to be complete, 20 mL water was added, methanol removed under reduced pressure and the organic portion extracted into DCM. The DCM was then removed under reduced pressure.

Step 3 Deprotection of diMEM-protected chalcones

Approximately 50 mg of crude diMEM-protected chalcones were either purified on silica gel column using 50 % (v/v) EtOAc in hexane followed by acid treatment [30 mL methanol containing 1 % (v/v) HCl in 10 mL Et_2O] to remove the MEM-protecting group or they were simply acid treated and the MEM-free chalcone purified on preparative TLC using 50 % (v/v) EtOAc in hexane to obtain the final chalcones products (**BM 06**, **BM 07**, **BM 08**, **BM 09** and **BM 10**).

Confirmation of this group of chalcones is done in the same manner as that described in section 2.3.2.1 for **BM 01**.

Chapter 3 RESULTS

3.0 Molecular biology aspects, protein expression, purification and activity determination

3.1 Molecular cloning

The objective of this segment of the project was to transfer the malaria HGXPRT gene from pET-15b (with his-tag) to pET-17b (without his-tag) and incorporate the recombinant plasmid in an expression strain of *E. coli*.

The first step was to increase the quantity of the two plasmids by making competent cells, transforming them with the plasmids, and generating plasmid preparations.

3.1.1 Preparation of competent *E. coli* XL1 blue cells and their transformation

Competent *E. coli* XL1 blue cells were successfully made using the $CaCl_2$ method and stored in aliquots at - 80 ^{o}C. The plasmids were incorporated into the competent cells by use of a standard heat shock protocol. The transformed *E. coli* XL1 blue cells were grown for 1 h in 2x TY medium and plated on LB agar plates. The transformation efficiency (using pUC 18) was 2.1×10^6 colony forming units per µg DNA.

3.1.2 Plasmid DNA preparations

Individual colonies were selected and grown in LB liquid medium. In preliminary experiments, difficulties were experienced in extracting the plasmids, and two methods were tried, standard alkaline lysis combined with organic solvent (isopropanol) precipitation and alkaline lysis followed by DNA-binding silica. A culture of cells was split into equal volumes and processed to yield the same volume, and equal aliquots were analysed by agarose gel electrophoresis. The results are shown in Figure 3.1, and clearly the rapid alkaline method provided superior yields of both plasmids, and was adopted

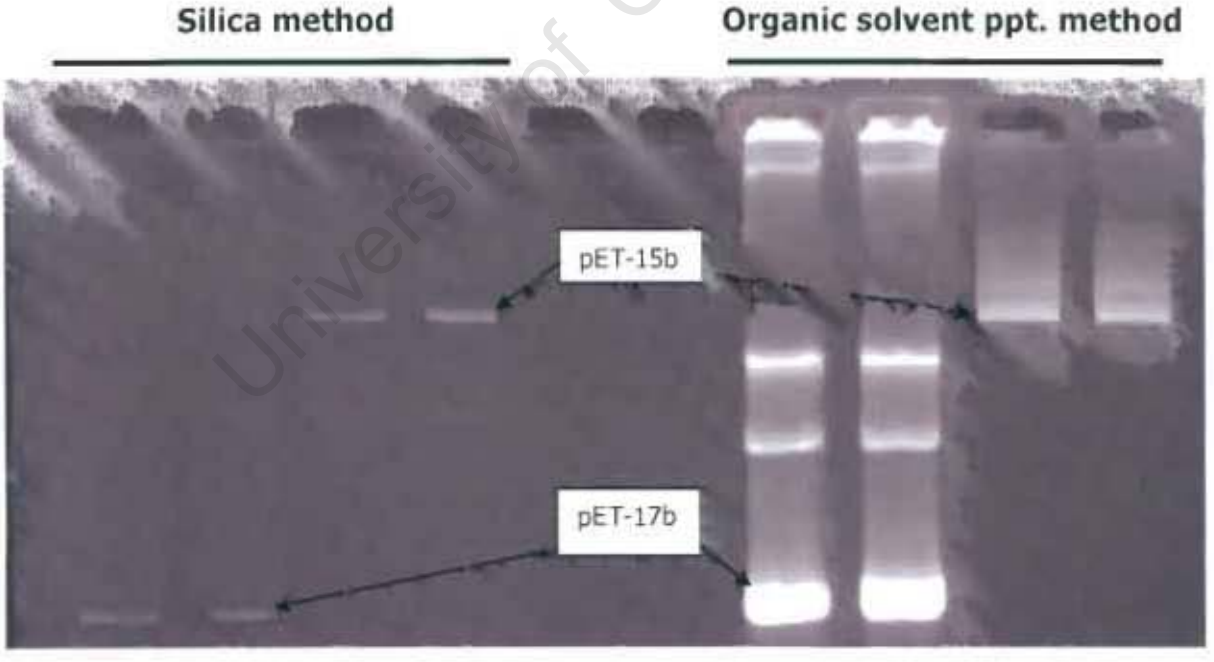

Figure 3.1 **Comparison of DNA-binding silica vs organic solvent precipitation methods for plasmid DNA preparation**. Plasmid DNA was analysed on 0.8 % agarose gel and visualised under UV light using ethidium bromide

Figure 3.3 **Digestion of Lambda DNA by *Bam* HI and *Nde* I.** Digestion was at 37 ^{0}C for 2 h. The digests were analysed on 0.8 % agarose gel. The control had no restriction enzyme.

Both pET-17b and recombinant pET-15b were capable of being digested by *Nde* I and *Bam* HI, as shown in Figure 3.4, indicating the presence of the cleavage sites.

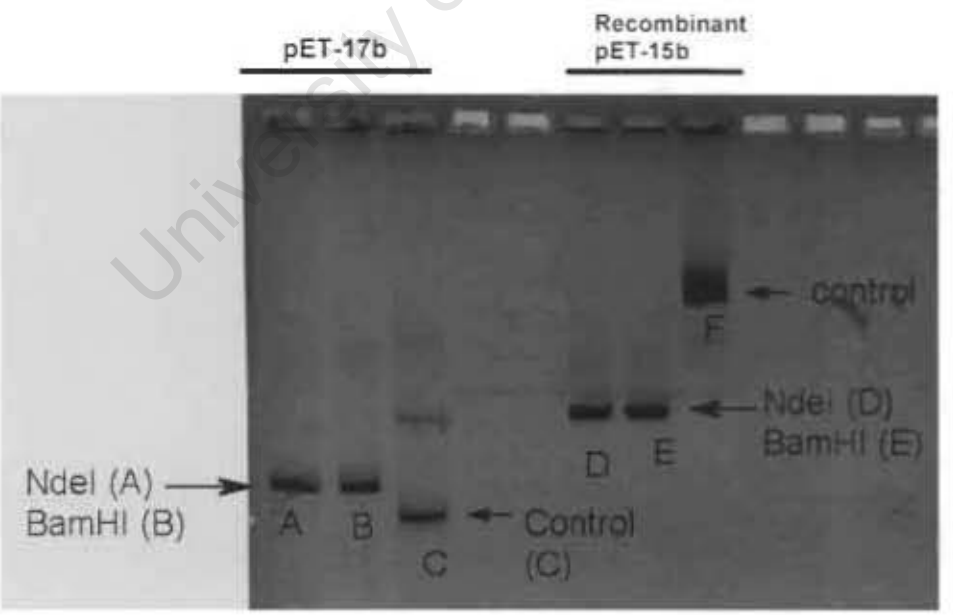

Figure 3.4 **Single digestions of pET-17b and the recombinant pET-15b plasmid DNA with *Bam* HI and *Nde* I.** The digests were analysed on 0.8 % agarose gel and visualised under UV light.

3.1.4 Purification of insert and cleaved pET-17b and their ligation

The restriction digests of pET-17b and recombinant pET-15b were run in a thick agarose gel with ethidium bromide and visualised briefly under UV light (Figure 3.5). The gel bands containing the cleaved pET-17b and HGXPRT cDNA (insert) from the recombinant pET-15b were excised and the DNA extracted using an extraction kit.

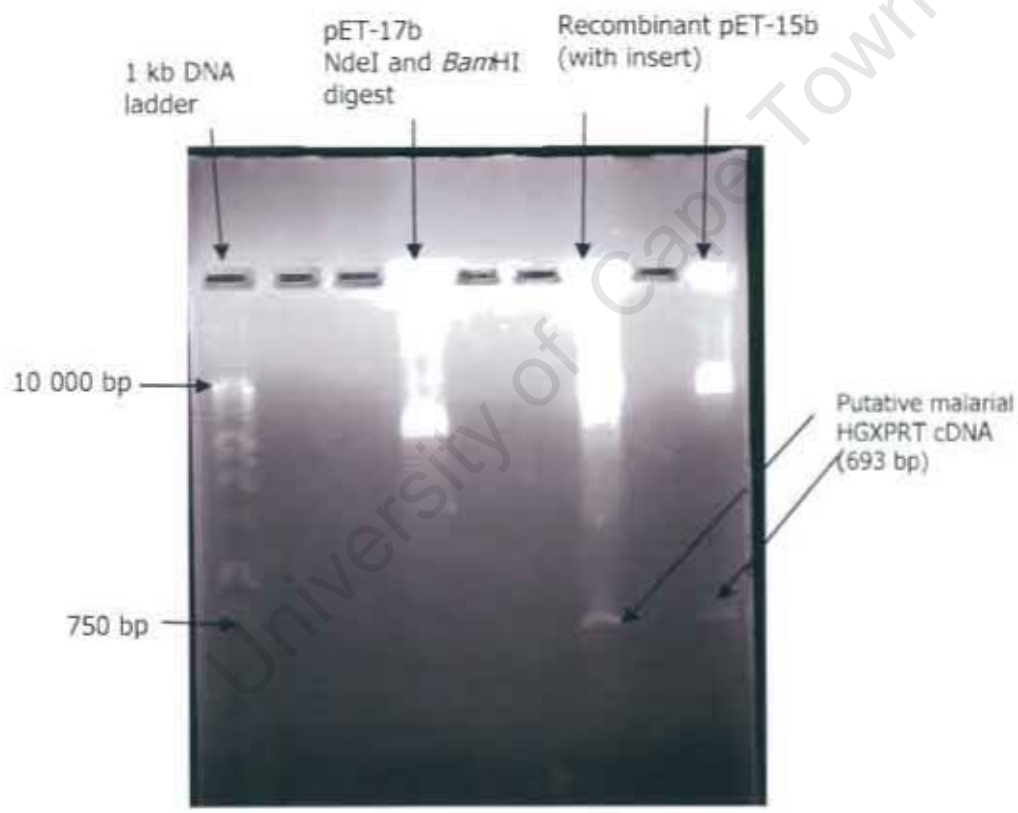

Figure 3.5 **Combined *Nde* I and *Bam* HI restriction digestion of pET-15b and pET-17b.** Digestion was carried out at 37 °C overnight with both enzymes. The bands corresponding to the insert and cleaved pET-17b were cut out and the DNA extracted.

The extracted DNA was then ligated and transformed into either XL1 Blue or BL21(DE3)pLysS cells. The plasmid preparations of selected colonies were analysed on 0.8 % agarose gel (Figure 3.6). Lanes 1, 2, 3 and 7 (from XL1 Blue cell colonies) each had one prominent plasmid DNA band, although one plasmid (lane 7) was obviously different from the other three. Lanes 4, 5, and 6 (from BL21(DE3)pLysS cells) showed that one colony had no plasmid, while the other two had several prominent bands. Two of the plasmids from XL1 Blue cells (lanes 3 and 7) and one of the BL21(DE3)pLysS

Figure 3.6 **Analysis of plasmid preparations following ligation of insert into pET-17b.** The ligation reaction products were transformed into XL1 Blue cells and BL21(DE3)pLysS cells and plasmid DNA obtained from the selected colonies analysed on 0.8 % agarose. The last lane shows pET-17b without insert for comparison.

(lane 5) were selected for analysis by restriction digestion with *Bam* HI, and the results are shown in Figure 3.7. Only lanes B and C showed bands of the correct molecular size (~4000 bp), and the plasmid prep in lane B was taken for further analysis. Figure 3.8 shows that combined digestion with *Bam* HI and *Nde* I released a fragment of approximately the correct size for the insert (693 bp).

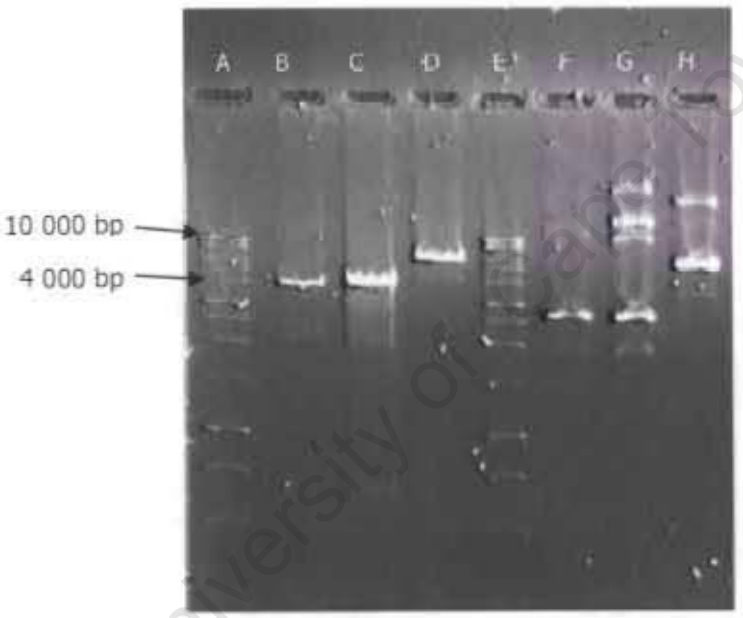

Figure 3.7 **Analysis of plasmid preparations by *Bam* HI digestion**. A 1 kb DNA ladder is in lanes A and E, while the *Bam* HI restriction digests of plasmid DNA from colonies shown in lanes 3, 5, and 7 of Figure 3.6 are in lanes B, C, and D and their respective control digests (no enzyme) in lanes F, G and H. The analysis was carried out on 0.8 % agarose gels.

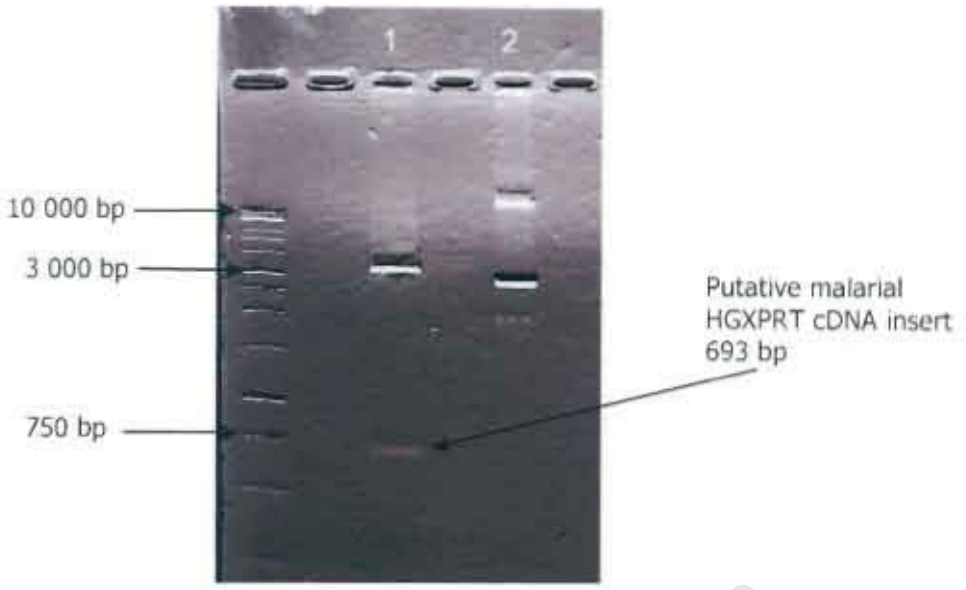

Figure 3.8 **Excision of insert from pET-17b**. Plasmid DNA obtained from colony shown in lane 3 of Figure 3.6 was digested with both *Nde* I and *Bam* HI. The restriction digest lane labelled 1 and the respective control lane labelled 2 analysed on a 0.8 % agarose gel.

3.1.5 Transformation of BL21(DE3)pLysS with pET-17b

Transformation of BL21(DE3)pLysS with pET-17b and recombinant pET-17b was carried out. The transformation efficiency (using pUC 18) attained was 2.1×10^6 colony forming units per µg DNA. Glycerol stocks of transformed BL21 (DE3)pLysS cells were made and stored at - 80 ^{0}C.

3.2 Malaria HGXPRT expression

3.2.1 Induction and control by IPTG

Figure 3.9 shows the time dependence of expression of a protein of the correct molecular size of malaria HGXPRT (26 232 Daltons). The protein is present at 30 min following induction with IPTG and becomes more obvious after longer times. No such protein is expressed in the control cells (without insert).

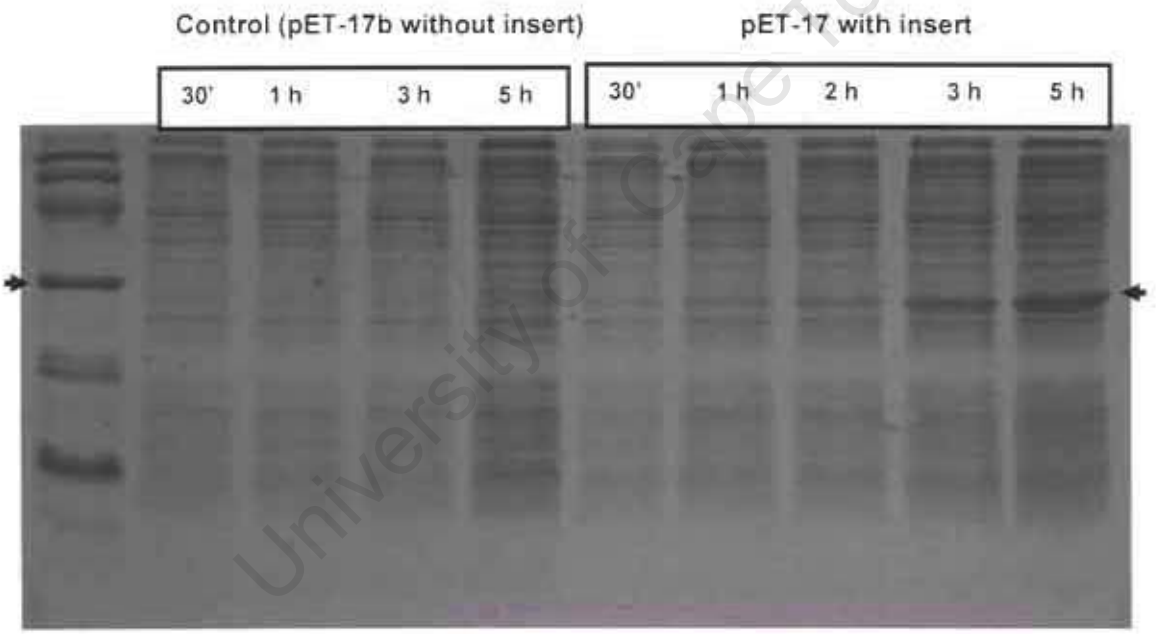

Figure 3.9 **Time course of expression of malaria HGXPRT in *E. coli* BL21(DE3)pLysS cells.** Cultures of E coli cells containing pET-17b without or with insert were grown to optical density of 0.4-0.6 and then treated with 0.4 mM IPTG for the indicated times. The cells were analysed by SDS-PAGE with 15 % (w/v) acrylamide and stained with Commassie Blue. The arrowhead on the left indicates the 30 000 MW marker protein. The arrowhead on the right points to the putative HGXPRT protein (MW 26 232 daltons).

Figure 3.10 shows the response of BL21(DE3)pLysS cells containing malaria HGXPRT gene to the presence of IPTG. As can be seen, the malaria HGXPRT enzyme is produced in both the presence and absence of IPTG indicating that its expression is not tightly controlled by IPTG. This is despite the fact that the cells were grown in the presence of chloramphenicol, which makes this strain maintain the pACYC plasmid. This plasmid is meant to ensure a tight control of protein expression in this strain. However, slightly more recombinant protein is produced and host protein expression is lower in the presence of IPTG than in its absence, and therefore we continued to use IPTG in future experiments.

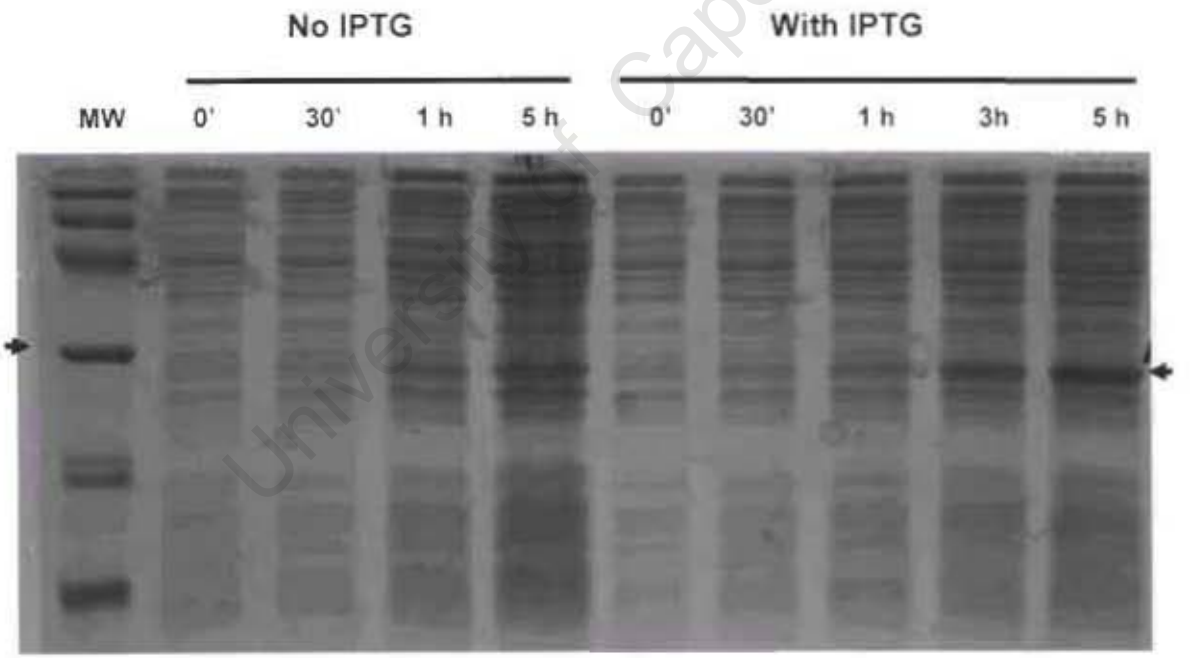

Figure 3.10 **Effect of IPTG on malaria protein expression**. In these experiments, two cultures were grown until the optical density was 0.4-0.6 (~16 h), at which stage IPTG (0.4 mM) was added to the one and the cultures continued for 5 h with aliquots taken at the indicated times and analysed by SDS-PAGE. The arrowhead on the left indicates the 30 000 dalton MW marker protein and that on the right indicates the putative malaria protein.

3.2.2 Trial of three methods of lysis of *E. coli* cells

Lysis of BL21(DE3)pLysS cells containing malaria cDNA had previously been successfully achieved in our laboratory by resuspending the cells in Tris-Cl, pH 7.9 and 500 mM NaCl, and digestion with 1 mg/ml lysozyme for 1 h on ice, followed by freeze-thawing rapidly with liquid nitrogen and a bath of room temperature water (Phehane, 2002). However, we wanted to use ion exchange chromatography as the first step in the purification of HGXPRT (see below) and needed a buffer with a low salt content. This procedure failed to provide adequate lysis under these conditions. Therefore a trial of 3 different methods, which are elaborated on in the legend to Figure 3.11, but essentially consisted of (i) a single freeze over a long period and thaw, (ii) lysozyme treatment at high $MgCl_2$, or (iii) lysozyme treatment at low salt. The results in Figure 3.11 show that the lengthier freezing followed by a thaw in the absence of lysozyme provided almost as much HGXPRT in the supernatant as the other two procedures in the presence of lysozyme. It will be seen later that some purification experiments, especially those on a small scale, were carried out with lysozyme, but the procedure we finally adopted was the first, namely prolonged freezing without lysozyme, in order not to contaminate the preparation with another protein added in large amounts (see Figure 3.11 for level).

It can be seen that most of the expressed HGXPRT remains with the pellet fraction, probably in inclusion bodies. This was the usual result we obtained,

but occasionally a better proportion in the supernatant was achieved (see below). The pellet fraction was discarded.

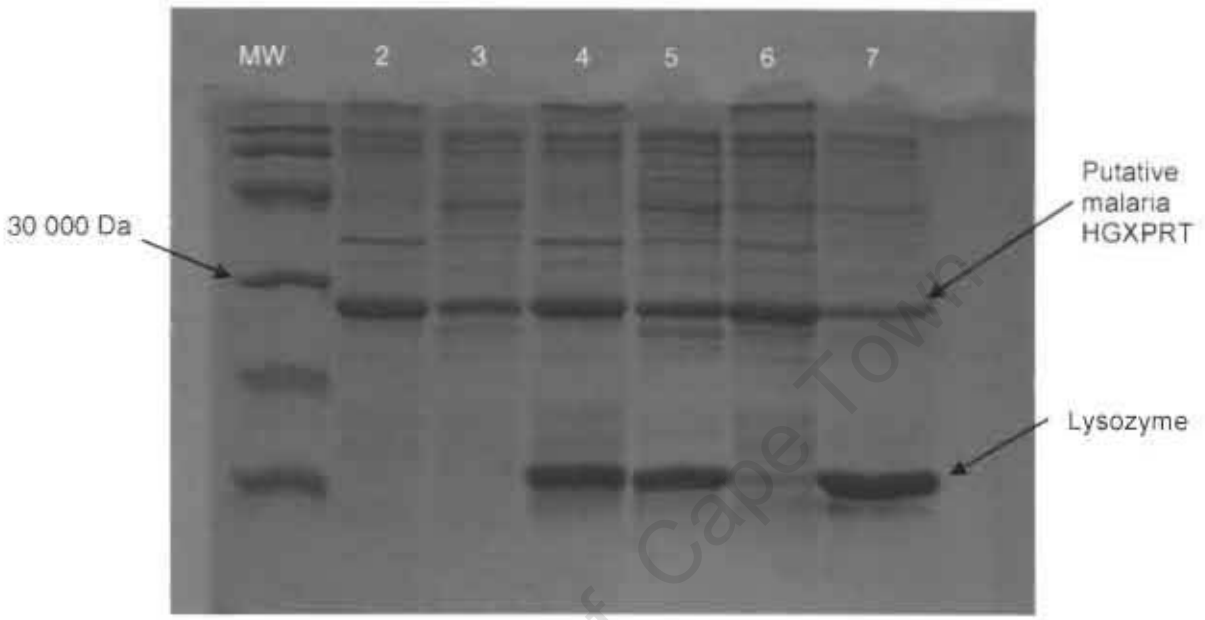

Figure 3.11 **Lysis of BL21(DE3)pLysS cells using three different methods** BL21(DE3)pLysS cells containing malaria HGXPRT cDNA were cultured, centrifuged, and the pellet lysed using three different methods. Method 1: Pellet frozen at - 80 ^{0}C for 1 h followed by re-suspension in 50 mM Tris-Cl, pH 8.0, 25 mM NaCl, 1 mM PMSF, 2 mM EDTA, 1 mM DTT (lanes 2 and 3). Method 2: Re-suspension of pellet in 100 mM Tris-Cl, pH 7.4, 110 mM $MgCl_2$, 1 mM PMSF, 1 mM β-mercaptoethanol, and 1 mg/mL lysozyme (lanes 4 and 5); Method 3: Re-suspension of pellet in 50 mM Tris-Cl, pH 8.0, 25 mM NaCl, 1 mM PMSF, 2 mM EDTA, 1 mM DTT and 1 mg/mL lysozyme (lanes 6 and 7). The suspension was centrifuged at 21000 x g for 20 min. The pellet was resuspended in the same volume as the supernatant and the same buffer solution, and both were analysed by SDS-PAGE, with Commassie Blue stain. Lanes 2, 4, 6 are resuspended pellets and 3, 5, 7 supernatants.

3.3 Purification of Malaria HGXPRT

Various purification procedures have been tried for the purification of non-his-tagged HGPRTs from a variety of sources. Early purification of the human enzyme was achieved with ammonium sulfate precipitation, heat treatment, and anion exchange chromatography (Olsen and Milman, 1978). This enzyme is extremely stable and such harsh treatments are not suitable for malaria HGXPRT. Later purifications include ammonium sulfate precipitation combined with phenyl Sepharose (hydrophobic interaction) and anion exchange chromatography (Eads *et al.*, 1994). Recombinant malaria enzyme has been purified from *E. coli* using either Hg-sepharose directly or following anion exchange chromatography (Keough *et al.*, 1999). Another group used anion exchange chromatography and gel filtration (Li *et al.*, 1999). A peculiarity was that the former study found that the malaria enzyme did not bind to anion exchange resin, whereas the latter did.

3.3.1 Small scale purification

3.3.1.1 Ion exchange chromatography

We tested the ability of the malaria enzyme and all other proteins to bind the ion exchange resins on a small scale by using cation and anion exchange Sep-Pak cartridges. The results are shown in Figure 3.12. In these experiments and some subsequently, the expressed HGXPRT appeared to migrate in SDS-PAGE as two bands, for an unknown reason. It will be seen

that the bottom band disappears with further purification. In general HGXPRT bound poorly to both resins at all three pH conditions, but significant

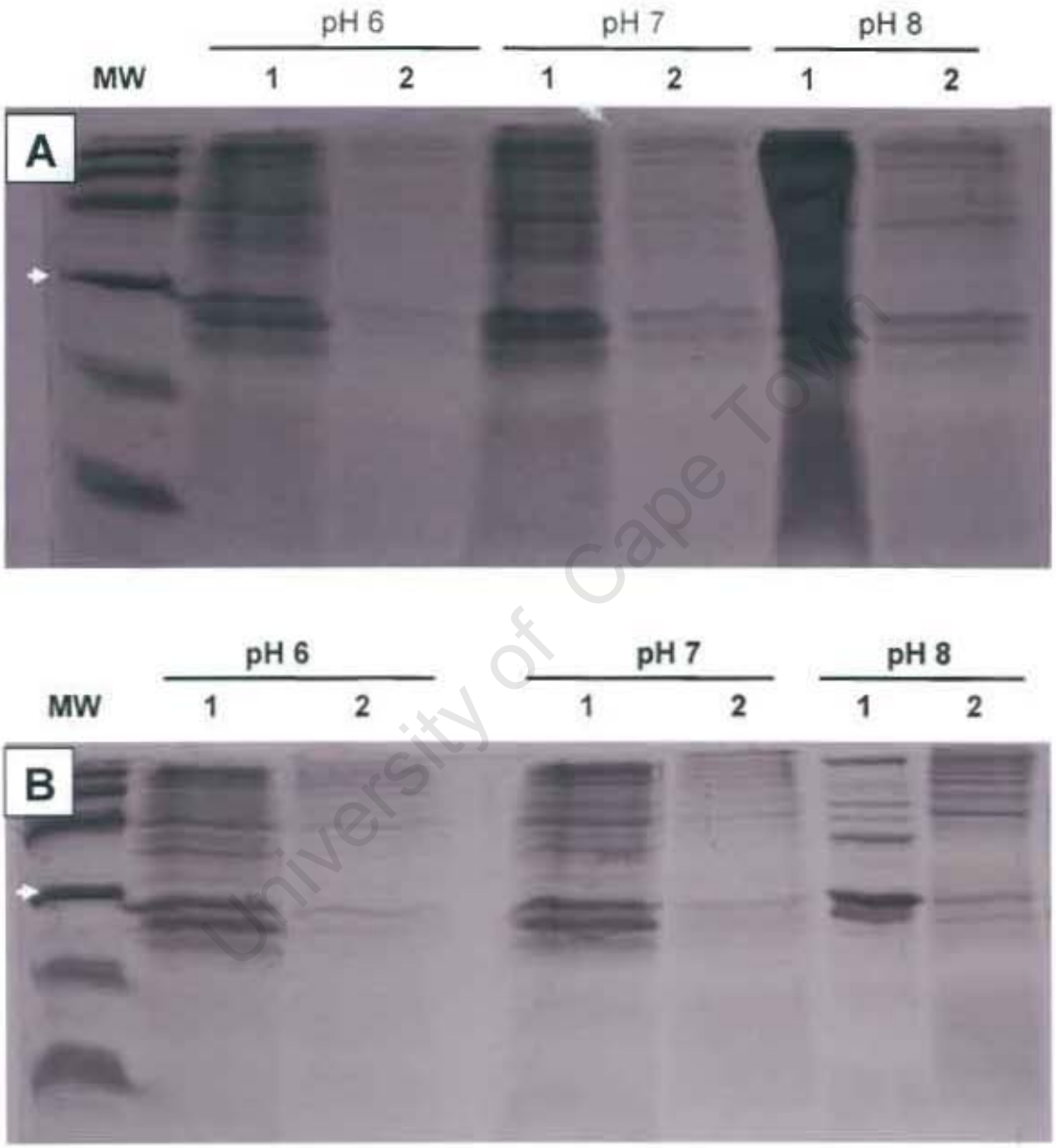

Figure 3.12 **Effect of pH on binding of proteins in crude supernatant to cation (A) and anion (B) exchange Sep-Pak cartridges**. 2 ml of supernatant was passed through each Sep-Pak after adjusting the pH to the required value. In the case of the pH 6 experiment, 10 mM sodium phosphate was added as well. Lanes 1 show the flow-through fraction and Lanes 2 show the proteins eluted from the cartridge with 1 M NaCl and made to the same volume. Analysis by SDS-PAGE.

purification was achieved at alkaline pH with the anion exchange resin, through contaminating proteins binding well, consistent with the results of Keough *et al.*, 1999.

The difference between the two resins is better demonstrated in Figure 3.13, where the experiment is performed at pH 8.9. It can be seen that virtually no proteins, HGXPRT and other proteins, bound to the cation exchange resin, whereas with the anion exchange resin the malaria protein is virtually the only protein that does not bind, providing a significant purification.

Figure 3.13 **Comparison of protein binding to cation and anion exchange Sep-Pak cartridges at pH 8.9.** A 4 ml E. coli lysate was pelleted (and resuspended to 4 ml) and the supernatant divided into two and passed through each Sep-Pak cartridge. The proteins bound to the cartridges were eluted with 1 M NaCl wash to the same volume. Equal aliquots of the fractions were analysed by SDS-PAGE. The arrowhead indicates putative HGXPRT.

3.3.1.2 Reactive Red 120 chromatography

Reactive Red 120-agarose is commonly used to purify enzymes with NAD/NADP cofactors or nucleoside/tide substrates (e.g. Coll and Murphy, 1984; Storts and Bhattacharjee, 1987; Buki *et al.*, 1987; Nakajin *et al.*, 1989; Muro-Pastor and Florencio, 1992; Pech and Nelson, 1994; Urbatsch *et al.*, 1994). On this basis we tested whether it could be used to purify malaria HGXPRT following an anion exchange Sep-Pak cartridge.

Figure 3.14 shows the purification achieved using a small column of Reactive Red 120-agarose. A comparison of Lanes 4 (sample applied to the column after passage through Sep-Pak cartridge) and 6 (sample afterwards), demonstrates how HGXPRT (and some other proteins, e.g. lysozyme) is retained on the column. The column was then washed with buffer containing 200 mM NaCl (Lane 7), followed by almost selective elution of HGXPRT with 50 mM PPi. The proteins remaining on the column, including lysozyme are shown in Lane 10.

We tried to elute HGXPRT with 10 mM IMP or 1 mM PRPP in the presence of 10 mM $MgCl_2$ without success. 50 mM Pi could elute the protein, but not as effectively as PPi (results not shown).

HGXPRT could also be eluted with high salt concentrations, but not selectively. Figure 3.15 shows the effect of increasing NaCl concentrations on protein elution from the Reactive Red 120 column. Virtually all proteins

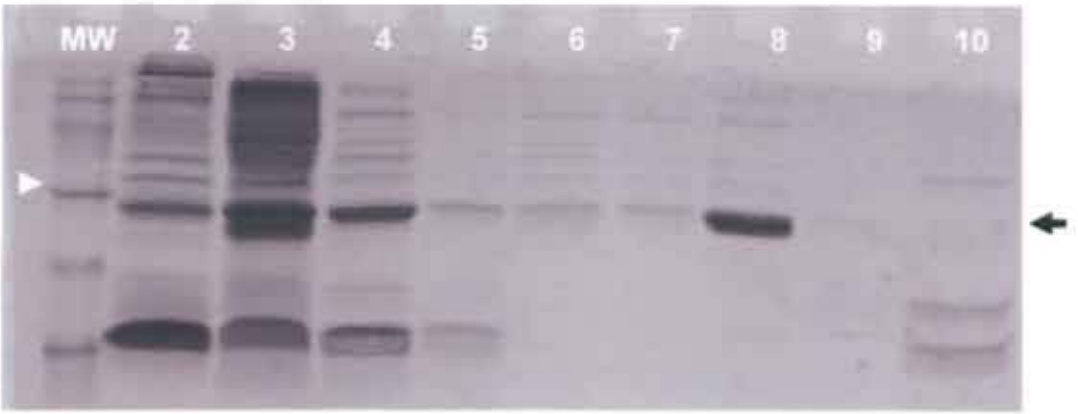

Figure 3.14 **Purification of malaria HGXPRT on Reactive Red 120 column**. A culture of 40 ml was pelleted and re-suspended to 4 ml, cells lysed, centrifuged, and the supernatant passed through an anion exchange Sep-Pak cartridge, washed with 1 ml buffer (combined with flow through), and then the combined sample was applied to a small column of Reactive Red 120. The column was washed with 1 mL buffer containing 200 mM NaCl, and then proteins eluted with 2 x 1 mL aliquots of 50 mM PPi, and then 1 mL 1 M NaCl. Lane 1, protein marker; Lane 2, pellet fraction (re-suspended to same volume as supernatant); Lane 3, supernatant fraction; Lane 4, Sep-Pak flow though; Lane 5, Sep-Pak wash; Lane 6, Reactive Red 120 flow though; Lane 7, Reactive Red 120 wash; Lane 8 and 9, elution with PPi; Lane 10, 1 M NaCl wash. The white arrowhead shows the 30 000 Dalton MW marker protein and the black one the position of the putative HGXPRT. Analysis by SDS-PAGE.

started being eluted at 300 mM NaCl, but 1 M NaCl was needed to clear the column. This indicates that the Na_4-PPi is effective not merely because it is a salt, but there must be selective interaction with HGXPRT. As a result of this experiment, the Reactive Red 120 column was routinely washed with buffered 200 mM NaCl prior to elution with PPi (see below).

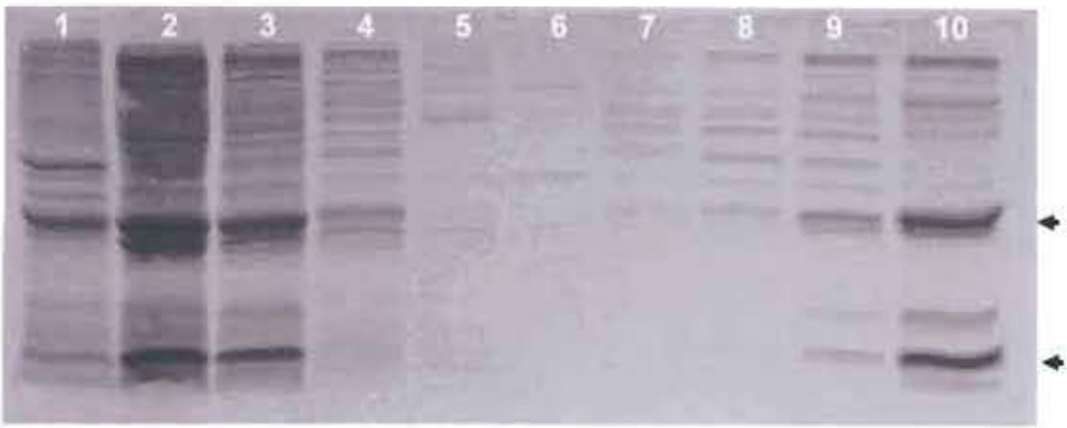

Figure 3.15 **Step-wise elution from Reactive Red 120 column by increasing salt concentration**. 40 mL of cell culture was pelleted, re-suspended to 4 mL, lysed, the debris pelleted (re-suspended to the same volume as the supernatant, Lane 1), and the supernatant (Lane 2) passed through an anion exchange Sep-Pak cartridge (Lane 3), and then placed on a small column of Reactive Red 120. The flow through is in Lane 4. The column was developed with 6 x 1 mL solutions of increasing NaCl concentration (50 mM, Lane 5; 100 mM Lane 6; 200 mM, Lane 7; 300 mM, Lane 8; 500 mM Lane 9; 1 M Lane 10). The top arrowhead indicates the position of the putative HGXPRT, and the lower one lysozyme. Analysis by SDS-PAGE.

Figure 3.16 shows the effect of omitting the anion exchange Sep-Pak cartridge and purifying by Reactive Red 120 on its own. Lane 4 (Reactive Red 120 flow through) indicates that all the HGPXRT bound to the resin and allowed several contaminating proteins through. Lane 7 shows the effectiveness of the 200 mM wash. PPi elutes the HGXPRT, but with significant contaminating proteins (Lane 8). On this basis it was considered preferable to use a prior anion exchange chromatography step. This also helped in preserving the expensive Reactive Red 120 resin for reuse.

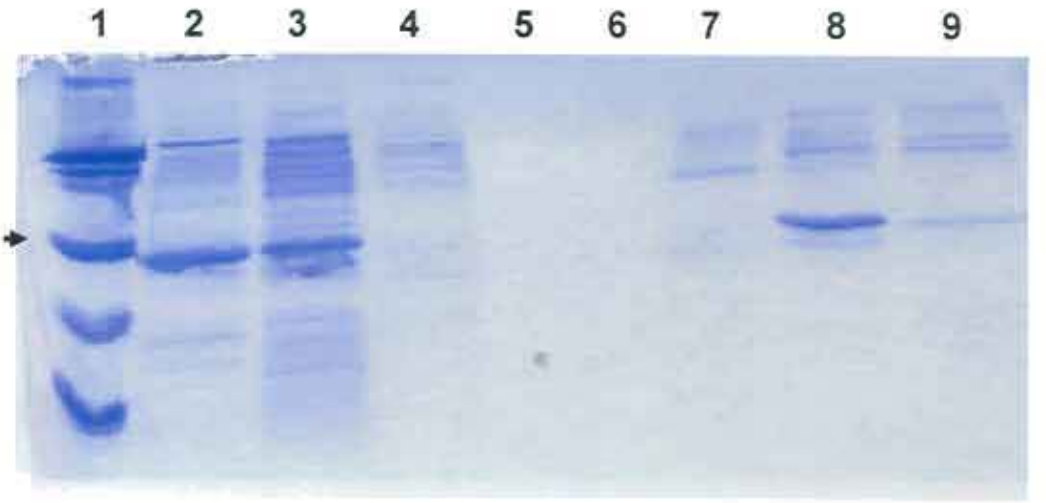

Figure 3.16 **Purification of HGXPRT by Reactive Red 120 column alone**. 40 ml of culture was processed by the standard procedure to yield pellet (Lane 2) and supernatant (Lane 3) fractions. The supernatant was passed directly through a small column of Reactive Red 120 to give the flow-through (Lane 4). The column was washed with buffered 200 mM NaCl (Lane 7), and eluted with first 50 mM PPi (Lane 8) and then 1 M NaCl (Lane 9). Lane 1 contains markers and Lanes 5 and 6 are empty. The arrowhead shows the 30 000 Dalton marker protein.

3.3.2 Large-scale purification

The results obtained with small-scale purification (using a Sep-Pak cartridge and a small column of Reactive Red 120) suggested that larger columns of anion exchange and Reactive Red 120 resins would achieve a large-scale purification. The amount of each resin for a 1 L culture was determined empirically. The result of a typical experiment using DE52 anion exchange resin is shown in Figure 3.17. The amount of soluble HGXPRT in the supernatant is approximately 40%, as before. A comparison of lanes 3 and 4 show that virtually all the HGXPRT passed through the column, but with

significant purification. The proteins bound to the column are seen in lane 5, and HGXPRT is a small proportion of these. Several non-HGXPRT proteins came straight through the Reactive Red 120 column (lane 6). Elution of HGXPRT occurs mainly in lanes 12-17, and is accompanied by a higher molecular weight protein of approximately 90 000 Daltons. This protein was difficult to eliminate. We had it sequenced by mass spectrometry (analysis of

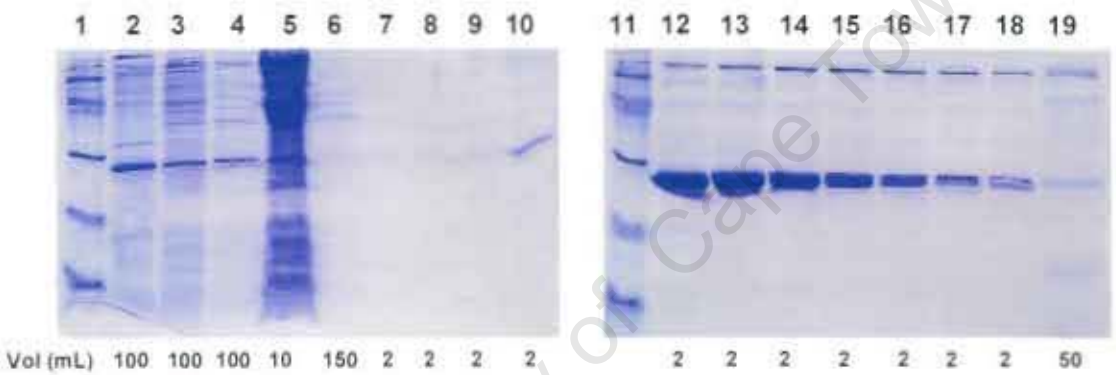

Figure 3.17 **Large-scale purification of HGXPRT using anion exchange and Reactive Red 120 columns**. 1 L cell culture was pelleted, the cells resuspended in 100 mL lysis buffer, lysed, and centrifuged to produce pellet (Lane 2, resuspended) and supernatant (Lane 3). The supernatant was passed through DE52 and then Reactive Red 120 columns. Material passing through the DE52 column is in Lane 4 and the proteins bound (eluted with 1 M NaCl) in Lane 5. The material passing straight through the Reactive Red 120 column and including a 50 ml buffered 200 mM NaCl wash is in Lane 6. Proteins were eluted from the Reactive Red 120 column with 11 x 2 mL PPi (Lanes 7-18) and finally 1 M NaCl (Lane 19). Equal volume aliquots of the samples were applied to the gel. The original volumes from which the aliquots were derived are shown below the gels. Molecular weight markers are shown in Lanes 1 and 11.

fragments of trypsin digestion, results not shown) , and identified it as *E. coli* maltodextrin phosphorylase, a dimeric protein with subunits of 90 000 Daltons. This contaminant is probably the same "persistent phosphatase" identified by Li *et al.*, 1999. They reduced its level by including 10 mM phosphate in the cell culture growth medium, and we adopted this ploy as well.

The success of this purification system suggested that the protocol could be combined into virtually a single manoeuvre, with tandem anion exchange and Reactive Red 120 columns, in which the crude supernatant is first passed through a top anion exchange column straight into a Reactive Red 120 column underneath, the columns separated, and the HGXPRT eluted from the second column with PPi.

The results of such a strategy are shown in Figure 3.18. The last lane (9) shows the result of the PPi elution, following dialysis of the eluate, concentration by lyophilisation, and dialysis again. The final sample was filtered through 0.45 μm filter, and, as can be seen in Lane 9, is approximately 95% pure. The volume was 2 ml and protein concentration 2.5 mg/ml. The yield was therefore 5 mg of protein from 1 L culture, rather similar to the yield of 10 mg from 2.5 L culture obtained by Keough *et al.*, 1999.

Further purification, mostly to eliminate the maltodextrin phosphorylase, was attempted with gel filtration, and some separation was achieved, but the differences in molecular weight (Tetrameric HGXPRT = 105 000 Daltons;

Dimeric phosphorylase = 180 000 Daltons), meant a long column and some loss of HGXPRT (results not shown).

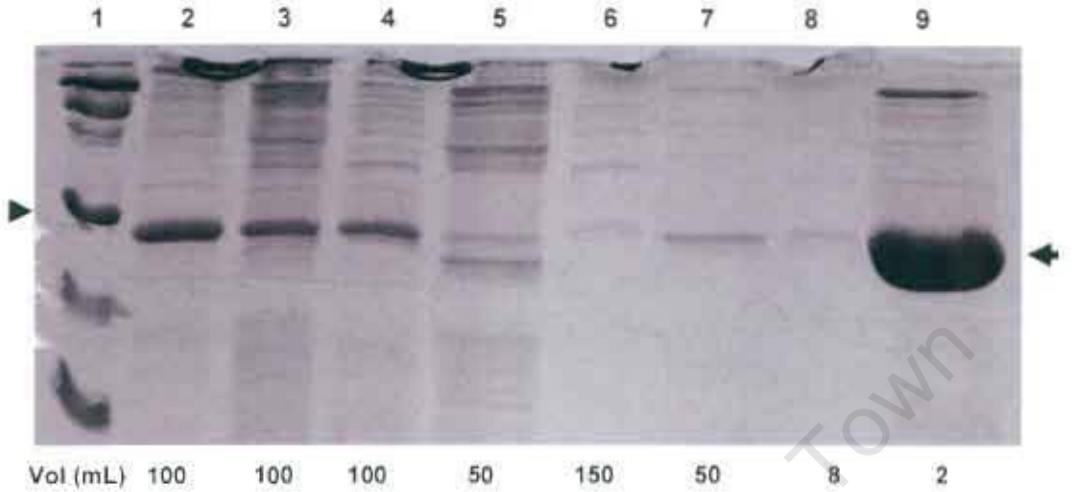

Figure. 3.18 **Large-scale purification with tandem anion exchange and Reactive Red 120 columns**. 1 L culture was processed as in Figure 3.17. The anion exchange column was placed directly on top of the Reactive Red 120 column, and the supernatant (Lane 3) passed through by gravity overnight. The columns were separated and an aliquot was taken of the material in between the columns (i.e. only been through DE52, for analysis only, Lane 4). The columns were rejoined and an additional 50 ml of lysis buffer was added to bring all the supernatant completely through both columns (Lane 6). The columns were separated and the proteins bound to the DE52 were eluted with 1 M NaCl (Lane 5), and the Reactive Red 120 column was washed with 50 mL buffered 200 mM NaCl (Lane 7), followed by 8 ml 50 mM PPi (Lane 8, no HGPRT), and then 15 ml (HGXPRT). The latter was dialysed, concentrated by lyophilization, redissolved with water, dialysed again, and filtered through 0.45 μm filter (Lane 9). Equal volume aliquots were analysed by SDS-PAGE. The relevant volumes of the original samples are shown below the gel. The left hand arrowhead indicates the 30 000 Dalton molecular weight marker, and the right hand one the putative HGXPRT.

3.4 Activity of malaria HGXPRT

The crude supernatant fraction exhibited very low HGXPRT activity. Partial or comprehensive purification by any of the procedures mentioned above resulted in inactive enzyme. Various modifications to the purification protocol were tried, including more rapid processing of the cell pellet, and inclusion of PRPP and/or 10% (v/v) glycerol in lysis buffer. These procedures had helped to obtain partially active his-tagged enzyme (Phehane, 2002). However, none of them did so in this instance.

Active HGXPRT could be obtained following activation by incubation with substrate, similar to the findings of Keough *et al.*, 1999, and Phehane, 2002 in our laboratory. We found dialysing the non his-tagged HGXPRT against 10 mM sodium phosphate or MOPS, pH 7.0, and 1 mM DTT overnight, prior to activation an important step. Activation was generally achieved by incubating overnight at 4 °C either with 1 mM PRPP + 10 mM $MgCl_2$ or 1 mM PRPP + 60 µM hypoxanthine. Guanine was also effective, but xanthine poorer. Without the prior dialysis, or even with 1 h dialysis, activation was ineffective. It appears that the just-isolated inactive protein changes to another inactive, but activatable, form during extended dialysis.

The time dependences of activation with PRPP + hypoxanthine at two temperatures are shown in Figure 3.19. Activation was complete in 5-10 h irrespective of whether it was done at 0 °C or room temperature. The maximum activity ranged from 1-6 µmol GMP formed/min/mg of protein for

different preparations, which is approximately 10-fold lower than the human enzyme, but comparable to what has been found for the malaria one (Keough *et al.*, 1999; Phehane, 2002).

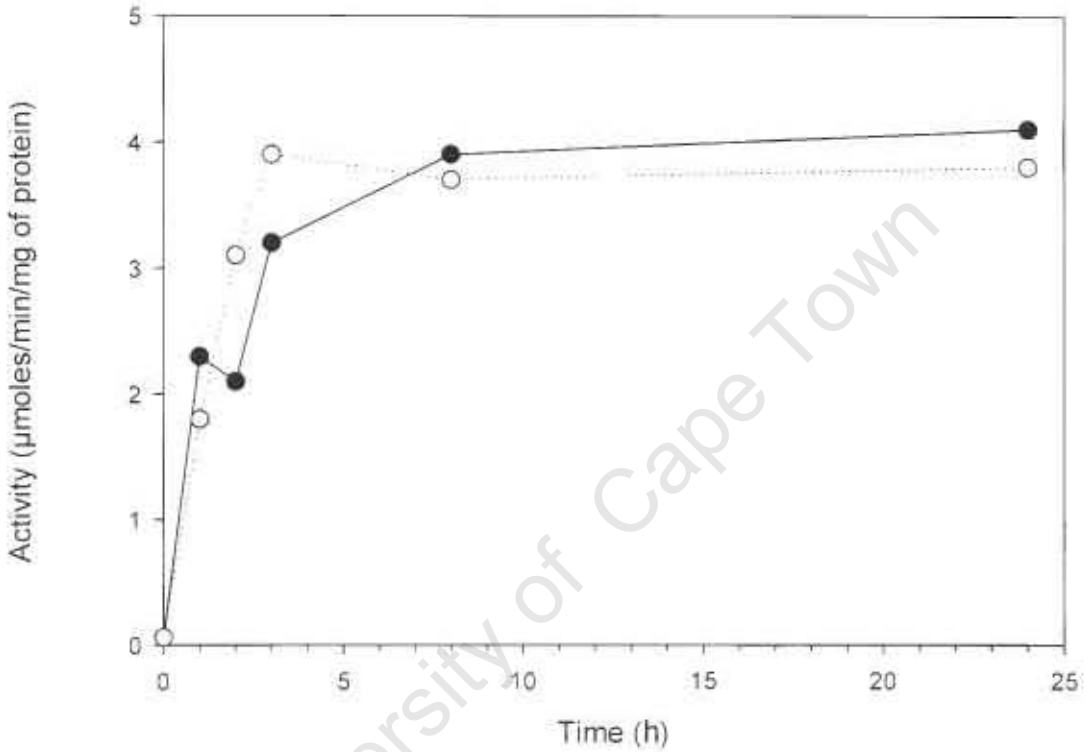

Figure 3.19 **Activation of HGXPRT**. Purified HGXPRT, which had been dialysed against 10 mM sodium phosphate, pH 7.0, and 1 mM DTT, overnight was activated by the addition of 1 mM PRPP + 60 µM hypoxanthine, and the sample either placed at room temperature (dotted line, open circles) or on ice (continuous line, dots) for the times shown and then activity measurements made on aliquots.

The activities at each step of one particular preparation of HGXPRT and with the three different purine substrates are shown in Table 3.1. The reason for negligible activity at the Supernatant step may be due to use of the activating

substrates by other enzymes in the mix. As reported by many others, there is substantial activity with xanthine as substrate.

Table 3.1 **The activity of malaria HGXPRT**. Activity of HGXPRT after Supernatant, Sep-Pak, and Reactive Red 120 steps. Overnight activation was in 60 μM hypoxanthine and 1 mM PRPP after dialysis in 10 mM sodium phosphate buffer pH 6.8, 1 mM DTT, and 1 mM PMSF. The assay conditions are in Materials and Methods, Section 2.2.11.

Malaria HGXPRT specific activity (μmol GMP/ min/ mg protein)			
Fraction	**Hypoxanthine pH 8.5**	**Guanine PH 8.5**	**Xanthine pH 7.4**
Supernatant	nda	nda	nda
Sep-Pak	1.4	3.6	2.5
Reactive Red 120	2.1	5.4	7.2

(nda = no detectable activity)

The protein prior to activation was quite stable at room temperature or on ice, in terms of being able to be subsequently activated (Figure 3.20). It was also stable once it had been activated with PRPP and hypoxanthine (Table 3.2). It

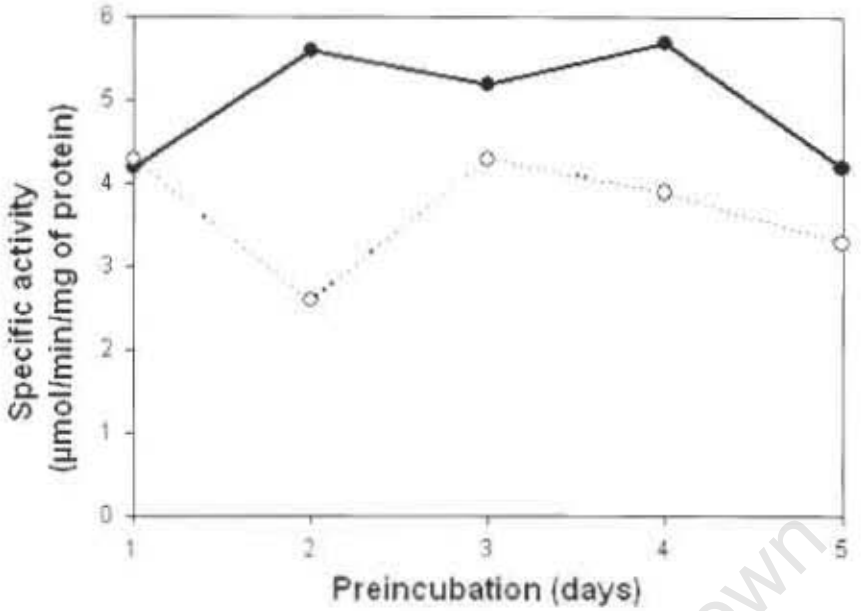

Figure 3.20 **Stability of HGXPRT prior to activation.** Following dialysis, HGXPRT was placed at room temperature (dotted line, open circles) or on ice (continuous line, dots) for the times indicated, and then activated overnight by addition of 1 mM PRPP + 60 µM hypoxanthine and assayed for activity with guanine as substrate.

Table 3.2 **Stability of activated HGXPRT**. HGXPRT was incubated under the conditions and times indicated, and then assayed for activity.

HGXPRT incubation conditions	Specific activity (μmol GMP/min/mg protein)	
	Day 1	Day 30
4 ^{0}C in 60 μM Hx + 1 mM PRPP	1.8	1.7
4 ^{0}C in 60 μM Hx + 1 mM PRPP + 50 % glycerol	2.8	2.8
- 20 ^{0}C in 60 μM Hx + 1 mM PRPP + 50 % glycerol	2.8	2.1
4 ^{0}C in 10 mM Mg^{2+} + 1 mM PRPP + 50 % glycerol	1.3	No detectable activity

was less stable with Mg^{2+} and PRPP over 30 days, due most probably to Mg^{2+} dependent hydrolysis of PRPP.

Rather remarkably, HGXPRT could be activated, inactivated, and reactivated several times with no decline in activity (Table 3.3). PRPP or Mg^{2+} alone was not sufficient for activation.

Table 3.3 Reversible activation and inactivation of HGXPRT. Dialysed HGXPRT (a) was activated by an overnight incubation with 10 mM Mg^{2+} and 1 mM PRPP (b), dialysed overnight against 10 mM sodium phosphate, pH 7.0 and 1 mM DTT (c), activated overnight with 1 mM PRPP + 60 µM hypoxanthine (d), dialysed again (e), attempted activation overnight with 1 mM PRPP (f), activated overnight with 10 mM Mg^{2+} + 1 mM PRPP (g), and finally dialysed against 10 mM Mg^{2+}, 10 mM sodium phosphate, and 1 mM DTT (g). The procedures were performed sequentially on the same sample and assayed for activity at the end of each procedure.

Stage	Procedure	Specific activity (µmol GMP/min/mg protein)
a	Prior to activation	**<0.2**
b	Activation with Mg^{2+} + PRPP	**3.0**
c	Removal of Mg^{2+} and PRPP	**0**
d	Activation with Hx + PRPP	**4.3**
e	Removal of Hx + PRPP	**0**
f	Activation with PRPP alone	**0**
g	Activation with Mg^{2+} and PRPP	**4.2**
h	Removal of PRPP	**0**

The activities reported in all the above experiments were deduced from the initial rates of the reaction as followed spectrophotometrically. Figure 3.21 shows a typical progress curve obtained for the conversion of guanine to GMP by malaria HGXPRT. The reaction ceases after about 300 s with a total absorbance change of approximately 0.06 units. This is not due to exhaustion of substrates, but rather inactivation of the enzyme because the total absorbance change for the formation of 60 µM GMP should be approximately 0.35 units. The slow fall off in activity is also indicative of inactivation, because the K_m is approximately 1 µM (Keough *et al.*, 1999) and therefore the rate should be linear until the K_m is approached.

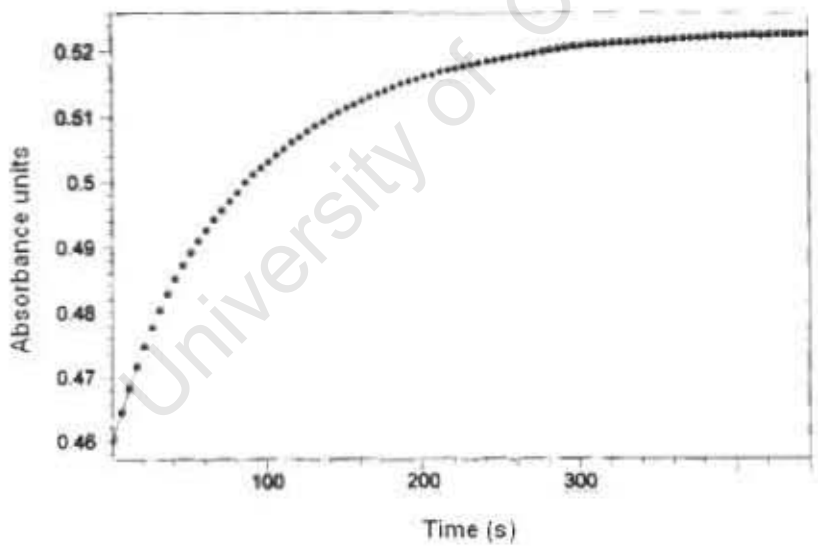

Figure 3.21 **Progress curve for conversion of guanine to GMP**. The reaction was performed in 100 mM Tris-Cl, pH 8.5, 110 mM $MgCl_2$, 1 mM PRPP, and 60 µM guanine. It was started with the addition of an aliquot of enzyme (to give 7.2 µg/ml) and monitored at 257 nm.

The fact that the amount of guanine is not limiting is shown more clearly in the series of experiments shown in Figure 3.22. In panel A, addition of another 60 µM guanine at approximately 800 s does not result in an increase in activity, which can also be seen in the *insert*. In panel B, an initial amount of 20 µM

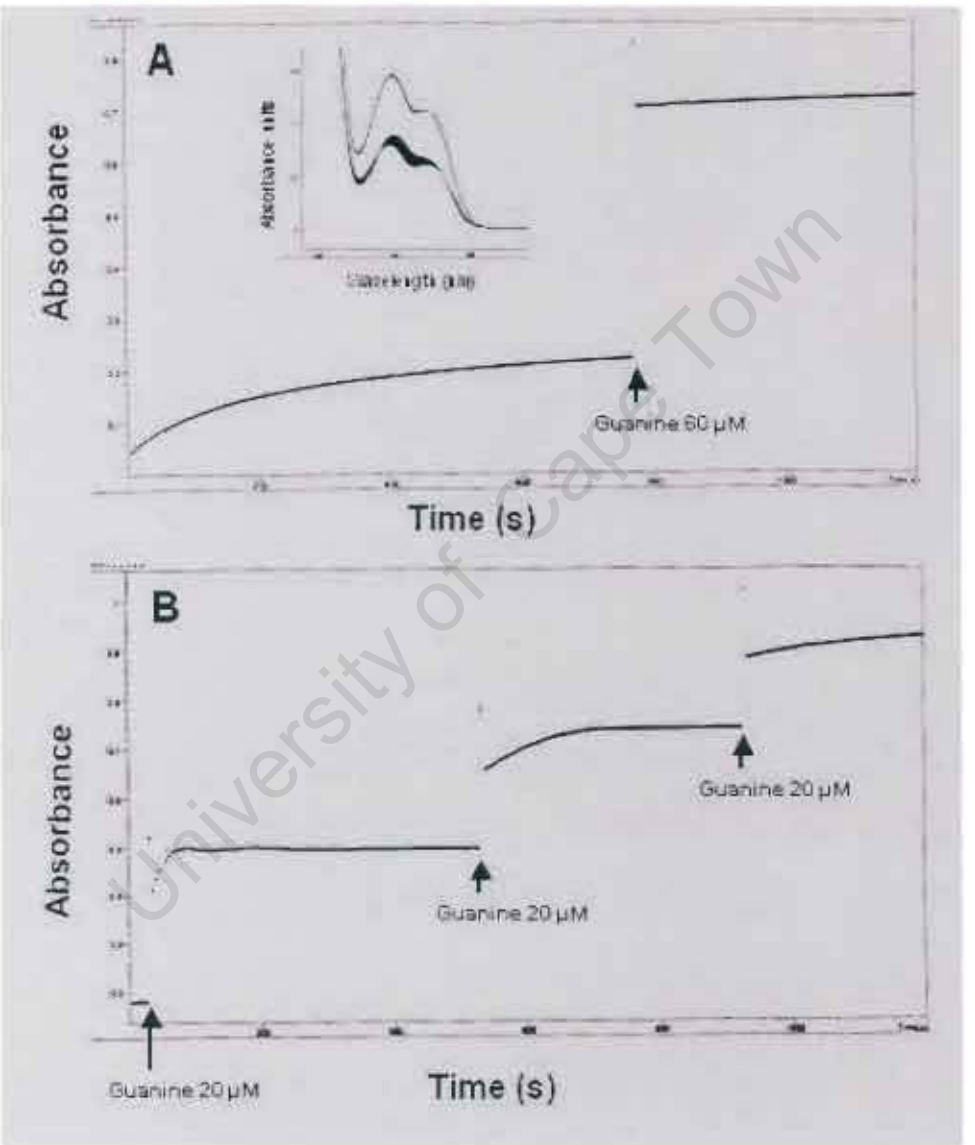

Figure 3.22 **Activity of HGXPRT**. Assays were performed as in Figure 3.21, except that the amount of guanine was variable. In A, 60 µM guanine was present initially, and more added later as shown. Insert: Spectra recorded during the experiment. In B, the additions of guanine are as indicated.

guanine was not sufficient to inactivate the enzyme, as a further addition after about 500 (s) produced detectable activity, but a third addition gave less activity. These results indicate that during enzyme turnover unstable intermediates are formed that decay to an inactive species. Following addition and consumption of 20 μM guanine, the enzyme reverts to the $E.Mg^{2+}PRPP$ complex, which is stable. A further addition results in the generation of unstable species again and inactivation.

The pH and Mg^{2+} dependence of activity is shown in Figure 3.23. Activities were highest at alkaline pH with intermediate Mg^{2+} concentrations. In the 1-30 mM range of concentrations of Mg^{2+}, the pH dependence is apparently biphasic. However, it is not clear whether the lack of activity at pH 5.0 is due to the protonation of catalytically important residues or denaturation, and therefore it is safer to conclude that there is merely activation in the alkaline pH range.

It will be seen later that the chalcone stock solutions are made in DMSO and therefore it was of interest to determine the effect of this organic solvent on HGXPRT activity.

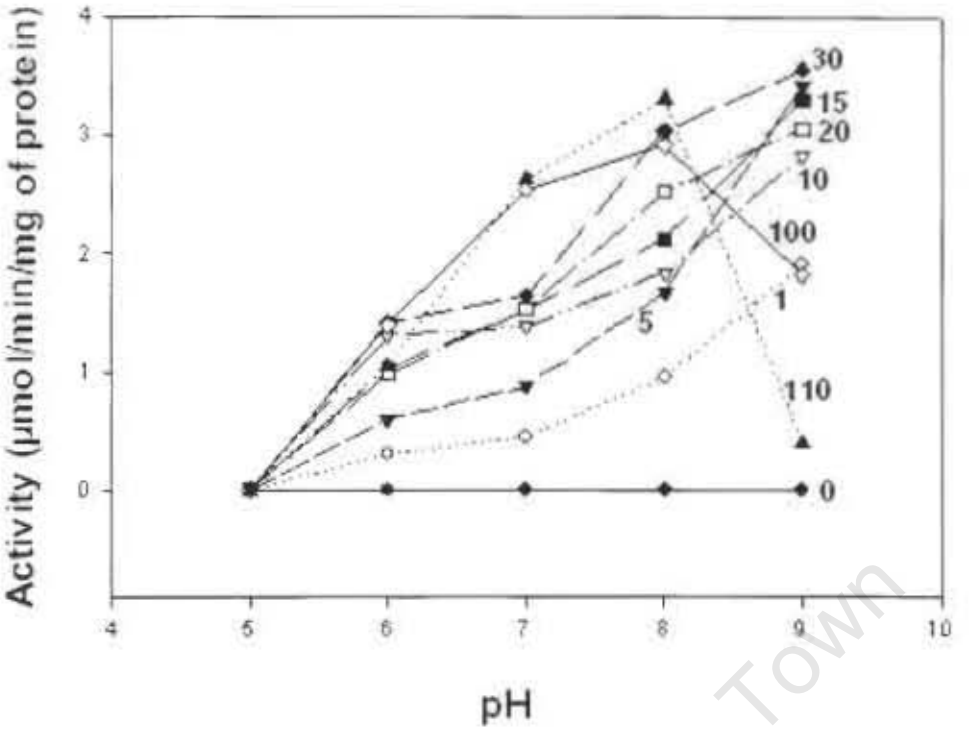

Figure 3.23 **pH and Mg^{2+} dependences of HGXPRT activity**. The assay was performed as in Figure 3.21, except the buffers (100 mM) were as follows: Acetate (pH 5.0), MES (pH 6.0), MOPS (pH 7.0), EPPS (pH 8.0), and CHES (pH 9.0), and the Mg^{2+} concentrations as shown.

Figure 3.24 shows that the effect depended on concentration of PRPP. At 0.2 mM of this substrate, low concentrations activated the enzyme approximately

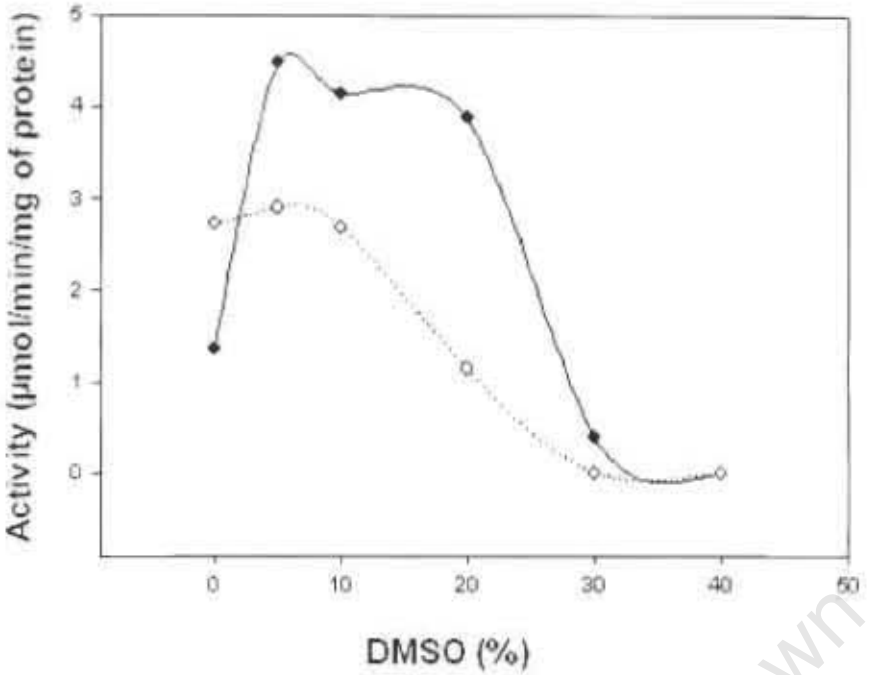

Figure 3.24 **Effect of DMSO on HGXPRT activity**. HGXPRT activity was performed as in Figure 3.21 with 0.2 mM (continuous line, dots) or 1 mM PRPP (open circles, dotted line) with the additions of DMSO shown.

3-fold, and high concentrations were inhibitory. At 1 mM PRPP, the solvent had no effect up until above 10 %, where it became inhibitory. Above 30 % DMSO there was evidence of precipitation, probably MgPRPP. The activation at low PRPP and low DMSO concentration is possibly due to increased formation of the complex Mg_2PRPP from Mg^{2+} and PRPP in the presence of the organic solvent.

Since the malaria HGXPRT bound to the Reactive Red 120 agarose column and was selectively eluted with PPi, it was of interest to determine whether the free dye affected the activity of the enzyme. The results with Reactive Red 120 and Reactive Blue 2 are shown in Figure 3.25. Both dyes are fairly

potent inhibitors of activity, with K_i values in the μM to sub-μM range (see legend for values with and without competition with PRPP).

The structures of the dyes are shown in Figure 3.26.

The binding of the Reactive dyes to HGXPRT was not irreversible (i.e. covalent derivatisation *via* the reactive Cl group) since both could be visibly separated from the protein by SDS-PAGE (results not shown).

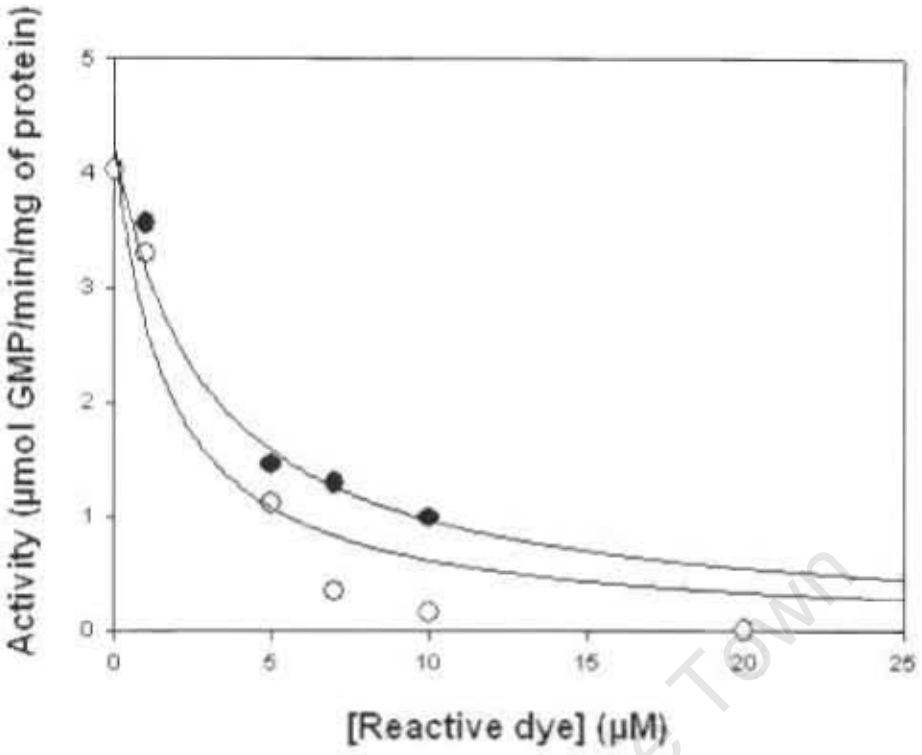

Figure 3.25 **Effect of Reactive dyes on HGXPRT activity**. Assays were performed as in Figure 3.21, with increasing concentrations of Reactive Red 120 (open circles) and Reactive Blue 2 (dots) as indicated. The concentration of HGXPRT was 0.32 µM. The data were fitted to a hyperbolic inhibition curve $y = Yo\ K_{0.5}/(K_{0.5} + S)$, where Y_o is the initial amount of material, $K_{0.5}$ the concentration of inhibitor at half- maximal activity, and S the concentration of inhibitor. The values for $K_{0.5}$ from the best fit of the data are 1.7 µM and 3.0 µM for Reactive Red 120 and Reactive Blue 2, respectively, assuming that the concentration of free dye is equal to the total concentration. This equation assumes that there is no competition between the inhibitor and the substrates. If the Reactive dyes are competing with PRPP for binding to the active site, then the competitive binding equation $K_i = K_{0.5}/(1 + [PRPP]/K_{d(PRPP)})$ takes this into account, and yields K_i = 0.5 µM and 0.8 µM for Reactive Red 120 and Reactive Blue 2 respectively, if $K_d \sim K_{M(PRPP)}$ and K_M is taken as 0.36 mM (Keough *et al.*, 1999) and the concentration of PRPP in the assay is 1 mM.

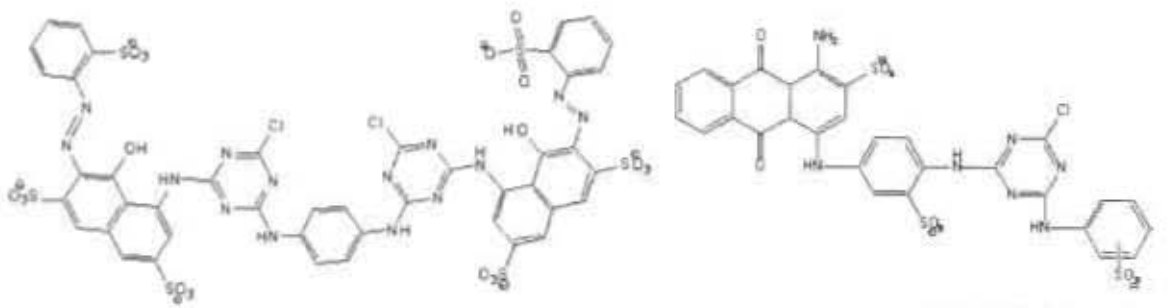

Reactive Red 120

Reactive Blue 2

Figure 3.26 **Structures of the Reactive dyes tested against malaria HGXPRT.**

3.5 Chemical synthesis

3.5.1 Synthesis of (2*E*)-1-(2',6'-dichloro-4'-hydroxyphenyl)-3-(4''-iodophenyl)prop-2-en-1-one

As indicated earlier (see Materials and Methods), synthesis of (2*E*)-1-(2',6'-dichloro-4'-hydroxyphenyl)-3-(4''-iodophenyl)prop-2-en-1-one (**BM 01**) was carried our in four reaction steps. These steps are summarised in scheme 3.1. Compound **1** (obtained from commercial sources) was used to synthesize compounds **2**, **3** and **4**. The final product in the scheme (compound **6**, chalcone, **BM 01**) was synthesized following the linking of compounds **4** and **5** (also obtained from commercial sources). The characerisation data for these products are given in the sections that follow below.

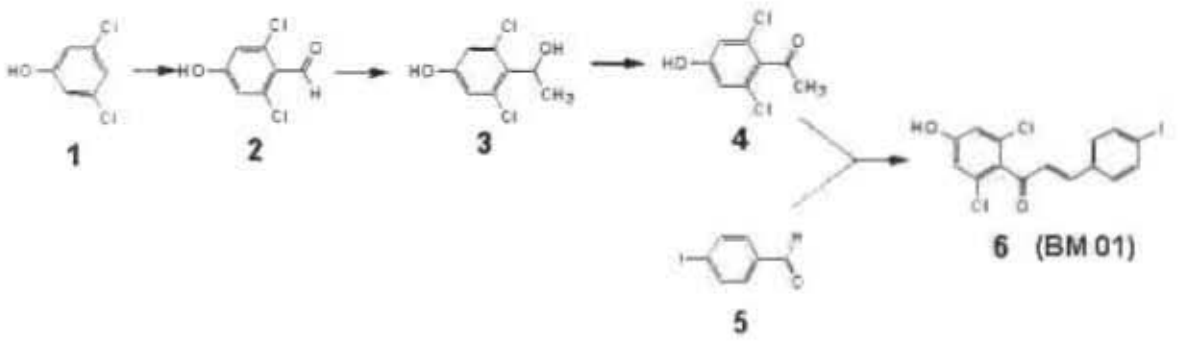

Scheme 3.1 **Summary of reactions leading to synthesis of a dichlorinated chalcone**, (2E)-1-(2',6'-dichloro-4'-hydroxyphenyl)-3-(4"-iodophenyl)prop-2-en-1-one (see text for details).

3.5.1.1 Synthesis of 2,6-dichloro-4-hydroxybenzyaldehyde

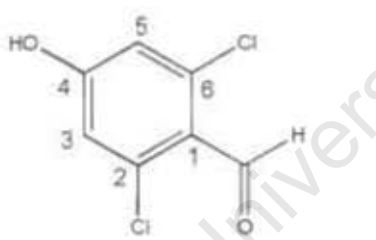

2,6-dichloro-4-hydroxybenzaldehyde

2,6-dichloro-**4**-hydroxybenzyaldehyde (labelled **2** in scheme 3.1) was obtained as yellow crystals in 19 % (205 mg) yield. R_f [20 % (v/v) EtOAc in hexane, 0.14]. Formation of this aldehyde was confirmed by carrying out a ^{1}H NMR (400 MHz, DMSO-d_6); δ_H 10.2 (s, 1H, -CHO), 6.9 (s, 2H, H-3', and H-5') and ^{13}C NMR (400 MHz, DMSO-d_6); δ_C 188 (-CHO), 163 (C-4), 139 (C-2 and C-6), 122 (C-1), 118 (C-3 and C-5).

3.5.1.2 Synthesis of 3,5-dichloro 4-(1'-hydroxyethyl) phenol

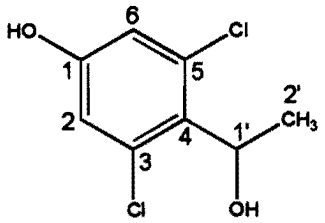

3,5-dichloro-4-(1'-hydroxyethyl)phenol

3,5-dichloro-4-(1'-hydroxy-ethyl)phenol (labelled **3** in scheme 3.1) was obtained as a yellow solid in 50 % (128 mg) yield; R_f [10 % (v/v) MeOH in DCM], 0.48. ^{1}H NMR (400 MHz, acetone-d_6); δ_H 6.8 (s, 2H, H-3, and H-5), 5.5 (q, 1H, J = 8.4, H-1'), 1.5 [d, 3H, J = 8.4, 3(H-2')]. ^{13}C NMR (400 MHz, acetone-d_6); δ_C 127 (C-1), 134 (C-3, and C-5), 129 (C-2'), 117 (C-4), 69 (C-1'), 21 (C-2').

3.5.1.3 Synthesis of 1-(2',6'-dichloro-4'-hydroxyphenyl) ethanone

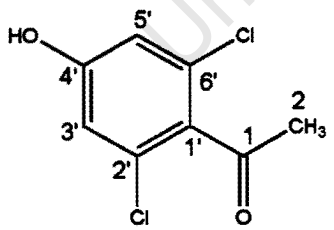

1-(2',6'-dichloro-4'-hydroxyphenyl)ethanone

1-(2',6'-dichloro-4'-hydroxyphenyl)ethanone (labelled **4** in scheme 3.1) was obtained as a cream coloured solid in 47.9 % (54 mg) yield and gave an R_f

[30 % (v/v) EtOAc-hexane, 0.37]. ^{1}H NMR (400 MHz, $CDCl_3$); δ_H 6.8 (s, 2H, H-3' and C-5'), and 2.6 (s, 3H, 3[H-2]).

3.5.1.4 Synthesis of (2*E*)-1-(2',6'-dichloro-4'-hydroxyphenyl)-3-(4"-iodophenyl)prop-2-en-1-one

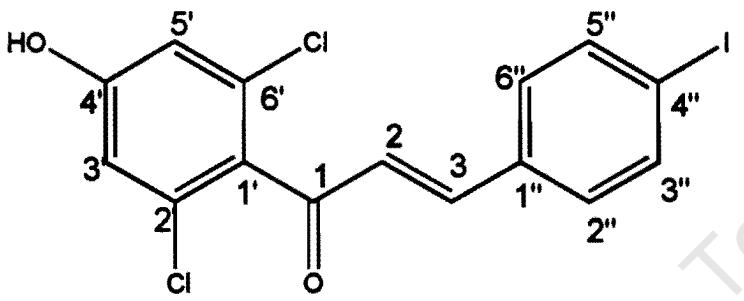

(2*E*)-1-(2',6'-dichloro-4'-hydroxyphenyl)-3-(4"-iodophenyl)prop-2-en-1-one
BM 01

The chalcone product (labelled **6** in scheme 3.1), (2*E*)-1-(2',6'-dichlorophenyl)-3-(4'-iodophenyl)prop-2-en-1-one (**BM 01**), was obtained as cream coloured crystals in yield 53.6 % (54 mg), mp 167-169 ^{0}C. R_f [30% (v/v) EtOAc in hexane], 0.25. ν_{max} (NaCl)/cm^{-1} 3287 (O-H), 3054 (C-H), 1656 (C=O), 1621 (C-C), 1602 (C=C aromatic), and 1260 (C-O). ^{1}H NMR (300 MHz, $CDCl_3$) gave the following peaks: δ_H 7.7 (*d*, 2H, *J* = 8.5, H-3" and H-5"); 7.3 (*d*, 2H, *J* = 8.5, H-2" and C-6"); 7.2 (*d*, 1H, *J* = 16.2, H-2); 6.9 (*d*, 1H, *J* = 16.2, H-3); 6.9 (*s*, 2H, H-3' and H-5'). ^{13}C NMR (300 MHz, $CDCl_3$); δ_C 194 (C1), 157 (C4'), 147 (C3), 138 (C2', C3", C5", C6'), 133 (C1"), 130 (C1'), 123 (C2", C6"), 127 (C2), 115 (C3', C5'), and 98 (C4"). Elemental analysis gave the following results: % C = 43.40, % H = 1.82 (calculated values; % C =

42.99, % H = 2.16, % O = 7.64, % Cl = 16.92, % I = 30.28, Mol. wt 419.0 and Mol. formula $C_{15}H_9Cl_2IO_2$); calculated *m/z* 417.9. Actual MS *m/z* 419.0 $[M+1]^+$.

3.5.2 Synthesis of (2*E*)-1-(2'-hydroxyphenyl)-3-(4"-iodophenyl)prop-2-en-1-one

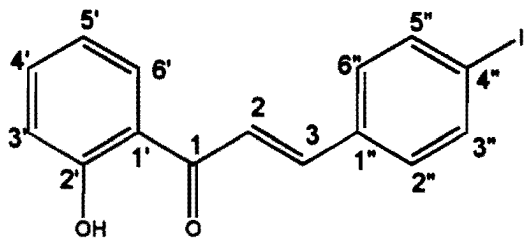

(2*E*)-1-(2'-hydroxyphenyl)-3-(4"-iodophenyl)prop-2-en-1-one
BM 02

The (2*E*)-1-(2'-hydroxyphenyl)-3-(4"-iodophenyl)prop-2-en-1-one (**BM 02**) was obtained as a orange crystals in 45 % (22 mg) yield, R_f [10 % (v/v) EtOAc in hexane, 0.78] and mp 144-146 ^{0}C. ^{1}H NMR (400 MHz, $CDCl_3$) δ_H 12.7 (s, 1H, -OH), 7.9 (dd, 1H, *J* = 1.5 and 7.8, H-6'), 7.8 (d, 1H, *J* = 15.6, H-3), 7.8 (dd, 2H, *J* = 2 and 4, H-2" and H-6"), 7.7 (d, 1H, *J* = 15.6, H-2), 7.5 (m, 1H, H-4'), 7.4 (dd, 2H, *J* = 2 and 4, H-3" and H-5"), 7.0 (dd, 1H, *J* = 1.5 and 7.8, H-3'), and 6.9 (m, 1H, H-5'). ^{13}C NMR (400 MHz, $CDCl_3$); δ_C 194 (C1), 163 (C2'), 144 (C2 and C3), 138 (C3", and C5"), 136 (C5'), 134 (C1"), 130 (C4' and C6'), 129 (C2" and C6"), 120 (C-1'), 116 (C3'), and 98 (C4").

3.5.3 Synthesis of chalcones containing both a nitro group as well as a hydroxyl group in ring A

3.5.3.1 (2*E*)-1-(4'-hydroxy-3'-nitrophenyl)-3-(4"-iodophenyl)prop-2-en-1-one

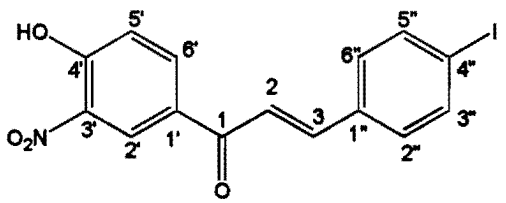

(2*E*)-1-(4'-hydroxy-3'-nitrophenyl)-3-(4"-iodophenyl)prop-2-en-1-one
BM 03

(2*E*)-1-(4'-hydroxy-3'-nitrophenyl)-3-(4"-iodophenyl)prop-2-en-1-one (**BM 03**) was obtained as yellow crystals in 25 % (31 mg) yield, R_f [20 % (v/v) EtOAc in hexane, 0.24] and mp 199 -200 ^{0}C. ν_{max} (NaCl)/cm^{-1} 3273 (O-H), 3055 (C-H), 1663 (C=O), 1597 (C=C aromatic), 1533 (NO_2) and 1240 (C-O). ^{1}H NMR (300 MHz, $CDCl_3$) gave δ_H 8.8 (d, 1H, *J* =2.1, H-2'), 8.3 (dd, 1H, *J* = 2.1 and 6.5, H-6'), 7.81 (d, 1H, *J* = 15.3, H-2), 7.77 (d, 2H, *J* = 8.4, H-2" and H-6"), 7.5 (d, 1H, *J* = 15.3, H-3), 7.4 (d, 2H, *J* = 8.4, H-3" and H-5"), 7.3 (d, 1H, *J* = 6.5, H-5') while ^{13}C NMR (300 MHz, $CDCl_3$) δ_C 186 (C-1), 158 (C-4'), 145 (C-3), 138 (C-6', C-3", and C-5"), 137 (C-3'), 134 (C1"), 130 (C-1'), 129 (C-2', and C-6'), 126 (C-2"), 120 (C-2, and C-5') and 97 (C-4"). Elemental analysis gave the following results: % C = 46.07, % H = 1.83, % N, 3.44 (calculated values; % C = 45.59, % H = 2.55, % I = 32.12, % N = 3.54, % O = 16.20. Mol. wt 395.15 and Mol. formula $C_{15}H_{10}INO_4$); calculated MS *m/z* 394.97. Actual *m/z* 396.0 $[M+1]^+$.

3.5.3.2 (2*E*)-1-(4'-hydroxy-3'-nitrophenyl)-3-(3"-iodophenyl)prop-2-en-1-one

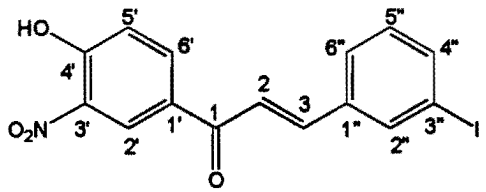

(2*E*)-1-(4'-hydroxy-3'-nitrophenyl)-3-(3"-iodophenyl)prop-2-en-1-one
BM 04

(2*E*)-1-(4'-hydroxy-3'-nitrophenyl)-3-(3"-iodophenyl)prop-2-en-1-one (**BM 04**) was obtained as yellow crystals in 22 % (31 mg) yield. mp 139-140 ^{0}C, R_f [60 % (v/v) EtOAc in hexane, 0.86]. ν_{max} (NaCl)/cm^{-1} 3300 (O-H), 3055 (C-H), 1668 (C=O), 1624 (C=C), 1600 (C=C aromatic), 1541 (NO_2) and 1265 (C-O). This chalcone gave the following ^{1}H NMR (300 MHz, $CDCl_3$); δ_H 10.9 (s, 1H, 4'-OH), 8.8 (d, 1H, *J* = 2.1, H-2'), 8.3 (dd, 1H, *J* = 2.1 and 9.0, H-6'), 8.0 (t, 1H, *J* = 1.8, H-2"), 7.8 (d, 1H, *J* = 15.6, H-3) 7.8 (d, 1H, J = 7.8, H-6"), 7.6 (broad d, 1H, *J* = 7.8, H-4), 7.5 (d, 1H, *J* = 15.6, H-2), 7.3 (d, 1H, *J* = 9, H-5'), and 7.2 (t, 1H, *J* = 7.8, H-5"). ^{13}C NMR ($CDCl_3$, 300 MHz), δ_C 186 (C-1), 158 (C-4'), 144 (C-3), 140 (C-3'), 137 (C-1', C-1" and C-6'), 131 (C-2" and C-4"), 130 (C-5"), 126 (C-6" and C-2'), 121 (C-2) 121 (C-5') and 95 (C-3"). Elemental analysis gave the following results: % C = 46.14, % H = 1.89, % N, 3.42 (calculated values; % C = 45.59, % H = 2.55, % N = 3.54. Mol. wt 395.15 and Mol. formula $C_{15}H_{10}INO_4$), calculated *m/z* 394.97. Actual *m/z* 396.1 $[M+1]^+$.

3.5.3.3 (2*E*)-1-(4'-hydroxy-3'-nitrophenyl)-3-(2"-iodophenyl)prop-2-en-1-one

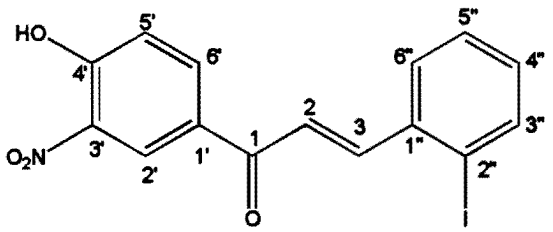

(2*E*)-1-(4'-hydroxy-3'-nitrophenyl)-3-(2"-iodophenyl)prop-2-en-1-one
BM 05

(2*E*)-1-(4'-hydroxy-3'-nitrophenyl)-3-(2"-iodophenyl)prop-2-en-1-one (**BM 05**) chalcone was also obtained as a yellow crystals in 25 % (29 mg) yield R_f [60 % (v/v) EtOAc in hexane, 0.81], and mp 186 -190 ^{0}C. ν_{max} (NaCl)/cm^{-1} 3419 (O-H), 3054 (C-H), 1664 (C=O), 1624 (C=C), 1600 (C=C), 1540 (NO_2) and 1260 (C-O). The ^{1}H NMR (300 MHz, $CDCl_3$): δ_H 10.9 (s, 1H, 4'-OH), 8.8 (d, *J* = 2.4,1H, H-2'), 8.3 (dd, 1H, *J* = 2.4 and 9.0, H-6'), 8.0 (d, 1H, *J* = 15.6, H-3), 7.9 (dd, 1H, *J* = 1.5 and 8.4, H-6"), 7.7 (dd, 1H, *J* = 2.1 and 8.0, H-3"), 7.4 (broad d, 1H, *J* = 7.8, H-4"), 7.3 (d, 1H, H-2, *J* = 15.6) 7.3 (d, 1H, J = 8.7, H-5'), 7.1 (td, 1H, *J* = 1.5 and 7.8, H-5"). ^{13}C NMR ($CDCl_3$, 300 MHz), δ_C 189 (C-1), 158 (C-4'), 149 (C-3), 140 (C-1", C-3"and C-6'), 137 (C-3'), 127 (C-6" and C-5"), 130 (C-4"), 126 (C-2'), 124 (C-2 and C-1'), 120 (C-5'), and 102 (C-2"). Elemental analysis gave the following results: % C = 46.07, % H = 1.98, % N, 3.40 (calculated values; % C = 45.59, % H = 2.55, % N = 3.54. Mol. wt 395.15 and Mol. formula $C_{15}H_{10}INO_4$), calculated MS *m/z* 394.97. Actual MS *m/z* 395.6 $[M+1]^+$.

3.5.4 Synthesis of chalcones containing 2,4,6-trihydroxy groups in ring A

The synthesis of chalcones containing a trihydroxyl moiety was carried out following a sequence of reactions summarized in scheme 3.2 (see Materials and Methods for details). While compounds labelled **2** and **5** were characterised (see below), compound labelled **4** was directly converted to **5** (final chalcone product of this series). The characterisation of type **5** chalcone products as well as the MEM-protected acetophenone (compound labelled **2**) is shown in the sections that follow. Compounds **1** and **3** were obtained from commercial sources.

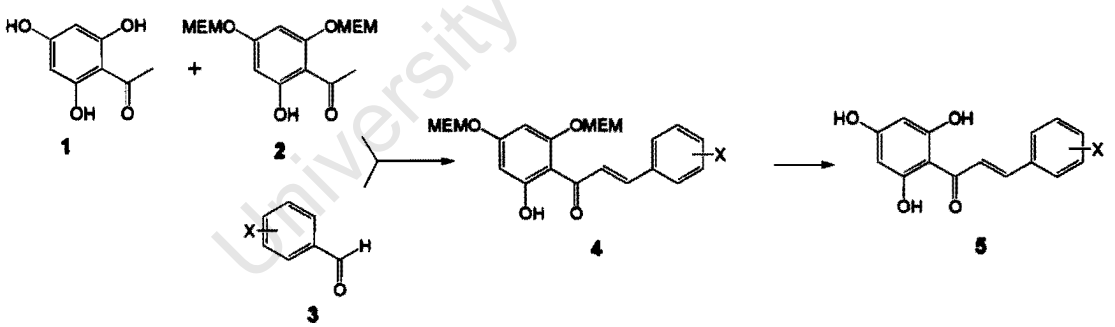

Scheme 3.2 **Sequence of reactions in the synthesis of chalcones containing trihydroxyl moiety.** X stands for a halogen at the *ortho*, *meta*, or *para* position of the benzaldehyde.

3.5.4.1 Protection of 2',4',6'-Trihydroxyacetophenone using methoxyethoxymethoxy chloride (MEM-Cl)

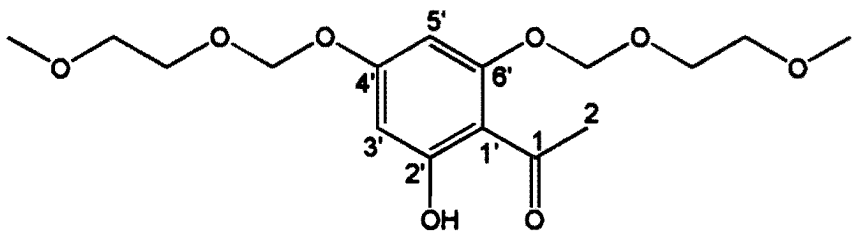

1-{2'-hydroxy-4',6'-bis[(2-methoxyethoxy)methox]phenyl}ethanone

Or simply,

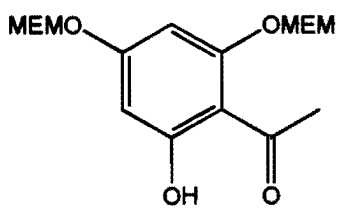

DiMEM protected 2',4',6'-trihydroxyacetophenone (compound **2** in scheme 3.2) was obtained as a clear oil in 83 % (90 mg) yield. ^{1}H NMR analysis (300 MHz; $CDCl_3$ solvent); δ_H 6.2 (s, 2H, H-3' and H-5'), 5.3 (s, 2H, Ar-OCH_2-), 5.2 (s, 2H, Ar-OCH_2-), 3.8 [m, 4H, -$O(CH_2)_2$-], 3.6 [m, 4H, -$O(CH_2)_2$-], 3.4 (s, 3H, -OCH_3), 3.3 (s, 3H, -OCH_3), 2.6 (s, 3H, 3[H-2]).

3.5.4.2 Synthesis of (2*E*)-3-(4"-iodophenyl)-1-(2',4',6'-trihydroxyphenyl)prop-2-en-1-one (4"-I-chalcone)

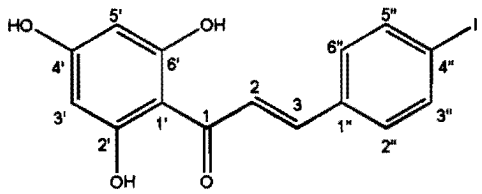

(2*E*)-3-(4"-iodophenyl)-1-(2',4',6'-trihydroxyphenyl)prop-2-en-1-one
BM 06

[(2*E*)-3-(4"-iodophenyl)-1-(2',4',6'-trihydroxyphenyl)prop-2-en-1-one] also referred to as 4"-I-chalcone (**BM 06**) was obtained as a yellow powder in 83 % (31 mg) yield, R_f [50 % (v/v) EtOAc, 0.41] and mp 189 - 190 ^{0}C. The ^{1}H NMR (400 MHz, acetone-d_6); δ_H 8.2 (d, 1H, J = 15.6, H-3), 7.8 (d, 2H, J = 8.3, H-2" and H-6"), 7.7 (d, 1H, J = 15.6, H-2), 7.5 (d, 2H, J = 8.3, H-3" and H-5"), 5.9 (s, 2H, H-3' and H-5').

3.5.4.3 Synthesis of (2*E*)-3-(3"-iodophenyl)-1-(2',4',6'-trihydroxyphenyl)prop-2-en-1-one (3"-I-chalcone)

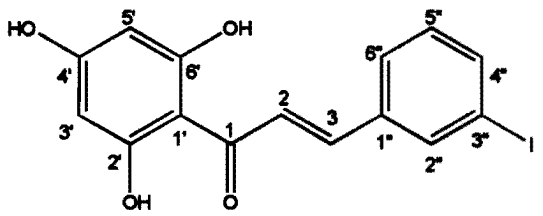

(2*E*)-3-(3"-iodophenyl)-1-(2',4',6'-trihydroxyphenyl)prop-2-en-1-one
BM 07

[(2*E*)-3-(3"-iodophenyl)-1-(2',4',6'-trihydroxyphenyl)prop-2-en-1-one] or 3"-I-chalcone (**BM 07**) was also obtained as orange crystals in 49 % (27 mg) yield, R_f [50 % (v/v) EtOAc in hexane, 0.52] and mp 95 - 98 ^{0}C. ν_{max} (KBr)/cm^{-1} 3100 (O-H), 1631 (C=O), and 1218 (C-O). ^{1}H NMR (300 MHz, acetone-d_6); δ_H 8.2 (d, 1H, J = 15.6, H-3), 8.0 (t, 1H, J = 1.5, H-2"), 7.7 (dd, 1H, J = 8.1 and 1, H-4"), 7.7 (dd, 1H, J = 8.1 and 1, H-6"), 7.6 (d, 1H, J = 15.6, H-2), 7.2 (t, 1H, J = 8.1, H-5"), 5.9 (s, 2H, H-3' and H-5'). ^{13}C NMR (300 MHz, acetone-d_6); δ_C 186 (C-1), 166 (C-6'), 158 (C-4'), 158 (C-3), 140 (C-1'), 139 (C-1"), 137 (C-2", C-4", and C-5"), 126 (C-2' and C-6"), 120 (C-2) 104 (C-3'), and 95 (C-3" and C-5'). Elemental analysis gave the following results; % C = 45.14 and % H = 2.96 (calculated values; % C = 47.14, % H = 2.90. Mol. wt 382.15 and Mol. formula $C_{15}H_{11}IO_4$); calculated MS *m/z* 381.97 $[M]^+$. Actual MS *m/z* 382.8 $[M+1]^+$. From elemental analysis, expected molecular weight is 17 units higher than actual. A water molecule (18 MW) accounts for this difference. Hence, actual molecular formula is $C_{15}H_{11}IO_4.H_2O$.

3.5.4.4 Synthesis of (2*E*)-3-(2"-iodophenyl)-1-(2',4',6'-trihydroxyphenyl)prop-2-en-1-one (2"-I-chalcone)

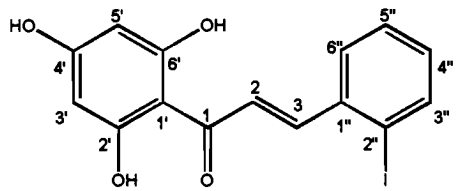

(2*E*)-3-(2"-iodophenyl)-1-(2',4',6'-trihydroxyphenyl)prop-2-en-1-one
BM 08

[(2*E*)-3-(2"-iodophenyl)-1-(2',4',6'-trihydroxyphenyl)prop-2-en-1-one] or 2"-I-chalcone (**BM 08**) was obtained as yellow crystals in 55 % (21 mg) yield, R_f [50 % (v/v) EtOAc in hexane, 0.41] and mp 157 - 159 ^{0}C. ν_{max} (KBr)/cm^{-1} 3100 (O-H), 1620 (C=O), and 1268 (C-O). ^{1}H NMR (400 MHz, acetone-d_6); δ_H 8.1 (d, 1H, *J* =15.6, H-3), 8.0 (dd, 1H, *J* = 1.2 and 8, H-3"), 8.0 (d, 1H, *J* = 15.6, H-2), 7.8 (dd, 1H, *J* = 1.6 and 8, H-6"), 7.5 (t, 1H, *J* = 8, H-5"), 7.2 (td, 1H, *J* = 1.6 and 8, H-4"), 6 (s, 2H, H-3' and H-5'). ^{13}C NMR (400 MHz, acetone-d_6); δ_C 205 (C-1), 166 (C-2', C-4' and C-6'), 144 (C-3), 140 (C-1"), 129 (C-4", and C-6"), 128 (C-2, C-3" and C-5"), 97 (C-1', C-3' and C-5') and 95 (C-2"). Elemental analysis gave the following results; % C = 47.95 and % H = 3.11 (calculated values; % C = 47.14, % H = 2.90. Mol. wt 382.15 and Mol. formula $C_{15}H_{11}IO_4$); calculated MS *m/z* 381.97 $[M]^+$. Actual MS *m/z* 382.6 $[M+1]^+$.

3.5.4.5 Synthesis of (2*E*)-3-(4"-chlorophenyl)-1-(2',4',6'-trihydroxyphenyl)prop-2-en-1-one (4"-Cl-chalcone)

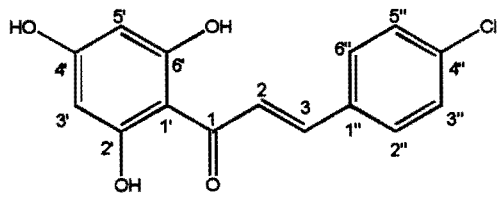

(2*E*)-3-(4"-chlorophenyl)-1-(2',4',6'-trihydroxyphenyl)prop-2-en-1-one
BM 09

[(2*E*)-3-(4"-chlorophenyl)-1-(2',4',6'-trihydroxyphenyl)prop-2-en-1-one] or 4"-Cl-chalcone was obtained as yellow crystals in 72 % (21 mg) yield; R_f [50 % (v/v) EtOAc in hexane, 0.37], mp 157 - 158 ^{0}C. The H NMR (acetone-d_6 solvent, 400 MHz); δ_H 8.2 (d, 1H, J = 15.3, H-3), 7.7 (d, 1H, J = 15.3, H-2), 7.6 (d, 2H, J = 8.3, H-3" and H-5"), 7.4 (d, 2H, J = 8.3, H-2" and H-6"), 5.9 (s, H-3' and H-5').

3.5.4.6 Synthesis of (2*E*)-3-(4"-bromophenyl)-1-(2',4'6'-trihydroxyphenyl)prop-2-en-1-one (4"-Br-chalcone)

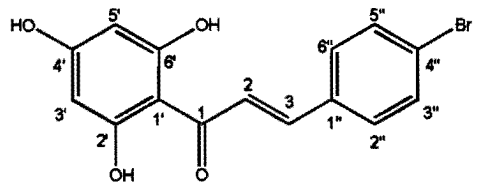

(2*E*)-3-(4"-bromophenyl)-1-(2',4',6'-trihydroxyphenyl)prop-2-en-1-one
BM 10

[(2*E*)-3-(4"-bromophenyl)-1-(2',4',6'-trihydroxyphenyl)prop-2-en-1-one] or 4-Br-chalcone (**BM 10**) was also obtained as a yellow solid in 64 % (31 mg) yield. R_f [50 % (v/v) EtOAc in hexane, 0.49], mp 160 - 164 ^{0}C. ^{1}H NMR analysis (acetone-d_6 solvent, 400 MHz); δ_H 8.3 (d, 1H, J = 15.6, H-3), 7.7 (d, 1H, J = 15.6, H-2), 7.6 (m, 4H, H-2", H-3", H-5" and H-6"), 6.0 (s, H-3' and H-5').

3.6 Attempted synthesis of other chalcones

An attempt at synthesizing other chalcones [(2*E*)-1-(2',6'-difluoro-4'-hydroxyphenyl)-3-(4"-iodophenyl)prop-2-en-1-one and (2*E*)-3-(4"-iodophenyl-1-(2'-nitrophenyl)prop-2-en-1-one] was made, see structures in Figure 3.27. The attempted synthesis of the difluorinated chalcone was to be carried out in the same way as described for the dichlorinated chalcone following the retrosynthetic scheme given in Figure 1.22. However, in the case of the

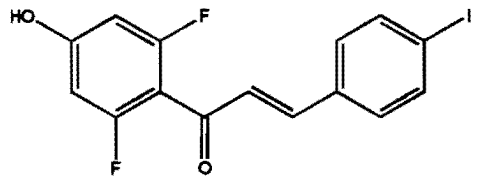

(2*E*)-1-(2',6'-difluoro-4'-hydroxyphenyl)-3-(4''-iodophenyl) prop-2-en-1-one

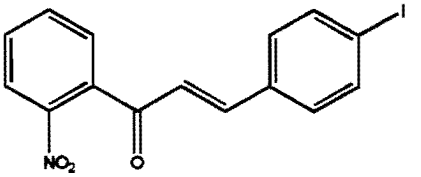

(2*E*)-3-(4''-iodophenyl)-1-(2'-nitrophenyl)prop-2-en-1-one

Figure 3.27 **Structures and names of other chalcones for which synthesis was attempted.**

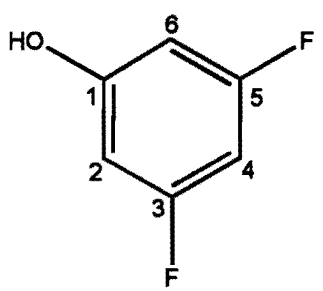

3,5-difluorophenol

difluorinated chalcone, the Reimer-Tiemann reaction conditions (see section 1.6.2.1) could not generate the required benzaldehyde. Instead of the expected 2',6'-difluoro-4'-hydroxybenzaldehyde, analogous to the 2',6'-dichloro-4'-hydroxybenzaldehyde, only the 3,5-difluorophenol (starting material, see structure above) was obtained as identified by TLC and ^{1}H NMR at the end of this reaction. The ^{1}H NMR analysis was identical with that of the commercial product, 3,5-difluorophenol; ($CDCl_3$ solvent, 300 MHz), δ_H 6.4 (m, 3H, H-2, H-4, H-6). The aldehyde proton, which is supposed to be a key spectroscopic indicator for the formation of the benzaldehyde, was absent in the ^{1}H NMR spectra. The strongly electron withdrawing nature of fluorine in

the 3,5-difluorophenol may be a reason for the failed Reimann-Tiemann reaction in this case (see mechanism in Figure 1.24).

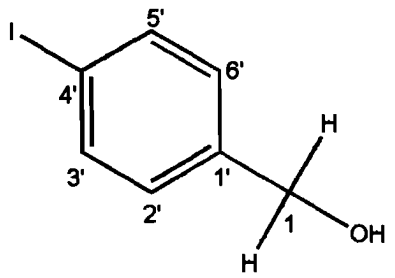

(4'-iodophenyl)methanol

Synthesis of the chalcone containing a nitro group at position 2' in ring A (see Figure 3.27) yielded a Cannizzaro reaction product. Instead of the Claisen-Schmidt reaction product (following the retrosynthetic scheme given in Figure 1.21), the benzaldehyde underwent a reduction to form a primary alcohol (4-iodophenyl)methanol, see structure above). The ^{1}H NMR ($CDCl_3$ solvent, 300 MHz) analysis of the reaction product gave the following: δ_H 7.7 (d, 2H, J = 8.4, H-2', H-6'), 7.11 (d, 2H, J = 8.4, H-3', H-5'), and 4.6 (s, 2H, 2[H-1]). This NMR spectral data is consistent with that of the 4-iodobenzaldehyde that has been reduced to a primary alcohol. One possible reason for this reaction occurring instead of the desired Claisen-Schmidt one, is that the base (KOH) used to carry out the reaction was too strong (see section 1.6.1). It ought to be pointed out however that this benzaldehyde was used successfully in the synthesis of several other chalcones using the same conditions (see sections 3.5.1.4 to 3.5.4.2 for examples).

Another possibility is that the strongly electron-withdrawing nitro group, which is in close proximity, renders the enolate generated poorly reactive. The extended conjugation (Figure 3.28) facilitates the electron-withdrawal by the nitro group. The poor reactivity of the enolate presumably makes the Cannizzaro reaction competitive to the Claisen-Schmidt.

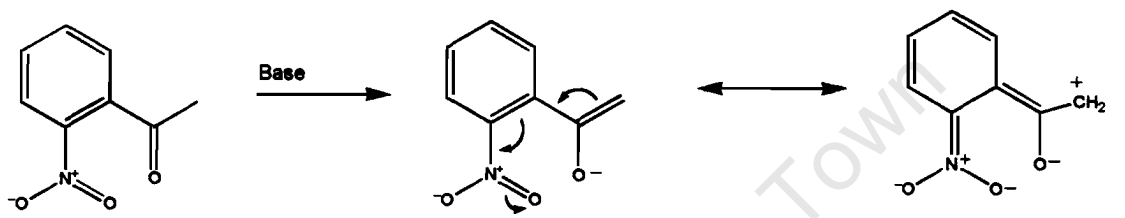

Figure 3.28 **Base initiated conjugation of enolate double bond with nitro group.**

3.7.0 Drug targeting

3.7.1 Effect of chalcones on HGXPRT activity

The effect of increasing concentrations of the various chalcones [see structures in Figure 3.29 (a) and (b)] on HGXPRT activity is shown in Figure 3.30. In addition to the chalcones synthesised, 4 chalcones (extracted from natural sources) obtained from University of Botswana were also tested. Two of these are somewhat similar to those synthesised and are included in Figure 3.31. The other two are fused chalcones and the results are shown in Figure 3.32.

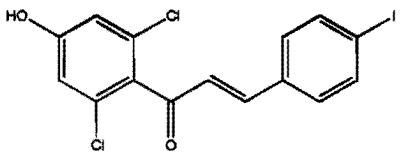

(2*E*)-1-(2',6'-dichloro-4'-hydroxyphenyl)-3-(4''-iodophenyl)prop-2-en-1-one
(BM 01)

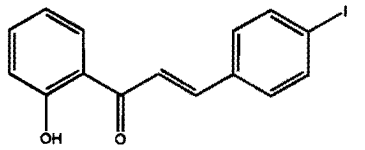

(2*E*)-1-(2'-hydroxyphenyl)-3-(4''-iodophenyl)prop-2-en-1-one
(BM 02)

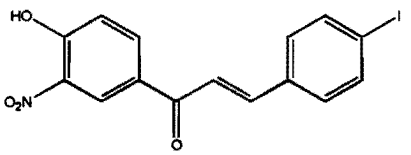

(2*E*)-1-(4'-hydroxy-3'-nitrophenyl)-3-(4''-iodophenyl)prop-2-en-1-one
(BM 03)

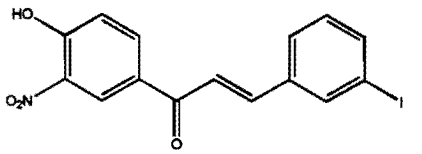

(2*E*)-1-(4'-hydroxy-3'-nitrophenyl)-3-(3''-iodophenyl)prop-2-en-1-one
(BM 04)

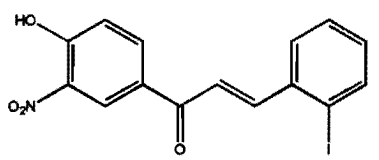

(2*E*)-1-(4'-hydroxy-3'-nitrophenyl)-3-(2''-iodophenyl)prop-2-en-1-one
(BM 05)

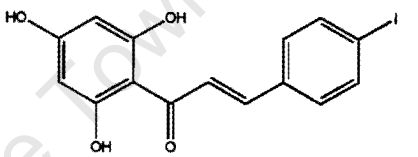

(2*E*)-3-(4''-iodophenyl)-1-(2',4',6'-trihydroxyphenyl)prop-2-en-1-one
(BM 06)

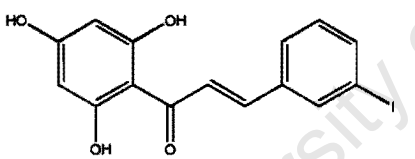

(2*E*)-3-(3''-iodophenyl)-1-(2',4',6'-trihydroxyphenyl)prop-2-en-1-one
(BM 07)

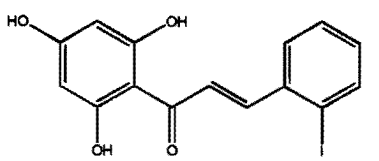

(2*E*)-3-(2''-iodophenyl)-1-(2',4',6'-trihydroxyphenyl)prop-2-en-1-one
(BM 08)

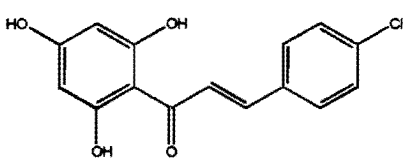

(2*E*)-3-(4''-chlorophenyl)-1-(2',4',6'-trihydroxyphenyl)prop-2-en-1-one
(BM 09)

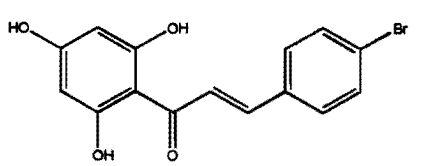

(2*E*)-3-(4''-bromophenyl)-1-(2',4',6'-trihydroxyphenyl)prop-2-en-1-one
(BM 10)

Figure 3.29 (a) **Structures, names and codes of the chalcones that were synthesized**.

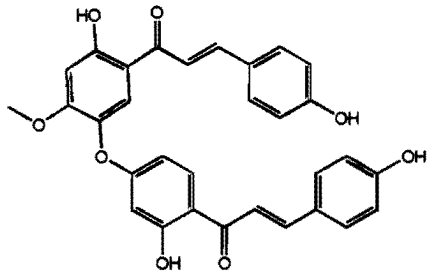

RHPR28-1

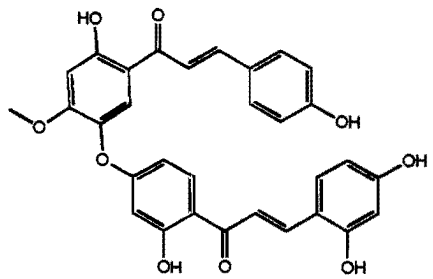

RHPR17-1

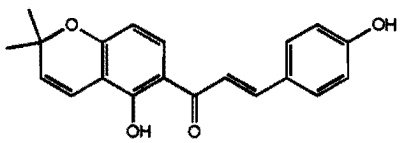

4-hydroxylonchocarpin

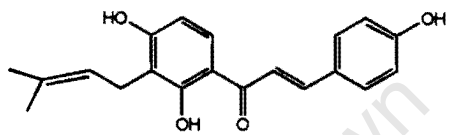

Isobavachalcone

Figure 3.29(b) **Structures, names (and/or codes) of the chalcones (extracted from natural sources) that were obtained from the University of Botswana.**

Only the 4''-I-, 4-Br''- and 4-Cl''-chalcones (**BM 06**, **BM 09** and **BM 10** respectively) showed significant acceleration of catalytic turnover, up to 2.5 fold. The concentration of half maximal effect is approximately the same for the three chalcones at ~10 μM. There seemed to be a small effect of the (*2E*)-1-(4'-hydroxy-3'-nitrophenyl)-3-(4''-iodophenyl)prop-2-en-1-one (**BM 03**). The experiment was repeated with 3 other preparations of HGXPRT at 30 μM chalcone and similar results were obtained.

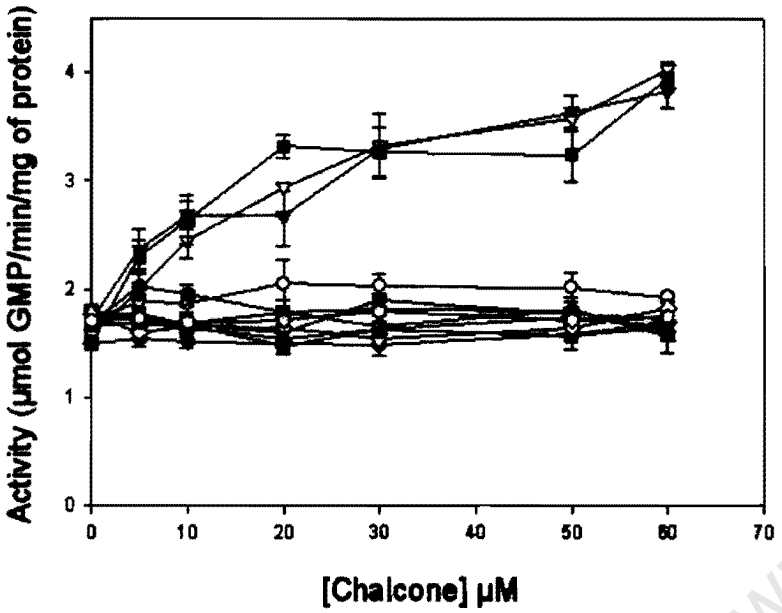

Figure 3.30 **Effect of chalcones on HGXPRT activity**. The assay conditions were 100 mM Tris-Cl, pH 8.5, 30 mM $MgCl_2$, 1 mM PRPP, 60 µM guanine, 0 - 60 µM chalcone as indicated, and 7 µg HGXPRT/ml at room temperature. The reaction was started with a small aliquot of protein and the initial rate determined. Each data point represents mean +/- SEM (n = 4). The identity of the chalcones [structures provided in Figure 3.29 (a) and (b)] is as follows:

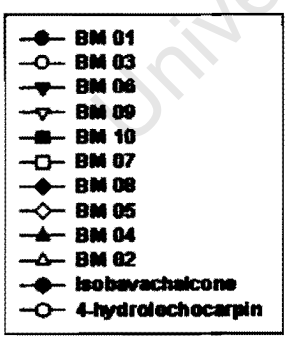

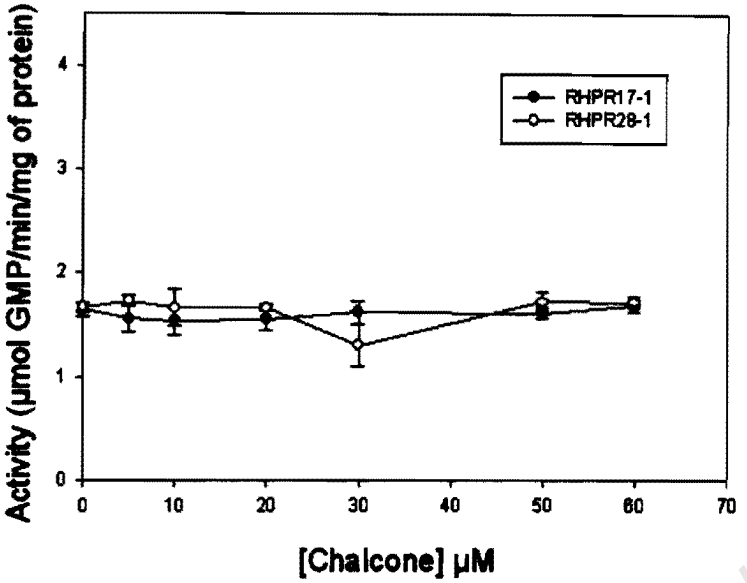

Figure 3.31. **Effect of fused chalcones on HGXPRT activity.** The assay conditions are the same as in Figure 3.30. The data points are mean +/-SEM (n = 4). The code names for the chalcones are provided in the box and their structures are in Figure 3.29 (b).

3.7.2 Attempts to alter the rate-limiting step and effect of chalcones

The main rate-limiting step in the catalytic cycle of human HGPRT has been found to be release of nucleotide (Xu *et al.*, 1997), but it is not known for the malaria enzyme. The identity of the particular step that slows catalysis has implications for the nature of the accelerating site and the underlying mechanism. The true catalytic acceleration of turnover provided by the chalcones may also be obscured due to rate-limitation being spread over several steps. In order to probe these possibilities, we attempted to change

the rate-limiting step(s) through changing pH and divalent cation cofactor. For example, in the latter case, if the chemical interconversion was slowed significantly, and acceleration by the chalcones persisted, then the chalcone binding site had to be located outside of the catalytic site.

3.7.2.1 Varying pH

It has been shown above (Figure 3.23) that malaria HGPRT was increasingly more active as the pH became more alkaline (pH 6 to 9). It was therefore of interest, as indicated above, to determine if the accelerating effect of the chalcones persisted in the low pH range. Table 3.4 shows results of including the chalcones in assays at pH 6 compared with at pH 9. Even though limited experiments were performed (no repeats) all three chalcones seemed to exhibit a similar activating effect at both pHs.

Table 3.4 **Effect of chalcones on activity at pH 6 and 9.** The assay was performed in either 100 mM MES or 100 mM CHES, at pH 6.0 and 9.0 respectively, 30 mM $MgCl_2$, 30 µM chalcone, 1 mM PRPP, and 60 µM guanine at room temperature. Structures of the chalcones are given in Figure 3.29.

Chalcone (30 µM)	**Activity (µmol GMP/min/mg of protein)**	
	pH 6	**pH 9**
Control (no chalcone)	0.6	1.2
4"-I-chalcone (or **BM 06**)	0.9	2.0
4"-Cl-chalcone (or **BM 09**)	1.1	2.0
4"-Br-chalcone (or **BM 10**)	0.8	1.8

3.7.2.2 Varying divalent cation cofactor

When Mg^{2+} was replaced with other divalent metal ions (Mn^{2+}, Ca^{2+}, and Sr^{2+}) in the reaction assay, concentrations higher than 1 mM resulted in problems with precipitation, and therefore 1 mM was chosen. As shown in Figure 3.32, no activity was detectable in the absence of added divalent cations. In 1 mM Mg^{2+}, the two halogenated chalcones (**BM 06** and **BM 09**) examined provided approximately 2-fold acceleration, close to what was observed at 30 mM. The activity in Mn^{2+} was identical to that of Mg^{2+}, but the in presence of chalcones

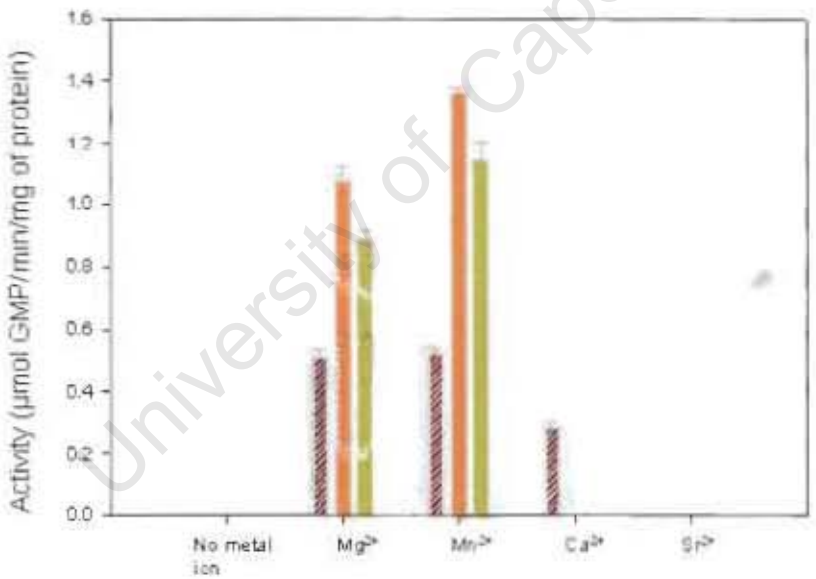

Figure 3.32. **Effect of divalent cations and accelerating chalcones on HGXPRT activity.** The assay conditions were 100 mM Tris-Cl, pH 8.5, 1 mM divalent cation as indicated, without (brown bar) or with 60 µM 4'-Cl-chalcone **BM 09** (orange bar) or 4'-I-chalcone **BM 06** (green bar), 1 mM PRPP, 60 µM guanine, and 0.014 mg HGXPRT/ml at room temperature. The concentrated enzyme was first dialysed in 10 mM MOPS, pH 7.0, to remove Pi, and converted to the active form by overnight incubation with PRPP + hypoxanthine. The values are mean +/- SEM (n = 4). In the cases where no bar is indicated the activity was zero.

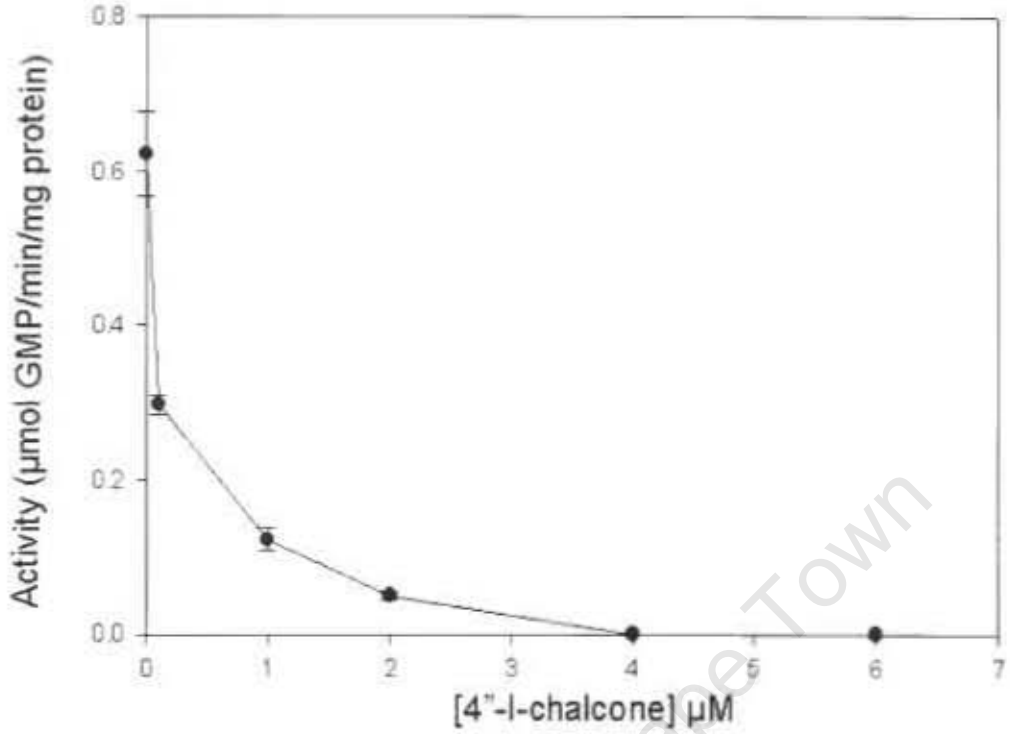

Figure 3.33 **Inhibition of malaria HGXPRT in 1 mM Ca^{2+}**. The enzyme was dialysed in MOPS, pH 7.0 as described in Figure 3.32. The assay was carried out in 100 mM Tris-Cl, pH 8.5, 1 mM $CaCl_2$, 1 mM PRPP, 30 µM guanine, variable 4''-I-chalcone (**BM 06**) as indicated, and 0.014 mg/mL protein (0.53 µM monomer HGXPRT) at room temperature. The data shows the mean +/- SEM (n=4) and was also fit to standard binding algorithm to yield IC_{50} = 0.11 µM. Note that total chalcone concentration is plotted on the x-axis and the concentration of enzyme is 0.53 µM monomer. Thus the $K_{0.5}$ would be lower if free chalcone concentration (the appropriate parameter) could be plotted. If the binding is competitive with PRPP, then this also needs to be taken into consideration using the competitive binding equation (McIntosh *et al.*, 1996), $K_{d(chalcone)} = K_{0.5(chalcone)}/\{1 + ([PRPP]/K_{d(PRPP)})\}$. With the above reservation about $K_{0.5}$, and assuming $K_{d(PRPP)} \sim K_{M(PRPP)}$, and the latter is similar in Ca^{2+} as Mg^{2+} (0.36 mM Keough *et al.*, 1999), then $K_{d(chalcone)}$ = 0.029 µM. If $K_{d(chalcone)} = K_{M(PRPP)}/50$ as it is for the human enzyme with guanine as substrate (Xu *et al.*, 1997), then $K_{d(chalcone)}$ = 0.8 nM.

(**BM 06** and **BM 09**), significant activation was observed. The activity in 1 mM Ca^{2+} was about half but the chalcones (**BM 06, BM 09,** and **BM 10**) unexpectedly completely inhibited this. There was no activity with 1 mM Sr^{2+}.

The inhibition by the chalcones in Ca^{2+} was investigated further. Figure 3.34 shows the inhibition by **BM 06** in 1 mM Ca^{2+}, which yielded an IC_{50} of 0.11 µM, when total chalcone concentration is plotted on the x-axis. It should be noted that the concentration of HGXPRT was in this range as well (0.53 µM monomer, not all of which may be active), and essentially the protein is being titrated. The $K_{0.5}$ (obtained when free chalcone is plotted on the x-axis) would be lower than the IC_{50}. If competition with PRPP is occurring, then this needs to be taken into account to provide a K_d. This value could be extremely low, as the K_d may be much lower than the K_M (0.36 mM, Keough *et al.*, 1999) – it is 50-fold lower for the human enzyme (Xu *et al.*, 1997). For example, if a value of 0.11 µM is taken as an indication of the $K_{0.5}$, then the K_d works out to be 0.8 nM, if competition with PRPP is occurring and the above parameters are incorporated (see Figure 3.34 for equations and calculations).

Importantly, chalcones that do not accelerate the rate of turnover in the presence of Mg^{2+}, such as **BM 07**, **BM 08**, and **BM 01**, showed no inhibition of activity in 1 mM Ca^{2+} (results not shown).

3.7.3 Effect of chalcones on transition from inactive to active HGXPRT

The above experiments demonstrated that, in the presence of Ca^{2+}, and under turnover conditions, the critical chalcones (**BM 06**, **BM 09** and **BM 10**) bound tightly to HGXPRT. The importance of the divalent cation identity and the fact that such cations are only known to bind at the catalytic site, strongly suggests that the chalcones bind at this site. Another possible way of monitoring binding to the catalytic site may be through the requirement for substrate binding to convert the isolated inactive HGXPRT to an active form. Here activation normally requires preincubation with either Mg^{2+} + PRPP or PRPP + hypoxanthine, as seen above in Section 3.4. If the chalcones compete with PRPP or hypoxanthine, they could either inhibit or substitute for the substrates in the activation process. Such an experiment is shown in Table 3.5, where a preincubation under certain conditions is performed, and then the enzyme assayed for activity in high concentrations of Mg^{2+} following a large dilution of the protein, in order to reduce the effect of possible inhibition during the assay from Ca^{2+} + chalcone. Under our two standard activating conditions the activity was changed from zero to 1.2 µmol GMP/min/mg of protein for this particular preparation (rows 1, 2 and 9). Substituting **BM 06** for PRPP in Mg^{2+} gave good activation (row 3). Addition of this chalcone with Mg^{2+} and PRPP gave a similar result (row 4). Ca^{2+} (1 mM) could not substitute for Mg^{2+} in the activation with PRPP (row 5). However, addition of chalcone with Ca^{2+} and PRPP produced activation (row6). Prior incubation with Ca^{2+} + **BM 06** for 30 min followed by Mg^{2+} +

Table 3.5 **Activation of malaria HGXPRT**. HGXPRT (1.4 mg of protein/ ml, 53 μM monomer concentration) was pre-incubated as indicated on ice for 16 h, after which aliquots were diluted 100-fold into the assay medium of 100 mM Tris-Cl, pH 8.5, 110 mM $MgCl_2$, 1 mM PRPP and 60 μM guanine and the initial activities measured. Structures of the chalcones are in Figure 3.29.

Row	Pre-incubation conditions	Activity (μmol GMP/min/mg protein)
1	HGXPRT alone	No detectable activity
2	10 mM Mg^{2+} + 1 mM PRPP	1.2
3	10 mM Mg^{2+} + 60 μM **BM 06**	1.9
4	10 mM Mg^{2+} + 60 μM **BM 06** + 1 mM PRPP	1.7
5	1 mM Ca^{2+} + 1 mM PRPP	<0.3
6	1 mM Ca^{2+} + 60 μM **BM 06** + PRPP	1.1
7	1 mM Ca^{2+} + 60 μM **BM 06** for 30 min, then added 1 mM PRPP + 10 mM Mg^{2+}	1.6
8	1 mM Ca^{2+} + 60 μM **BM 06**	1.3
9	60 μM Hx + 1 mM PRPP	1.2
10	60 μM Hx + 1 mM PRPP + 1 mM EDTA	No detectable activity
11	60 μM Hx + 1 mM PRPP + 1 mM EGTA	1.1
12	60 μM Hx + 60 μM **BM 06**	0.74
13	60 μM Hx + 60 μM **BM 06** + 1 mM EDTA	1.2
14	60 μM **BM 06**	1.2
15	60 μM Hx + 60 μM **BM 01**	No detectable activity

PRPP, also resulted in activation, showing that the Ca^{2+}-chalcone did not covalently modify the protein in an inhibitory manner (row 7). A surprising result was that Ca^{2+} + **BM 06** alone provided activation (row 8). EDTA destroyed the activating effect of hypoxanthine and PRPP (row 10), suggesting the presence and a requirement for contaminating divalent cations. EGTA was not effective, further suggesting Mg^{2+} is the most important cation (row 11). Activation was also achieved with hypoxanthine and **BM 06**, or **BM 06** alone, in a manner that did not require divalent cations (row 12, 13, and 14). A non-accelerating chalcone (**BM 01**) plus hypoxanthine failed to activate (row 15).

These results demonstrate that the **BM 06** mimics PRPP in activation, but, contrary to PRPP, does so both in Ca^{2+} and in the absence of divalent cations.

Chapter 4 Discussion

4.1 Molecular biology aspects

The construction of a recombinant pET-17b with the gene for malaria HGXPRT was successfully carried out. The malaria HGXPRT cDNA was excised from recombinant pET-15b using *Nde* 1 and *Bam* H1 and inserted into pET-17b that had been cut by the same enzymes. Problems were experienced with plasmid extraction and different methods of isolating the plasmid were tried, including a silica-binding method. However, the standard and faster isopropanol precipitation eventually worked the best. We think that initially there were problems with removing all of the 70 % ethanol in the final wash, which may have had an effect on the activity of the restriction enzymes. Ligation of the insert into the pET-17b vector also gave trouble. A procedure that eventually worked was to combine the agarose cut-outs of insert and vector, with the former DNA in excess over the latter, and extract together in the same tube. The ligation was successful when the volume was reduced from the recommended 50 µL to 15 µL.

4.2 Protein expression and purification

Expression of malaria HGXPRT was achieved by growing the cells overnight at 37 ^{0}C to OD_{600} 0.4 - 0.6, and then inducing with IPTG over 3 h. The recombinant protein was visible on SDS-PAGE gels after 30 min of induction. The expression was not under tight control by IPTG, but this method of

inducing appeared to increase the proportion of HGXPRT over the background protein synthesis.

HGXPRT is a soluble protein and expected to be in the crude supernatant. However, we consistently found that a significant proportion appeared in the crude lysed-cell pellet, most likely as inclusion bodies. We tried lowering the temperature during the induction phase in order to increase the proportion of folded (soluble) protein, but it did not appear to help.

We initially experienced some problems with cell lysis, which may have contributed to the poor release of protein into the supernatant. Malaria HGXPRT has been found to be unstable, both in our hands (Phehane, 2002) and others (Queen *et al.*, 1988; Keough *et al.*, 1998; Keough *et al.*, 1999), and therefore a harsh lysis method like sonication was avoided. Phehane, in our laboratory, routinely lysed the cells containing the His-tagged protein by combining osmotic shock (500 mM NaCl), lysozyme treatment, and rapid freeze-thaw. We wanted to avoid high salt as we planned to use ion exchange chromatography as the first step in the purification. Our initial attempts at lysis using just lysozyme treatment and rapid freeze-thaw were not successful, as judged by the lack of increase in viscosity (DNA release) and analysis by SDS-PAGE. Some success was achieved by adding EDTA and a small amount of salt (25 mM NaCl). However, we found that prolonged freezing of the sample, prior to freeze-thaw, was very successful even in the absence of added lysozyme. BL21(DE3)pLysS cells produce their own lysozyme, and often obviates the need to add extra.

Initial purification of the enzyme was tested with anion and cation exchange Sep-Pak cartridges, and the protein did not bind well to either resin. This is rather a surprise, as it appears from the electrostatic surface of the protein that there may be an excess of positive charge, and could perhaps be expected to bind to a cation exchange resin (Figure 4.1). We found, however, that many of the contaminating cellular proteins bound well to the anion exchange resin at alkaline pH, and we could take advantage of the inability of HGXPRT to do so, as did Keough *et al.*, (1999).

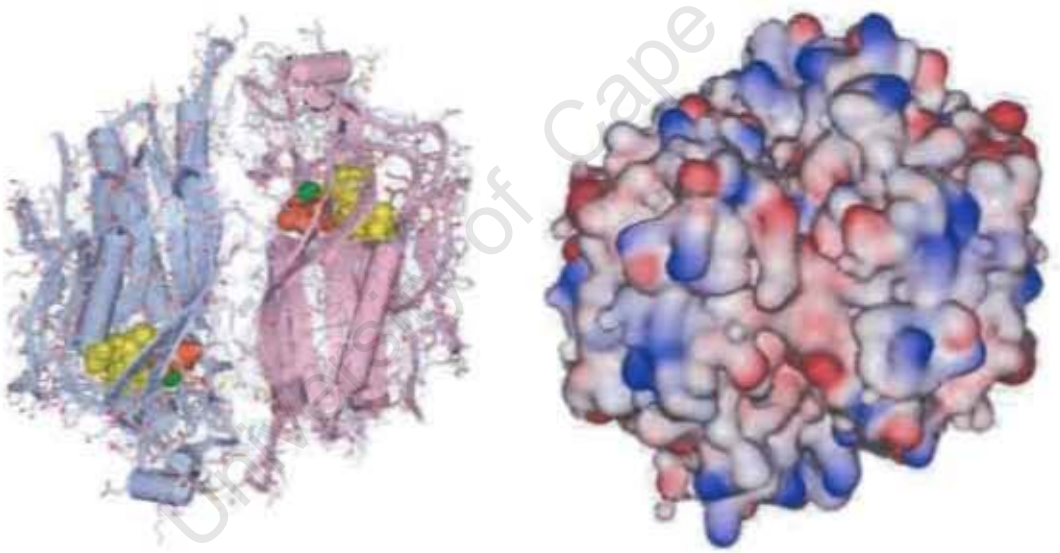

Figure 4.1 **Subunits A and B of malaria HGXPRT without (left) and with (right) electrostatic surface**. In the left hand image the substrate analogues, PPi, and Mg^{2+} are shown in CPK representation. The blue and red colours denote positive and negative electrostatic potential respectively. Subunits C and D (not shown) are positioned directly behind A and B in the particular view shown. Structure taken from Shi *et al.* (1999b) in a transition state complex.

Li *et al.*, (1999), employed an anion exchange (Q-sepharose) as the first step to purify this protein, and it appeared that the protein did in fact bind. Our inclusion of 25 mM NaCl may have contributed to this. We did find that the purer protein in 10 mM sodium phosphate, pH 7.0, bound to the resin, and that it was eluted in very low salt.

Reactive Red 120-linked agarose was used in the next purification step. Reactive Red 120 is a large symmetrical polycyclic ring system with 6 negatively charged sulfonate groups (Figure 4.2).

Figure 4.2 **Structure of Reactive Red 120** Reactive Red 120 is linked to agarose through the chloro groups (green). The S of the sulphonate groups is coloured orange.

Selective elution of the HGXPRT from the Reactive Red 120 was achieved with PPi in Tris-Cl, pH 8.5. High salt (300 mM or greater) could also elute the protein, but in a non-selective fashion. Specific interaction of protein and dye was also suggested from the fact that the protein bound to what is actually a cation exchange resin (negatively charged), which, as shown in the results, the HGXPRT protein did not bind to. Furthermore, the free dye strongly

inhibited activity. All these results point to a portion of the dye occupying the catalytic site. As alluded to in the Results section, Reactive Red 120 agarose is often used for the purification of NADH and/or nucleotide binding proteins, and it is possibly interacting with the IMP site of HGXPRT. However, as can be seen in Figure 4.3, the portion of Reactive Red 120 containing the sulphonate groups overlays PRPP, as bound in the ternary complex with PRPP, 9-deazaguanine and Mg^{2+} in *T. gondii*, rather well.

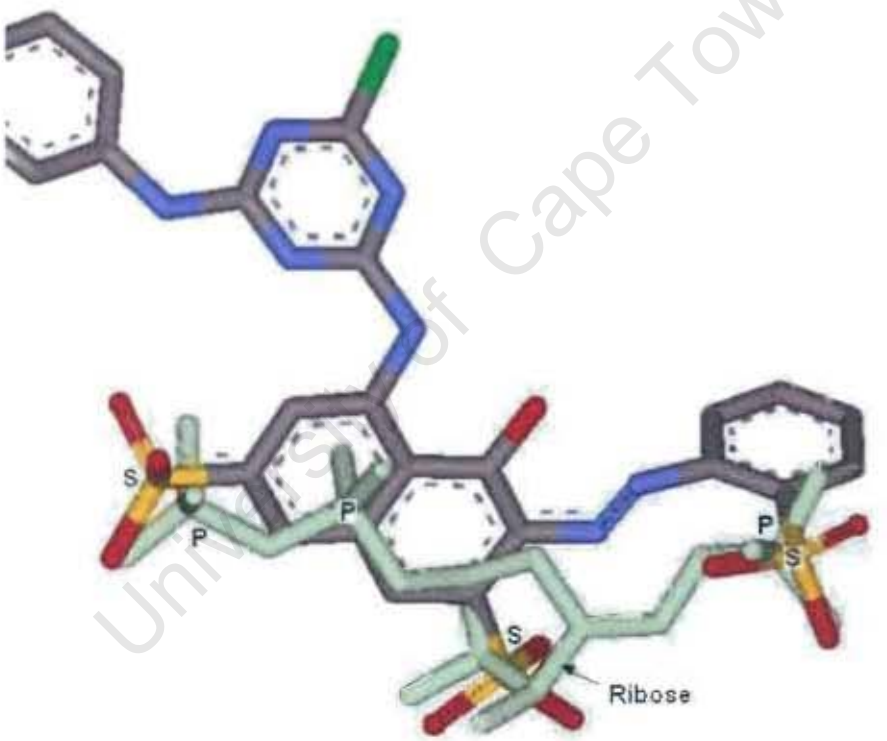

Figure 4.3 **Overlay of PRPP and a portion of Reactive Red 120**. The structure of PRPP (light green) was taken unaltered from *T gondii* HGXPRT (Heroux *et al.*, 2000). The phosphorous atoms of PRPP and the sulphur atoms of Reactive Red 120 are indicated.

4.3 HGXPRT activity

The recombinant malaria HGXPRT, both in crude fractions and in almost pure form, was inactive. It could be activated by dialysing in 10 mM sodium phosphate buffer, pH 6.8, over several hours followed by incubation at 4 ^{0}C in the presence of hypoxanthine + PRPP (Keough *et al.*, 1999) or Mg^{2+} + PRPP (Phehane, 2002). The process is reversible - dialysing out the substrates causes inactivation, and reintroducing them activates. The inactive protein is stable in the sense that it can remain at room temperature for several days and still be able to be activated with substrates.

It appears that the activation by hypoxanthine + PRPP requires contaminating divalent cations, in particular Mg^{2+}. Hence slow catalysis may be taking place and, in fact, Raman *et al.* (2005) report that IMP is the major activator. However, as mentioned above, Mg^{2+} + PRPP is equally effective. 4''-I-chalcone (**BM 06**) substitutes for PRPP in Mg^{2+}, but, in addition, has the property of activating in the presence of Ca^{2+}, as well as with hypoxanthine when divalent cations are absent. Thus the chalcone binds and activates in the absence or presence of divalent cation, unlike PRPP, which cannot bind without cation (Xu *et al.*, 1997).

The mechanism of activation and inactivation is not known, but there seem to be two possibilities (see Figure 4.4), one in which there is a slow equilibrium of inactive and active forms and only the latter binds substrate (**A**), and in the other case where the inactive enzyme binds substrate and slowly converts to

the active form (**B**). The fact that we have not been able to pick up any activity at all with the enzyme as isolated perhaps suggests that the second alternative is operating.

These mechanisms could be distinguished if one could find a method for measuring binding fairly rapidly, as only in the second case would the binding of substrate to all protein species be fast.

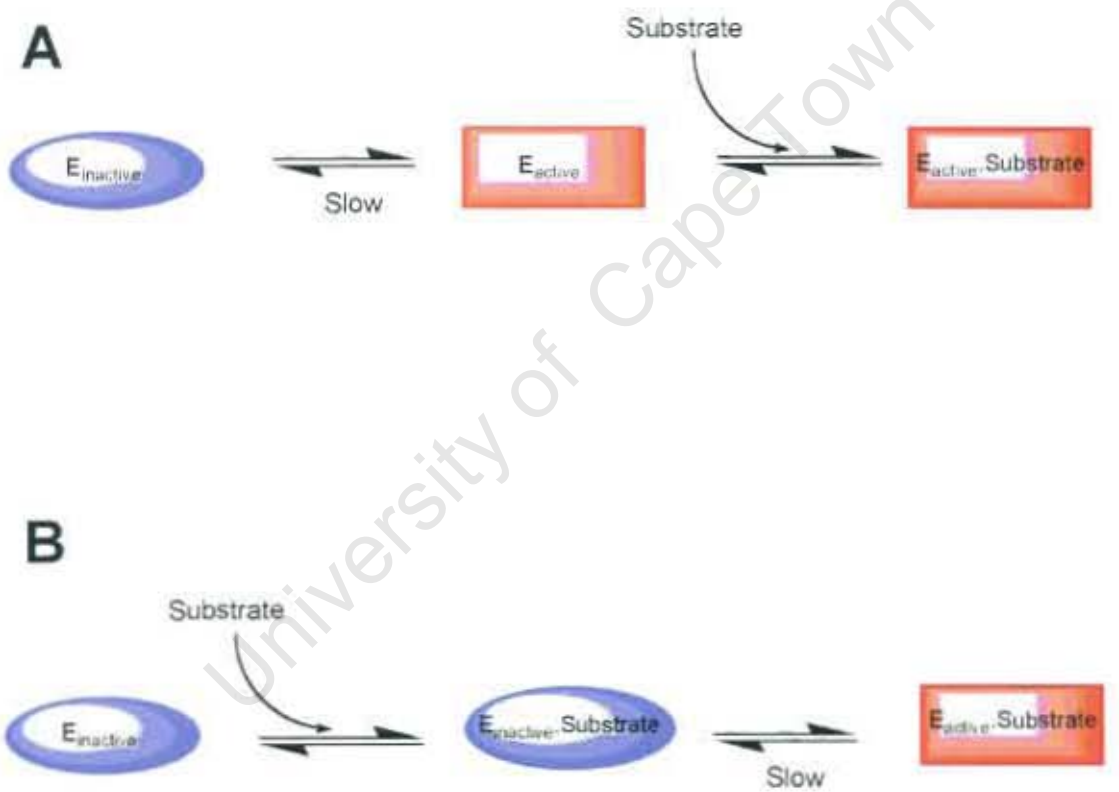

Figure 4.4 **Possible routes by which malaria HGXPRT is activated.**

The HGPRT enzymes from a variety of sources exist as a tetramer. Keough *et al.* (1999) found that the malaria enzyme was much more sensitive to KCl than the human, and 1.2 M converted the former into an inactive dimer, whereas it did not affect the latter. Inactivation therefore may be related to the requirement for tetramer formation, with correct subunit interactions.

Activation experiments are done with fairly concentrated enzyme (~1 mg of protein/ml). Under conditions of assay the enzyme is much more diluted (~100-fold) and turnover with the full complement of substrates causes rather rapid (~1 min) inactivation. Diluting the enzyme could favour break-up of the tetramer, but enzyme cycling through unstable intermediates that do not contain substrates or products probably also contributes to instability.

The motivation for expressing the malaria HGXPRT without a his-tag was to try to express active enzyme and increase its stability. A previous study in our laboratory (Phehane, 2002) had found that malaria HGXPRT with a his-tag was expressed as an inactive, largely soluble protein, with poor stability during enzyme turnover once it had been activated with substrate. The instability seemed much more than that found by Keough *et al.* (1999), who found approximately 50% activity remaining after dialysis in 10 mM phosphate, pH 7.1, over 5 h and then a further 50% decline over 90 h. However, we found that the tag-less protein was inactive in the crude homogenate and remained so in the pure form, unless activated. Once activated, it had the same inactivation kinetics as we had found previously for the tagged enzyme, and was much more unstable during dialysis in

phosphate buffer (no activity after 16 h) than found by the Keough group. We conclude that recombinant tagless and tagged proteins have equivalent instability. We do not understand the discrepancy with respect to the Keough findings. It is not due to an incorrect sequence, as it had been checked previously (Phehane, 2002).

We opted to continue with the tagless protein because the purification procedure was not all that more cumbersome than the Ni-chelate protocol, and, in the future, we wanted to produce crystals of the protein, for which the tagless protein would be preferable.

4.4 Structure activity relationships (SARs)

Prior to this study, we had identified a halogenated-chalcone (**BM 06**) as an accelerator of the catalytic cycle in the presence of Mg^{2+}. This we refer to as the accelerating activity of the chalcones. The present study has uncovered that the chalcones also show inhibitory activity in the presence of Ca^{2+}, as well as an activating activity that converts the inactive isolated protein to an active form.

4.4.1 Accelerating activity

Nine chalcones had been tested previously for any inhibitory effect on human, *T. gondii*, and *P. falciparum* HGPRT (Phehane, 2002). Of these, seven were 2',4',6'-trihydroxylated, but changed at position 4'' (see Figure 4.5 for

numbering). Four had O-aliphatic chains, C_2H_5, C_4H_9, C_6H_{13}, and C_8H_{17}. The other three were substituted with I, F, or OH. The other two were 2',4',4''-OH, with either a prenyl substitution at 5' (also called broussochalcone A) or 3''. None were found to be inhibitory, but, as mentioned before, 4''-I-chalcone (**BM 06**) unexpectedly accelerated catalytic turnover, and only of the malaria HGXPRT.

The above results, together with what has been found in this study, allow structure activity relationships to be explored with respect to the accelerating activity of the chalcones. A summary is provided in Figure 4.5. Looking at the 2',4',6'-trihydroxylated chalcones first, the iodo group at position 4'' can be replaced with Br and Cl, but not with F or O-aliphatics. The position of the iodo group cannot be changed to 2'' or 3''.

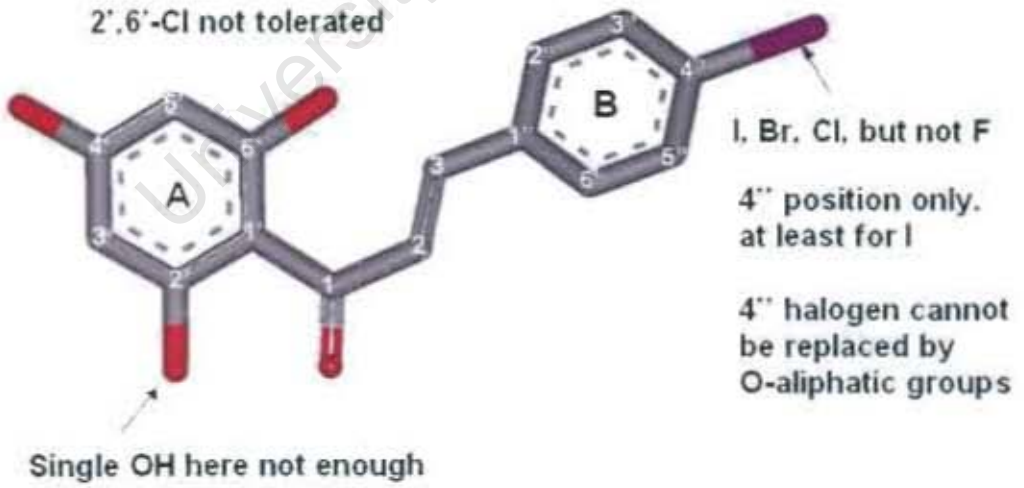

Figure 4.5 **Summary of structure activity relationships for the accelerating effect on catalysis.**

Substitutions at ring A, when the 4''-I is fixed, are also not tolerated. Changing 2',6'-OH to two chloro groups destroys the activating effect. Removing the 4',6'-OH also prevents it. Adding a 3'-NO_2 group to the chalcone without 2',6'-OH has little effect. With this grouping in ring A, changing the position of the iodo group in ring B to 2'' or 3'' does not lead to activation.

The chalcones fused through ring A showed no activity.

Therefore the requirements for exhibiting the accelerating effect are very stringent, the only changes allowed in the lead compound were replacing the 4'-iodo group in ring B with Br or Cl.

The mechanism for acceleration of the catalytic cycle is not known, but some speculation is warranted. The kinetics of catalytic cycle of HGPRT enzymes has only been explored in detail for the human form (Xu *et al.*, 1997). The rate constants for each step are shown in Figure 4.6 at pH 7.4 and 23 ^{0}C in 12 mM $MgCl_2$ 0.5 mM PRPP, and 0.01 mM hypoxanthine. Rate limitation in the forward direction is primarily associated with nucleotide release ($k = 6\ s^{-1}$). The chemical conversion is very rapid at $k = 131\ s^{-1}$. The human enzyme is at least 10-fold faster than the malaria one, and it is not known what is slowing the latter. If nucleotide release remains the primary slow step, then the accelerating chalcones may be binding either at an allosteric site outside of the catalytic site or at the vacant PPi site to augment the release of nucleotide (assuming ordered release). On the hand if the chemical interconversion is

rate limiting (slowed about 100-fold with respect to the human enzyme) then it can only be at an allosteric site, because the active site is occupied.

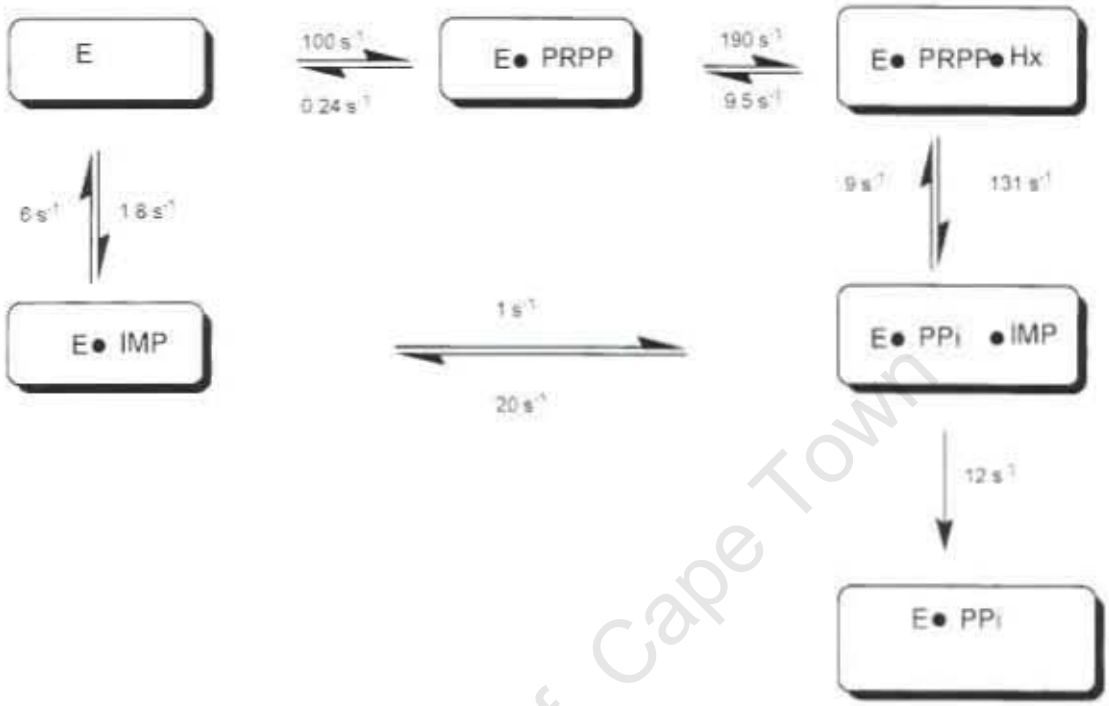

Figure 4.6 **Catalytic cycle of human HGPRT with rate constants (Xu *et al.*, 1997).** The second order rate constants for substrate and product binding were converted into single order constants for 0. 5 mM PRPP, 10 μM hypoxanthine, 1 μM PPi.

We attempted to alter the slow step(s) by altering the pH and the identity of the divalent cation. The latter, we felt, could be particularly interesting as changing the cation cofactor could dramatically slow the chemical interconversion, making it the rate-limiting step, and retention of an accelerating effect of the chalcones would point to an allosteric mechanism for activation.

The activity was lowered about 3-fold at pH 6 compared with pH 9. However, the accelerating effect of the chalcones remained about the same at the two pH values, suggesting that the rate-limiting step(s) had not changed much.

The activity of the enzyme in Mn^{2+} was very similar to that in Mg^{2+}, and replacement with Ca^{2+} slowed it about 1/3, whereas no activity was detected with Sr^{2+}. If Ca^{2+} was only affecting the chemical interconversion step, it could mean that the chemical interconversion had slowed considerably and become rate limiting. However, addition of chalcone unexpectedly produced potent inhibition.

4.4.2 Inhibitory activity

The transformation of accelerating chalcones into inhibitors by Ca^{2+} strongly suggests that they are capable of binding at the active site and that the binding affinity changes from medium (acceleratory) to very tight (inhibitory). This conclusion is in harmony with the finding that the 4''-I-chalcone (**BM 06**) in the presence of Ca^{2+} activates inactive to active enzyme by binding to the PRPP site (see later). Taking the competitive effect of PRPP into account, the K_d for Ca^{2+}-chalcone binding may be as low as 1 nM, making it one of the most potent inhibitors found for any PRT. Examination of a few of the non-accelerating chalcones showed that they did not act as inhibitors in Ca^{2+}.

4.4.3 Activating activity

Investigating the effect of the chalcones on the conversion of inactive to active HGXPRT (activating activity) also provided insights into the nature of chalcone binding. Normally the activation process is achieved with either hypoxanthine + PRPP or Mg^{2+} + PRPP. It now appears that under the first conditions, with both substrates, there is a requirement for Mg^{2+}, and that in fact IMP may be the activator (Raman *et al.*, 2005). Ca^{2+} + PRPP, PRPP alone or hypoxanthine alone are ineffective (this work and Keough *et al.*, 1999). Very surprising is that 4''-I-chalcone (**BM 06**) alone, hypoxanthine + chalcone, and Ca^{2+}/Mg^{2+} + chalcone could activate the enzyme.

It is difficult to explain why Ca^{2+} + PRPP was ineffective, but given that the Ca-chalcone may be binding several orders of magnitude tighter than Mg-PRPP, and perhaps Ca-PRPP, the binding interactions could be much more extensive (see below).

The inhibitory and activating effects of specifically the accelerating chalcones suggest a single unique chalcone binding site, and together place the site at the catalytic site in proximity to PRPP. The size and shape of the chalcones fit very well over that of bound PRPP as it appears in the active site of the *T. gondii* enzyme (Figure 4.7). The rotation around three of the bonds in the chain linking the two rings provides for many alternative ways of superimposing the structures.

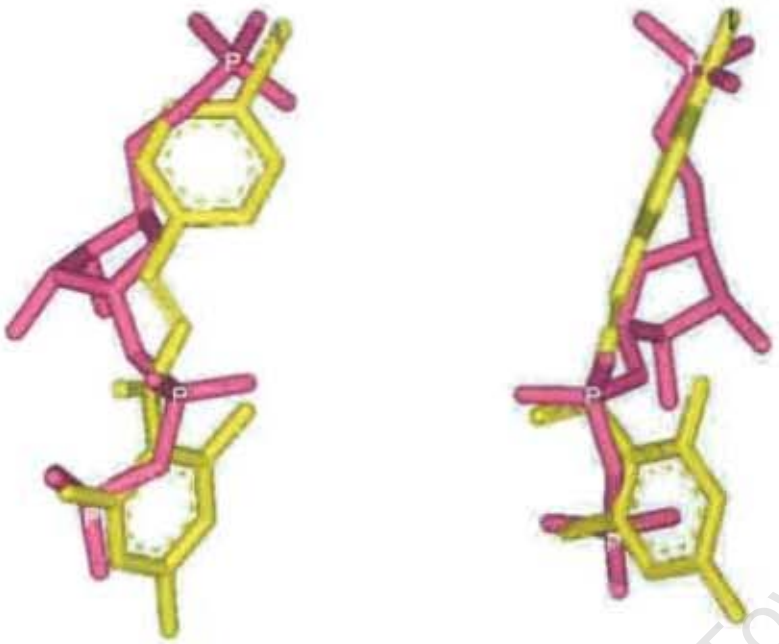

Figure 4.7 **Superimposition of 4''-I-chalcone (BM 06, yellow) and PRPP (pink).** The structure of PRPP is taken unaltered from how it is bound in the *T. gondii* HGXPRT (Heroux *et al.*, 2000). The fit was performed manually.

It is insightful to compare the sizes of the accelerating/inhibiting chalcones and in particular the contribution of the halogen. In Figure 4.8 these chalcones as well as the ineffective 4''-F-chalcone aligned in a linear form. The size of the halogen increases with the increase in atomic number, from F to I.

The other parameters that vary in this series are polarizability, electronegativity, hydrophobicity, and halogen and hydrogen bonding characteristics. A halogen bond is formed between a halogen and an oxygen atom, and its strength depends on the polarizability of the bond linking the

halogen to the carbon of the halogenated species (Auffinger et al., 2004). There is an increase in the polarizability of the carbon-halogen link and increasing electropositive character on the halogen in the series F to I (Auffinger *et al.*, 2004). Fluorine atoms are not polarizable and remain entirely electronegative in halogenated methane and model halogenated aliphatic and aromatic compounds. The magnitude of the electropositive area increases with the radius or polarizability of the halogen. Therefore I (iodine) develops the strongest halogen bond, and F the weakest. The strength of hydrogen bonding decreases in the opposite series OMe > OH > F > Cl > Br > I (Raevsky *et al.*, 1995, as quoted in Bois *et al.*, 1998), and the effectiveness of the latter three halogens, and not the second and third groups, appears not related to this type of bonding. Lipophilicity, which increases in this series (Hansch and Leo, 1979, quoted in Bois *et al.*, 1998), may play a role.

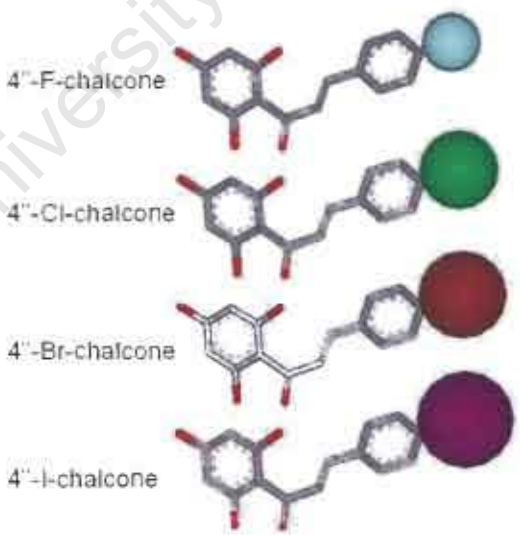

Figure 4.8 **Comparison of 4''-halogenated chalcones** The halogen group is shown in CPK representation. Only the bottom three chalcones accelerated catalytic turnover with Mg^{2+} as divalent cation cofactor.

Therefore the important parameters relating to the halogen could be size, halogen bonding, and lipophilicity.

Turning to the other end of the molecule, the combination of tri-hydroxyl aromatic and carbonyl groups seems to mirror the pyrophosphate moiety rather well (Fig 4.7). The 3 O-atoms potentially overlay those of the chalcone. A difference is that the one compound is charged and the other not, and this evidently relates to the inability of PRPP to bind to HGPRT in the absence of divalent cation (Xu *et al.*, 1997), whereas the chalcone, judging from its ability to activate the inactive protein, can.

4.4.4 Models of chalcone binding

The layout of the active site of HPRT with bound substrates is shown in schematic form in Figure 4.9. It is presented to remind the reader of the organisation of loops and the fact that only one of the Mg^{2+}s bonds to the protein, and that is only a single link at Loop IV.

The binding site for PRPP can be taken from the position of PPi and the ribose and 5'-phosphate moieties of ImmucillinHP in the transition state complex of the malaria HGXPRT (Shi *et al.*, 1999b), since the same hydrogen bond contacts are made for PRPP in the *T. gondii* enzyme in complex with PRPP and deazaguanine - each have 13 substrate-protein contact distances ≤ 3 Å (Heroux *et al.*, 2000, compare Figures 1.11 and 1.15). A possible

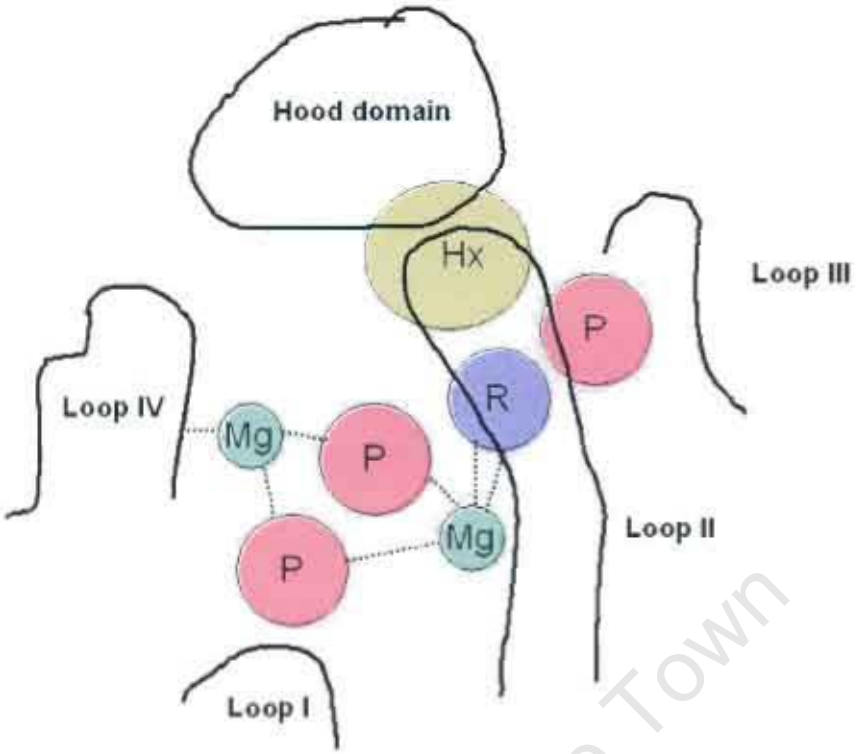

Figure 4.9 **Schematic diagram of HGXPRT active site**. Note that only one Mg^{2+} is directly linked to the protein, via Loop IV.

position of the chalcone with it overlaying the PRPP site is shown in Figure 4.10. In this position, the keto group and one hydroxyl of ring A replaces two hydroxyls of the PPi, another hydroxyl is 2.9 Å from the second Mg^{2+}, and the third makes good contact with the amide of lys77, and the carbonyl of the previous amino acid. On the other end, the halogen interacts with thr149 to form a hydrogen (H-) and a halogen bond. Aromatic π interactions are possible with tyr116 if catalytic loop II is folded down. Without the nucleotide, there is nothing holding the Mg^{2+} ion in position and its locality need not be fixed.

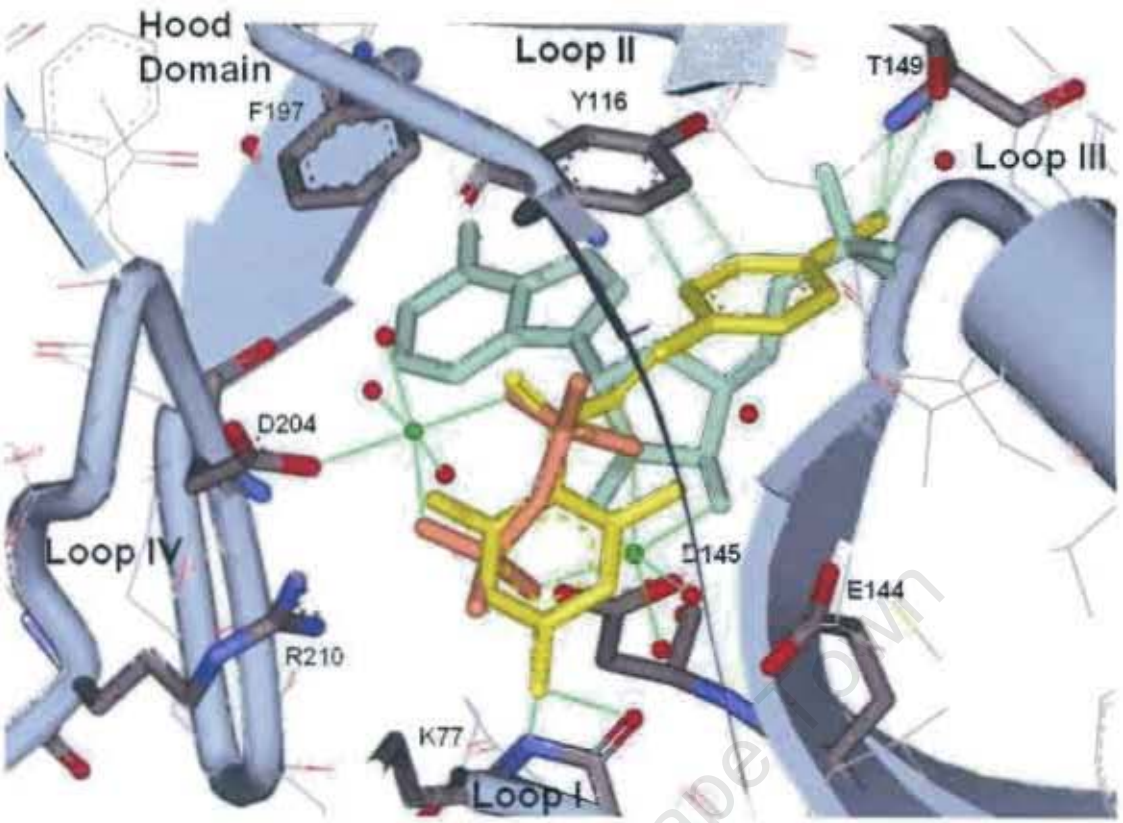

Figure 4.10 **Docking 4''-I-chalcone (BM 06) into malaria HGXPRT with Mg^{2+}** ImmucillinHP is in green, PPi orange, chalcone yellow, and Mg^{2+} green. The chalcone was docked manually using Accelrys DS ViewerPro. Interactions with chalcone and protein of < 3 A are shown in green lines. The coordinations of the Mg^{2+}s are also shown by green lines.

In the absence of bound Mg^{2+}, other configurations for ring A are possible, including H-bond contacts with asp145, ser202, asp204, and arg210 (docking not shown).

The alkene double bond in the chalcone limits configurations to linear forms, which precludes it assuming a U-shape that would make it resemble a nucleotide.

The docking in Figure 4.10 with or without Mg^{2+} could have relevance to the activating activity of the chalcone. The chalcone would interact first with an open inactive enzyme structure and with time the loops could come together and close over the chalcone so that the protein structure assumes something more like what is presented. Activation is achieved in the absence of purine and added divalent cation (as well as in their presence) suggesting that closure of the hood domain may not be necessary, which fits with the finding that Mg-PRPP is also sufficient.

It seems possible that the conversion of inactive to active conformation of the protein may involve an improvement in inter-subunit contacts, and that this requires a more compact or constrained structure around the active site. Once the correct inter-subunit contacts have been made, the activators may dissociate to yield the active conformation with empty active and attendant mobility of the loops. There is evidence from the human enzyme that substrate occupancy of one subunit influences the characteristics of the neighbouring subunit, suggesting co-operativity between subunits (Keough *et al.*, 2005).

The chalcones became potent inhibitors when Ca^{2+} was substituted for Mg^{2+} in the standard activity assay. In considering possible docking for the inhibitory chalcones, we reasoned that extra interaction with the protein must have been occurring when Ca^{2+} replaces Mg^{2+}. In all relevant PRT structures determined to date, only one of the Mg^{2+}s makes contact with the protein (at asp204 for malaria enzyme), the other only contacts the ribose moiety and

PPi. With Ca^{2+} all the interactions that are present with Mg^{2+} are possible, but there is the intriguing possibility that use may be made of the two carboxylate amino acids glu144 and asp145, just below the one Mg^{2+}, when Ca^{2+} is present. In this regard it is interesting that Ca^{2+} has variable coordination (6, 7 or 8), whereas Mg^{2+} is restricted to 6, Ca^{2+}- donor distances are longer than Mg^{2+} (2.37 versus 2.11 Å in model compounds), Ca^{2+} often coordinates carboxyls in a bi-dentate manner and for Mg^{2+} it is extremely rare, Ca^{2+} tolerates deviation for ideal geometry much more than Mg^{2+}, and Ca^{2+} can move twice as far from the OCO plane compared with Mg^{2+} (Harding 1999, 2000, 2001). All these features of Ca^{2+} make it more versatile and capable of stronger interactions compared with Mg^{2+}. In Figure 4.11, ring A of the chalcone has been moved towards glu144 and asp145 and a Ca^{2+} ion placed in between at suitable bonding distances. The keto group and one hydroxyl coordinate the Ca^{2+}, as well as asp145 in a bi-dentate fashion. The coordination includes glu146 and a backbone carbonyl of loop I. While the geometry is not ideal, variations are possible. With regard to the other metal ion binding site, replacement of Mg^{2+} with Ca^{2+} could introduce the possibility of a bi-dentate link to asp204 and one of the hydroxyls of ring A is also in a suitable position for coordination, which may be completed with water molecules. It is interesting that in one apo structure of *T. gondii*, a Mg^{2+} was bound at the residues equivalent to glu144 and asp145 (see Figure 1.10). At this stage it is not known whether purine binding is required for the very tight Ca-chalcone to protein interaction. An intriguing possibility, in view of the tightness of the interaction, is that the complex may resemble a transition state. Maybe the electron withdrawing capability of the halogen, creates an

electron deficient aromatic ring. It can be seen from the Figure that this aromatic ring is in proximity to the protonated N in the imino-ribitol ring, and it is the positive charge on the latter which creates the very tight binding affinity of the ImmucillinHP when PPi is included. However, against this idea is the fact that the inhibition with the Ca-chalcone is immediate, whereas the binding of transition state inhibitors is typically much longer (Li *et al.*, 1999).

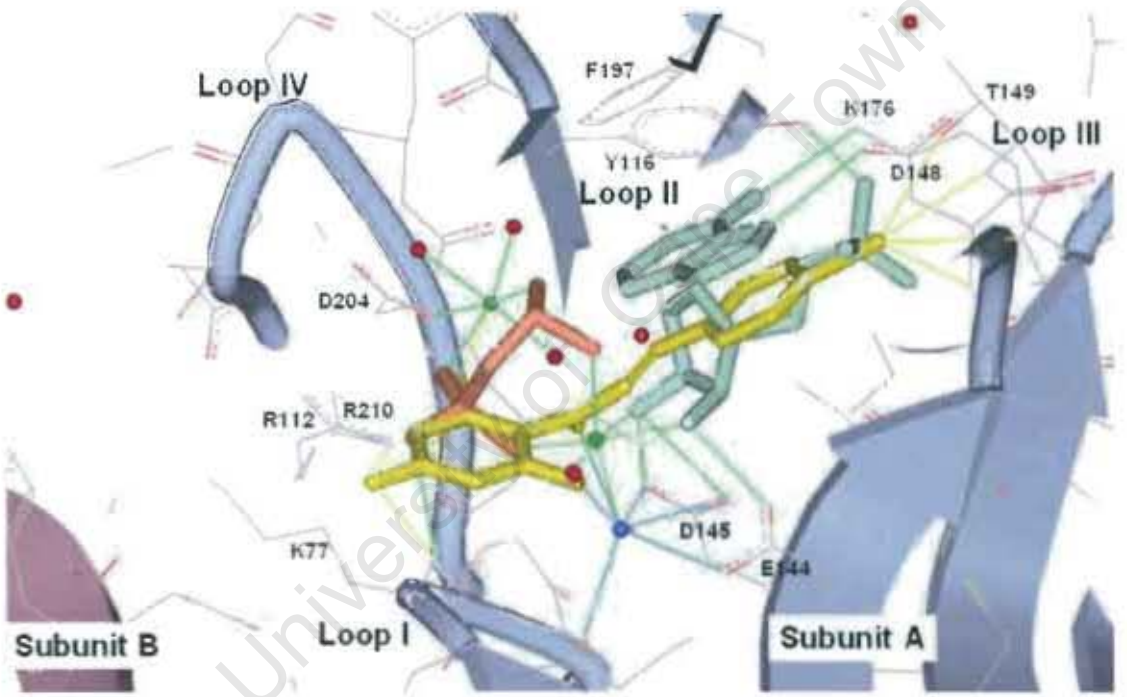

Figure 4.11 **Docking of 4''-I-chalcone (BM 06) in malaria HGXPRT with Ca^{2+}.** ImmucillinHP is in green, PPi orange, Mg^{2+} green, Ca^{2+} blue and chalcone yellow. The chalcone and Ca^{2+} were docked manually with Accelrys DS ViewerPro.

In regard to the accelerating effect, the rate-limiting step for the malaria HGXPRT is not known, but if it is the same as the human enzyme, it would be nucleotide release. In which case, the relevant structure would be the complex of enzyme + IMP/GMP. However, in this case it seems not possible for the chalcone to bind as a PRPP analogue as discussed above, since the nucleotide is bound. Nucleotide release probably consists of several phases (Heroux *et al.*, 1999), and one outside possibility that we considered is that the ribose + 5'-phosphate is loosened first, and the slower step is the pulling back of the hood domain to release the purine portion and the complete nucleotide. In this scenario, Loops II, III, III', and IV move away following departure of the Mg^{2+}s and PPi allowing the detachment of the ribose and 5'-phosphate moieties while the purine ring part is trapped between ile146 and phe197 of the hood domain. Only once the hood domain opens away from the core domain is nucleotide released. Binding of chalcone to the PRPP site, particularly at the site of the ribose and 5'-phosphate, would disallow the nucleotide to regain purchase to this region, and help its release. The rebinding of the ribose-phosphate section may be also be retarded by a fast conformational change of the nucleotide from its strained bound state to a more stable one. Making Hood Domain movement the slow step is attractive because the domain is relatively large, probably moves as a rigid body, and is constrained by inter-subunit contacts. In this series of events, the binding of the chalcone may be driven by interactions with some of the disordered loops mentioned above, and the structure of the enzyme with nucleotide and chalcone, in the vicinity of the latter, may not be all that different from the

transition state complex. However, it seems doubtful whether chalcone would be able to compete with the partially bound nucleotide.

There are several alternative possibilities for the accelerator-binding site, if nucleotide release is the rate-limiting step, and the chalcone binds elsewhere. For example, in the transition-like structure, ring A (the tri-hydroxyl moiety) could remain at the PPi site, but flipped so that ring B with the halogen is pointing outside the catalytic site (Figure 4.12). His109 and glu130 of the

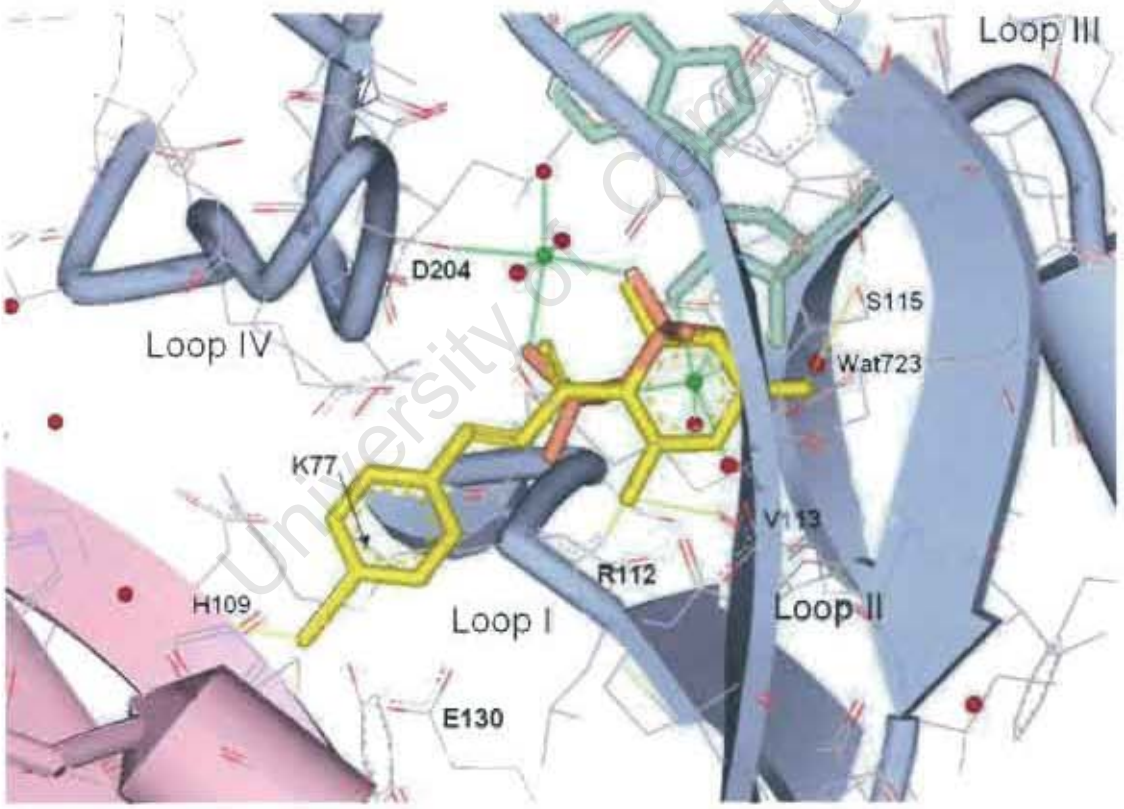

Figure 4.12 **Docking of 4''-I-chalcone (BM 06) in malaria HGXPRT with ring B outside of the catalytic site.** The HGXPRT structure is taken from Shi *et al.* (1999b). Interaction distances of <3 Å are shown in yellow lines. Coordination of Mg^{2+}s is shown in green lines.

neighbouring subunit are within bonding distance of the halogen. How this binding would accelerate IMP release is unclear, but it could be via Loop IV, which is next to the Hood Domain, which in turn needs to open. A more relevant structure could be that of the binary nucleotide-bound form, for which the *T. gondii* enzyme may be used as a model. The structure is shown in figure 1.12, and it is evident that there is a large open region vacated by the Mg^{2+}s and PPi. In Loop I, lys79 is facing in, the catalytic loop with tyr118 is pulled back, Loop III has less contacts with the 5'-phosphate, and Loop III' with arg182 has receded. There are many ways to dock the chalcone. Again interaction of the chalcone with Loop IV could aid pushing back the Hood Domain.

If the rate-limiting step is not nucleotide release, but rather a slow conformational change following, say IMP release, then the apo enzyme may be the more relevant structure to consider, and even more possibilities for binding at the active site present themselves. If the slow step is the chemical interconversion, then an allosteric site needs to be considered.

4.5 Concluding remarks

As mentioned earlier, **BM 06**, **BM 09** and **BM 10**, but none of the other chalcones and flavonoids tested here or previously, accelerate the catalytic turnover of the malaria enzyme. These three chalcones also inhibit the malaria enzyme when Ca^{2+} replaces Mg^{2+} as the divalent cation cofactor. Furthermore, **BM 06** has been demonstrated to convert malaria HGXPRT

from an inactive into an active form. Since these three chalcones differ only in the halogen, it is reasonable to conclude that each binds at the same site for a particular activity. Further, since the same chalcones appear to exhibit each of the activities (accelerator, activator, and inhibitor - with the reservation that for the latter activities only limited non-accelerating chalcones were tested), it seems rational to conclude that they bind at the same/similar site for each activity. In the activating and inhibiting activities, there is evidence that the chalcones bind at the PRPP site. Therefore it is tempting to speculate that to induce an accelerating effect they also need to bind at the PRPP site, which, as we have seen, presents problems if nucleotide is still bound, and the possibility of a different rate limiting step needs to be considered. The transformation from an accelerator to inhibitor, if the binding is at the active site, would merely require that the binding energy changes from medium to tight depending on whether Mg^{2+} or Ca^{2+} is the cofactor, respectively.

The halogenated chalcones initially did not seem to have obvious structural similarity to PRPP, but the fact that they become tight binding inhibitors with Ca^{2+} strongly suggested that they bind divalent cations, and the only real possibility is through the keto group and a hydroxyl group of ring A. The other interesting aspect is that, unlike PRPP, they are not charged, and this feature appears to allow them to bind at the PRPP site in the absence of divalent metal ion. As far as we are aware, these are the first uncharged PRPP mimics, and at least in their accelerating activity, they are specific for the malaria enzyme. They raise hope that they or more potent analogues may inhibit growth of the malaria parasite itself, either targeting HGXPRT or

another essential PRPP-utilising enzyme. That said however, it may be difficult to prove that the death of the parasites is due to targeting such enzymes since other chalcones inhibit malaria growth (see section 1.5).

Chapter 5 Future work

A number of strategies could be followed in order to understand the nature of the chalcone-HGXPRT interaction in the three activities.

Foremost of these would be to try to crystallise the chalcone-HGXPRT complex. Malaria HGXPRT has proven difficult to crystallise and it has only been accomplished with the transition state inhibitor, ImmucillinHP + PPi, but the tight binding of the chalcones in the presence of Ca^{2+} provides some hope. It would be worth trying with purine, or even ImmucillinHP +/- PPi. It may be necessary to purify the enzyme further, and preliminary experiments with another DE52 column, under conditions in which the protein bound to the resin, showed that this is possible with this technique.

As time did not permit, SARs were not done for all chalcones in the activation (inactive to active protein) and inhibition (in the presence of Ca^{2+}) experiments. It would be instructive to ascertain if exactly the same profile is found for each activity.

It is desirable to determine the true K_d for Ca-chalcone binding. This presents problems due to the instability of the protein at low protein concentrations. One technique that may be suitable is equilibrium dialysis, but this would require the synthesis of a radiolabelled derivative.

It would also be interesting to determine whether the chalcones are inhibitory in mixtures of Mg^{2+} and Ca^{2+}, which may pertain to the situation *in vivo*. For example, at physiological concentrations of Mg^{2+} (~3 mM), could the chalcones exhibit inhibition at μM concentrations of Ca^{2+}? The concentration of Ca^{2+} in the parasite within the red blood cell may not be all that low, since there appear to be connections to the outside (New Permeability Pathways that develop upon parasite effection can possibly lead to a change in levels of Ca^{2+} in the parasite, see section 1.3.1).

Another avenue of investigation is to determine whether the Ca-chalcones inhibit the human and *T. gondii* enzymes. In Mg^{2+}, the 4''-I-chalcone did not accelerate these proteins (Phehane, 2002), but this may be because rate limitation in the catalytic cycle is different.

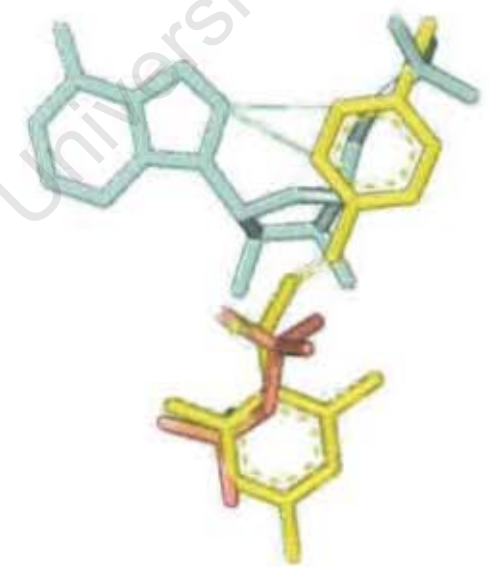

Figure 5.1 **Proximity of ImmucillinHP (light green), PPi (orange) and docked chalcone (yellow) as occurs in the structure of Figure 4.10**. The green lines show distances <3 Å.

Further more potent chalcone inhibitors could possibly be developed if the docking of chalcone into the active site of the transition state structure can be trusted, since the 8 position of the deazahypoxanthine ring comes close to the chalcone. This is shown in Figure 5.1, where the two structures are taken exactly as they occur in the docked structure of Figure 4.10. The distances are under 3 Å (green lines), and a chalcone derivatised with a purine on ring B could take advantage of the isoleucine-phenylalanine ring clamp and bind very tightly. If the synthetic chemistry does not allow this, perhaps a phenyl ring with an appropriate linker attached to the chalcone could serve as well. As mentioned above, the tight binding of the present chalcones in Ca^{2+} may actually require a bound purine. Such a compound would bear some resemblance to a half Reactive Red 120 molecule (Figure 4.2).

BIBLIOGRAPHY

Abdel-Rahman H.M., Kimura, T., Hidaka, K., Kiso, A., Nezami A., Freire, E., Hayashi, Y., and Kiso, Y. (2004). Design of inhibitors against HIV, HTLV-1 and *Plasmodium falciparum* aspartic proteases. Biol. Chem. **385**(11), 1035-9.

Adams, PA., Berman, PAM., Egan, TJ., Marsh, PJ., and Silver, J. (1996). The iron environment in heme and heme-antimalarial complexes of pharmacological interest. J. Inorg. Biochem. **63**, 69-77.

Aldieri, E., Altragene, D., Bergandi, L., Riganti, C., Constamagna, C., Bosia, A. and Ghingo, D. (2003). Artemisinin inhibits inducible nitric oxide synthase and nuclear factor NF-kB activation. FEBS Lett. **552**(2-3), 141-4.

Aufinger, P., Hays, F.A., Westhof, E. and Ho, P.S. (2004). Halogen bonds in biological molecules. Proc. Natl. Acad. Sci. U. S. A. **101**(48), 16789-94.

Basco, L.K., Tahar, R., Keundjian, A., and Ringwald, P. (2000). Sequence variations in the genes encoding dihydropteroate synthase and dihydrofolate reductase and clinical response to sulfadoxine-pyrimethamine in patients with acute uncomplicated falciparum malaria. J. Infect. Dis. **182**(2), 624-8.

Berman, P.A., and Human, L. (1990). Regulation of 5-phosphoribosyl 1-pyrophosphate and of hypoxanthine uptake and release in human erythrocytes by oxypurine cycling. J. Biol. Chem. **265**, 6562-6568.

Berman, P.A., Human, L. and Freese, J.A. (1991). Xanthine oxidase inhibits growth of *P. falciparum* in human erythrocytes in vitro. J.Clin. Invest. **88**, 1848 - 1855.

Birnboim, H.C., and Doly, J. (1979). A rapid alkaline extraction procedure for screening recombinant plasmid DNA. Nucleic Acids Research **7**, 1513-1523.

Bois, F., Beney, C., Boumenndjel, A., Mariotte, A., Conseil, G., and Di Pietro, A. (1998). Halogenated chalcones with high-affinity binding to P-Glycoproteins: Potential modulators of multidrug resistance. J. Med. Chem. **41**, 4161-4164

Bois, F., Beney, C., Boumenndjel, A., Mariotte, A., Conseil, G., and Di Pietro, A. (1999). Synthesis and biological activity of 4-alkoxy chalcones: Potential hydrophobic modulators of P-glycoprotein-mediated multidrug resistance. Bioorg. Med. Chem. **7**, 2691-2695.

Bray, P.G., Martin, R.E., Tilley, L., Ward, S.A., Kirk, K. and Fidock, D.A. (2005). Defining the role of PfCRT in *Plasmodium falciparum* chloroquine resistance. Mol. Microbiol. **56** (2), 323-333.

Brown, J.D. (1997) A rapid, non-toxic protocol for sequence-ready plasmid DNA. Technical Tips Online:
http://130.15.90.245/plasmid_preparations.htm

Brown, D.M., Netting, A.G., Chun, B.K, Choi, Y., Chu, C.K. and Gero, A.M. (1999). L-nucleoside analogues as potential antimalarials that selectively target *Plasmodium falciparum* adenosine deaminase. Nucleoside Nucleotides **18**, 2521-32.

Buki, K.G., Kirsten, E., and Kun, E. (1987). Isolation of adenosine diphosphoribosyltransferase by precipitation with reactive red 120 combined with affinity chromatography. Anal. Biochem. **167**(1), 160-6.

Butler, D., Maurice, J., and O'Brien, C. (1997). Time to put malaria control on the global agenda. Nature **386**, 535-6.

Bzik, D.J., Li, W.B., Horii, T. and Inselburg, J. (1987). Molecular cloning and sequence analysis of the *Plasmodium falciparum* dihydrofolate reductase-thymidylate synthase gene. Proc. Natl. Acad. Sci. U.S.A. **84**, 8360-4.

Carter, N.S., Ben Mamoun, C., Liu, W., Silva, O.E., Landfear, S.M., Goldberg, D.E., and Ullman, B. (2000). Isolation and functionl characterisation of the PfNT1 nucleoside transporter gene from *Plasmodium falciparum*. J. Biol. Chem., **275**, 10683-91.

Chen, M., Brogger Christensen, Zhai, L., Rasmussen, M.H., Theander, T.G., Frokjaer, S., Steffansen, B. Davidsen, J. and Kharazmi, A. (1997). The novel oxygenated chalcone, 2,4-dimethoxy-4'-butoxychalcone, exhibits potent activity against human malaria parasite *P. falciparum* In Vitro and rodent parasites *P. berghei* and *P. yoelii* In Vivo. J. Infect. Dis. **176**, 1327-33.

Chen, M., Theander, T.G., Christensen, S.B., Hviid, L., Zhai, L. and Kharazmi, A. (1994). Licochalcone A, a new antimalarial agent, inhibits in vitro growth of the human malaria parasite Plasmodium falciparum and protects mice from P. yoelii infection. Antimicrob. Agents Chemother. **38**(7), 1470-5.

Chen, M., Zhai, L., Christensen, S.B., Theander, T.G. and Kharazmi, A. (2001). Inhibition of fumarate reductase in Leishmania major and L. donovani by chalcones. Antimicrob. Agents Chemother. **45**(7), 2023-9

Chibale, K. and Musonda, C.C. (2003). The synthesis of parasitic cysteine protease and trypanothione reductase inhibitors. Current Medicinal Chemistry. **10**, 1241-53.

Chiyanzu, I., Clarkson, C., Smith, P.J, Lehman. J., Gut J., Rosenthal, P.J., Chibale K (2005). Design, synthesis and anti-plasmodial evaluation in vitro of new 4-aminoquinoline isatin derivatives. Bioorg. Med. Chem. **3**(9), 3249-61

Clark, J.D., Weisenburger, G.A., Anderson, K.D., Colson, P., Edney, A.D., Gallager, D.J, Kleine, P.H., Knable, A.M., Lantz, M.K., Moore, M.V., Murphy, J.B., Rogers, T.E., Ruminski, P.G., Shah, A.S., Storer, N., and Bruce, W. (2004). Pilotplant preparation of an $\alpha_v\beta_3$ integrin antagonist. Part 1. process research and development of (s)-β-amino acid ester intermediate: synthesis via a scalable, diastereoselective Imino-Reformatsky reaction. Organic Process Research & Development **8**, 51-61.

Choi, C.Y., Schneider, E.L., Kim, J.M., Gluzman, I.Y., Goldberg, D.E., Ellman, J.A. and Marlletta M.A. (2002). Interference with heme binding to histidine-rich protein-2 as an antimalarial strategy. Chem. Biol. **9**(8), 881-9.

Coll, R.J. and Murphy, A.J. (1984). Purification of the CaATPase of Sarcoplasmic Reticulum by Affinity Chomatography. J. Biol. Chem. **259**(22), 14249-54

Cowman, A.F., Morry, M.J., Biggs, B.A., Cross, G.A. and Foote, S.J. (1988). Amino acid changes linked to pyrimethamine resistance in the dihydrofolate reductase-thymidylate synthase gene of Plasmodium falciparum. Proc. Natl. Acad. Sci. U.S.A. **85**(23), 9109-13.

Craig, S.P. and Eakin, A.E. (2000). Purine Phosphoribosyltransferases. J. Biol. Chem. **275**, 20231-4.

Daddona, P.E., Wiesmann, W.P., Lambros, C., Kelley, W.N., and Webster, H.K. (1984). Human malaria parasite adenosine deaminase; Characterisation in host enzyme-deficient erythrocyte culture. J. Biol. Chem. **259**, 1472-5.

Dahl, E.L. and Rosenthal, P.J. (2005). Biosynthesis, localization, and processing of falcipain cysteine proteases of *Plasmodium falciparum*. Mol. Biochem. Parasitol. **139**, 205-12.

Dominguez, J.N., Charris, J.E., Lobo, G., Gamboa de Domininduez, N., Moreno, M.M., Riggione, F., Sanchez, E., Olson, J. and Rosenthal, P.J. (2001). Synthesis of quinolinyl chalcones and evaluation of their antimalarial activity. Eur. J. Med. Chem. **36**(6), 555-60.

Dua, M., Raphael, P., Sijwali, P.S., Rosenthal, P.J. and Hanspal, M., (2001). Recombinant falcipain-2 cleaves erythrocyte membrane ankyrin and protein 4.1. Mol. Biochem. Parasitol. **116**, 95-9.

Ducki, S., Forrest, R., Hadfield, J.A., Kendall, A., Lawrence, N.J., McGown, A.T. and Rennison, D. (1998). Potent antimitotic and cell growth inhibitory properties of substituted chalcones. Bioorg. Med. Chem. Lett. **8**(9), 1051-6.

Duraisingh, M.T. and Cowman, A.F. (2005). Contribution of the *pfmdr1* gene to antimalarial drug-resistance. Acta Trop. **94**(3), 181-90.

Eads, J.C., Scapin, G., Xu, Y., Grubmeyer, C., and Sacchettin, J.C. (1994). The crystal structure of human hypoxanthine-guanine phosphoribosyltransferase with bound GMP. Cell, **78**, 325-34.

Eckstein-Ludwig, U., Webb, R.J., Van Goethem, I.D., East, J.M., Lee, A.G., Kimura, M., O'Neil, P.M., Bray, P.G., Ward, S.A., and Krishna, S. (2003). Artemisinins target the SERCA of *Plasmodium falciparum*. Nature, **424**, 887-9.

Egan, T.J., Ross, T.J. and Adams, P.A. (1994). Quinoline anti-malarial drugs inhibit spontaneous formation of beta-haematin (malaria pigment). FEBS Lett. **352**(1), 54-7.

Egan, T.J. and Ncokazi, K.K. (2004). Effects of solvent composition and ionic strength on the interaction of quinoline antimalarials with ferriprotoporphyrin IX. J. Inorg. Biochem. **98**(1), 144-52.

Egan, T.J., Hempelmann, E. and Mavuso, W.W. (1999). Characterisation of synthetic beta-haematin and effects of the antimalarial drugs quinidine, halofantrine, desbutylhalofantrine and mefloquine on its formation. J. Inorg Biochem. **73**(1-2), 101-7.

Egan, T.J. (2003). Haemozoin (Malaria pigment): a unique crystalline drug target. Targets **2** (3), 115-24

Fidock, D.A., Nomura, T., Talley, A.K., Cooper, R.A., Dzekunov, S.M., Ferdig, M.T., Ursos, L.M., Sidhu, A.B., Naude, B., Deitsch, K.W., Su., X.Z., Wooton, J.C., Roepe, P.D., and Wellems, T.E. (2000). Mutations in the *P. falciparum* digestive vacuole transmembrane protein PfCRT and evidence for their role in chloroquine resistance. Mol. Cell **6**, 861-71.

Fitch, C.D., Cai, G.Z., and Shoemaker, J.D. (2000). A role for linoleic acid in erythrocytes infected with Plasmodium berghei. Biochim. Biophys. Acta. **1535** (1), 45-9.

Fitch, C.D., Cai, G.Z., Chen, Y.F. and Shoemaker, J.D. (1999). Involvement of lipids in ferriprotoporphyrin IX polymerization in malaria. Biochim. Biophys. Acta. **1454** (1), 31-7.

Fitch, C.D., Chen, Y. and Cai, G. (2003). Chloroquine-induced masking of a lipid that promotes ferriprotoporphyrin IX dimerization in malaria. J. Biol. Chem. **278** (25), 22596-9.

Focia, P.J., Craig, S.P., 3rd and Eakin, A.E. (1998). Approaching the transition state in the crystal structure of a phosphoribosyltransferase. Biochemistry. **37**(49),17120-7

Foote, S.J., Kyle, D.E., Martin, R.K., Oduola, A.M.J., Forsyth, K., Kemp, D.J., and Cowman, A.F. (1990). Several alleles of the multi-drug resistance gene are closely linked to chloroquine resistance in *Plasmodium falciparum.* Nature **345,** 255-8.

Foote, S.J., Thompson, J.K., Cowman, A.F., and Kemp, D.J. (1989). Amplification of multi-drug resistance in some chloroquine-resistant isolates of *P. falciparum.* Cell **57**, 921-930.

Francis, S.E., Banerjee, R. and Goldberg, D.E. (1997). Biosynthesis and maturation of the malaria aspartic hemoglobinases plasmepsins I and II. J. Biol. Chem. **272**(23),14961-8.

Gardner, M.J., Hall, N., Fung, E., White, O, Berriman, M., Hyman R.W., Calton, J.M., Pain, A., Nelson, K.E., Bowman, S., Paulsen, I.T., James, K., Eisen, J.A., Rutherford, K., Salzberg., S.L., Craig, A., Kyes, S., Chan, M.S., Nene, V., Shallom, S.J., Suh, B., Peterson, J., Angiuoli, S., Perta, M., Allen, J., Selengut, J., Haft, D., Mather, M.W., Vaidya., A.B., Martin., D.M.., Fairlamb., A.H., Fraunholz, M.J., Roos, D.S., Ralph, S.A., McFadden, G.I., Cummings, L.M., Subramanian, G.M., Mungall, C., Venter, J.C., Carucci., DJ., Hoffman., S.L., Newbold., C., Davis, R.W., Fraser, C.M., and Barrell, B.(2002). Genome sequence of the human malaria parasite *Plasmodium falciparum*. Nature **419**, 498-511.

Giacomello, A. and Salerno, C. (1978). Human hypoxanthine-guanine phosphoribosyltransferase. Steady state kinetics of the forward and reverse reactions. J. Biol. Chem. **253**(17), 6038 -44.

Gluzman, I.Y., Francis, S.E., Oksman, A., Smith, C.E., Duffin, K.L. and Goldbeerg, D.E.(1994). Order and specificity of the Plasmodium falciparum hemoglobin degradation pathway. J. Clin. Invest. **93**(4),1602-8.

Go, M.L., Liu, M., Wilairat, P., Rosenthal, P.J., Saliba, K.J., and Kirk, K. (2004). Antiplasmodial chalcones inhibit sorbitol-induced hemolysis of Plasmodium falciparum-infected erythrocytes. Antimicrob. Agents Chemother. **48**(9), 3241-5.

Go, M.L., Wu, X. and Liu, X.L. (2005). Chalcones: an update on cytotoxic and chemoprotective properties. Curr. Med. Chem. **12**(4), 481-99.

Goitein, R.K., Chelsky, D. and Parsons, S.M. (1978). Primary ^{14}C and alpha secondary ^{3}H substrate kinetic isotope effects for some phosphoribosyltransferases. J. Biol. Chem. **253**(9), 2963-71.

Greenbaum, D.C, Baruch, A., Graingen, M., Bozdech, Z., Medzihadszky, K.F., Engel, J., DeRisi, J., Holder, A.A., and Bogyo, M. (2002). A role for protease falcipain 1 in host cell invasion by the human malaria parasite. Science **298**, 1-6.

Greene, T.W. and Wuts, P.G.M. (1999). Protective Groups in Organics synthesis, 3rd Ed. John Wiley and Sons, NY. pp 249-291.

Greenwood, B. and Mutabingwa, T. (2002). Malaria in 2002. Nature **415**, 670 - 72.

Hansch, C. and Leo, A. (1979). Substituent constants for correlation analysis in chemistry and biology. Wiley. New York, pp 23 - 49.

Harding, M.M. (1999). The geometry of metal-ligand interactions relevant to proteins. Acta. Cryst. **D55**, 1432-43.

Harding, M.M. (2000). The geometry of metal-ligand interactions relevant to proteins. II. Angles at the metal atom, additional weak metal-donor interactions. Acta. Cryst. **D56**, 857-67.

Harding, M.M. (2001). The geometry of metal-ligand interactions in proteins. Acta. Cryst. **D57**, 401-11.

Haynes, R.K. (1996). The behaviour of qinghaosu (artemisinin) in the presence of heme iron (II) and (III). Tetrahedron Lett. **37**, 253-6.

Haynes, R.K., Pal, H.H.O., and Voerste, A. (1999). Ring opening of artemisinin (qinghaosu) and dihydroartemisinin and interception of the open hydroperoxide with formation of N-oxides- a chemical model for antimalarial mode of action. Tetrahedron lett. **40**, 4715-18.

Henderson, J.F, Brox, L.W., Kelley, W.N., Rosenbloom, F.M. and Seegmiller, J.E. (1968). Kinetic studies of hypoxanthine-guanine phosphoribosytransferase. J. Biol. Chem. **243**(10), 2514-22.

Heroux, A., White, E.L., Ross, L.J., and Borhani, D.W. (1999a). Crystal structures of the Toxoplasma gondii hypoxanthine-guanine phosphoribosyltransferase-GMP and -IMP complexes: comparison of purine binding interactions with the XMP complex. Biochemistry **38** (44), 14485-94

Heroux, A., White, E.L., Ross, L.J., Davis, R.L and Borhani, D.W. (1999b). Crystal structure of Toxoplasma gondii hypoxanthine-guanine phosphoribosyltransferase with XMP, pyrophosphate, and two Mg^{2+} ions bound: insights into the catalytic mechanism. Biochemistry **38** (44), 14495-506

Heroux, A, White E.L, Ross, L.J, Kuzin, A.P., and Borhani, D.W. (2000). Substrate deformation in a hypoxanthine-guanine phosphoribosyltransferase ternary complex: the structural basis for catalysis. Structure Fold. Des. **8**(12), 1309-18

von Hirschheydt, T. and Voss, E. (2004). Simple, short and efficient procedure for the preparation of hydroxymethyl-substituted 2,6-chlorobenzaldehydes. Synthesis, **12**, 2062-5

Hyde, J.E. (2005). Exploring the folate pathway in *Plasmodium faciparum*. Acta Trop. **94**(3), 191-206.

Jayasinghe, L. Balasoori, B.A.I.S., Padmini, W.C. Hara, N., and Fujimoto, Y. (2004). Geranyl chalcone derivatives with antifungal and radical scavenging properties from the leaves of *Artocarpus nobilis*. Phytochemistry **65**(9), 1287-90.

Kaschula, C.H., Egan, T.J., Hunter, R. Basilico, N. Parapini, S., Taramelli, D., Pasini, E. and Monti, D. (2002). Structure-activity relationships in 4-aminoquinoline antiplasmodials. The role of the group at the 7-position. J. Med. Chem. **45**, 3531-9.

Keough, D.T., Brereton, I.M., de Jersey, J. and Guddat, L.W. (2005). The Crystal Structure of Free Human Hypoxanthine-guanine Phosphoribosyltransferase Reveals Extensive Conformational Plasticity Throughout the Catalytic Cycle. J. Mol. Biol. **351**(1), 170-81.

Keough, D.T., Ng, A.L., Emmerson, B.T., and de Jersey, J. (1998). Expression and properties of recombinant P. falciparum hypoxanthine-guanine phosphoribosyltransferase. Adv. Exp. Med. Biol. **431**, 735-9

Keough, D.T., McConachie, L.A., Gordon, R.B., de Jersey, J. and Emmerson, B.T. (1987). Human hypoxanthine-guanine phosphoribosyltransferase. Development of a spectrophotometric assay and its use in detection and characterization of mutant forms. Clin. Chim. Acta. **163**(3), 301-8.

Keough, D.T., Ng, A., Winzor, D.J., Emmerson, B.T. and de Jersey, J. (1999). Purification and characterisation of *Plasmodium falciparum* hypoxanthine-guanine-xanthine phosphoribosyltransferase and comaparison with the human enzyme. Mol. Biochem. Parasitol. **98**, 29-41.

Kicska, G.A, Tyler, P.C., Evans, G.B., Furneaux, R.H., Kim, K., and Schramm, V. (2002). Transition state analogue inhibitors of purine nucleoside phosphorylase from *Plasmodium falciparum*. J. Biol. Chem., **277**(5), 3219-25.

Kirk, K., Horner, H.A., Spillett, D.J., and Elford, B.C. (1993). Glibenclamide and meglitinide block the transport of low molecular weight solutes into malaria-infected erythrocytes. FEBS Lett., **323**(1-2), 123-8.

Knuutinen, J.S. and Kolehmainen, E.T. (1983). Synthesis and spectroscopic data of chlorinated 4-hydroxybenzaldehyde. J. Chem. Eng. Data **28**, 139-141.

Kutner, S., Breuer, W.V., Ginsburg, H., and Cabantchik, Z.I. (1987). On the mode of action of phlorizin as an antimalarial agent in in vitro cultures of Plasmodium falciparum. Biochem. Pharmacol. **36**(1), 123-9.

Laemmli, U.K. (1970). Cleavage of structural proteins during the assembly of the head of bacteriophage T4. Nature **227**, 680 – 5.

Lee, C.C, Medrano, F.J, Craig, S.P. 3rd., and Eakin, A.E. (2001). Investigation of the functional role of active site loop II in a hypoxanthine phosphoribosyltransferase. Biochim. Biophys. Acta. **1537**, 63-70.

Li, C.M., Tyler, P.C., Furneaux, R.H., Kicska, G., Xu, Y., Grubmeyer, C., Girvin, M.E. and Shramm, V.L. (1999). Transition-state analogs as inhibitors of human and malarial hypoxanthine-gunaine phosphoribosyltransferases. Nat. Struct. Biol. **6**(6), 582-7

Li, R., Kenyon, G.L., Cohen, F.E., Chen, X., Gong, B., Dominguez, J.N., Davidson, E., Kurban, G., Miller, R.E., Nuzum, E.O., Rosenthal, P.J. and McKerrow, J.H. (1995). In vitro antimalarial actvity of chalcone and their derivatives. J. Med. Chem. **38**, 5031-7.

Lin, Y., Zhou, Y., Flavin, M.T., Zhou, L., Nie, W., and Chen, F (2002). Chalcones and flavonoids as Anti-Tuberculosis agents. Bioorg. Med. Chem. **10**, 2795-802.

Liu, M., Wilairat, P. and Go, M.L. (2001). Antimalarial alkoxylated and hydroxylated chalcones: structure activity relationship analysis. J. Med. Chem. **44**(25), 4443-52.

Liu, J., Gluzman, I.Y., Drew, M.E. and Goldberg, D.E. (2005). The role of *Plasmodium falciparum* food vacuole plasmepsins. J. Biol. Chem. **280**(2), 1432-7.

Liu, S.W., and Milman, G. (1983). Purification and characterization of Escherichia coli guanine-xanthine phosphoribosyltransferase produced by a high efficiency expression plasmid utilizing a lambda PL promoter and CI857 temperature-sensitive repressor. J. Biol. Chem. **258**(12), 7469-75.

McIntosh, D.B., Woolley, D.G., Vilsen, B. and Andersen, J.P. (1996). Mutagenesis of segment ^{487}Phe-Ser-Asp-Arg-Lys^{492} of Sarcoplasmic Reticulum Ca^{2+}-ATPase produces pumps defective in ATP binding. J. Biol. Chem. **271** (42), 25778-89.

Meng, C.Q., Zheng, NI., L., Ye, Z., Simpson, J.E., Worsencroft, K.J. Hotema, M.., Weingarten, M.D., Skudlarek, J.W., Gilmore, J.M., Hoong, L.K., Hill, R.R., Marino, E.M., Suen, K.L., Kunsch, C., Wasserman, M.A and Sikorki, J.A. (2004). Discovery of novel heteroaryl-substituted chalcones as inhibitors of TNF-α-induced VCAM-1 expression. Bioorg. Med. Chem. Lett. **14**, 1513-1517.

Meshnick, SR., Thomas, A., Ranz, A., Xu, CM., and Pan, HZ. (1991). Artemisinin (qinghaosu)-the role of intracellular hemin in its mechamism of antimalarial action. Mol. Biochem. Parasitol. **49**, 181-90.

Miller, L.H., Baruch, D.I., Marsh, K. and Doumbo, O.K. (2002). The pathogenic basis of malaria. Nature **415**, 673 – 8.

Muro-Pastor, M.I, and Florencio, F.J. (1992). Purification and properties of NADP-isocitrate dehydrogenase from the unicellular cyanobacterium Synechocystis sp. PCC 6803. Eur. J. Biochem. **203**(1-2), 99-105.

Mukherjee, S., Kumar, V., Prasad, A.K., Raj, G.H., Bracke, M.E., Olsen, C.E., Jain, S.C., and Parmar, V.S. (2001). Synthetic and biological activity evaluation studies on novel 1,3-diarylpropenones. Bioorg. Med. Chem. **9**, 337-45.

Munagala N.R, and Wang C.C. (1998). Altering the purine specificity of hypoxanthine-guanine-xanthine phosphoribosyltransferase from *Tritrichomonas foetus* by structure-based point mutations in the enzyme protein. Biochemistry. **37**(47), 16612-9.

Nakajin, S., Kawai, Y., Ohno, S., and Shinoda, M. (1989). Purification and characterization of pig adrenal 20 alpha-hydroxysteroid dehydrogenase. J. Steroid Biochem. **33**(6), 1181-9.

Narender, T., Shweta, Tanvir, K. Rao, M.S. Srivastava, K. and Puri, S.K. (2005). Prenylated chalcones isolated from *Crotalaria* genus inhibits in vitro growth of the human malaria parasite *Plasmodium falciparum*. Bioorg. Med. Chem. Lett. **15**(10), 2453-5.

Nerya, O., Musa, R., Khatib, S., Tamir, S., and Vaya, J. (2004). Chalcones as potent tyrosinase inhibitors: the effect of hydroxyl positions and numbers. Phytochemistry **65**, 1389-1395.

Nielsen, SF., Boesen, T., Larsen, M., Schonning, K. and Kromann, H. (2004). Antibacterial chalcones-bioisoteric replacement of the 4'-hydroxy group. Bioorg. Med. Chem. **12**, 3047-54.

Nielsen, S.F., Kharazmi, A., and Christensen, S.B. (2005). Cationic chalcone antibiotics. Design, synthesis, and mechanism of action. J. Med. Chem. **48**(7), 2667-77.

Pagola, S., Stephens, P.W., Bohle, D.S., Kosar, A.D., and Madsen, S.K. (2000). The structure of malaria pigment beta-haematin. Nature **404**, 307-10.

Parapini, S., Basilico, N., Mondani, M., Olliaro, P., Taramelli, D., and Monti, D. (2004). Evidence that haem iron in the malaria parasite is not needed for the antimalarial effects of artemisinin. FEBS Letters, 575(1-3), 91 - 94

Parker, M.D., Hyde, R.J., Yao, S.Y.M., McRobert, L., Cass, C.E., Young, J.D., McConkey, D.A. and Baldwin, S.A. (2000). Identification of a nucleoside/nucleobase transporter from *Plasmodium falciparum*, a novel target for anti-malarial chemotherapy. Biochem. J. **349**, 67-75.

pET-System Manual (2002) at: http://www.merckbiosciences.de/docs/NDIS/TB055-000.pdf

Phehane, V.N., (2002). The expression and drug targeting of parasitic hypoxanthine-guanine phosphoribosyltransferase (HGXPRT). Ph.D. Thesis, University of Cape Town, South Africa.

Pech, L.L, and Nelson, D.L. (1994). Purification and characterization of calmodulin (lysine 115) N-methyltransferase from Paramecium tetraurelia. Biochim. Biophys. Acta. **1199**(2), 183-94.

Peterson, D.S., Walliker, D., and Wellems, T.E. (1988). Evidence that a point mutation in dihydrofolate reductase-thymidylate synthase confers resistance to pyrimethamine in falciparum malaria. Proc. Natl. Acad. Sci. U.S.A. **85**(23), 9114-8.

Posner, G.H., and Oh, C.H. (1992). A regiospecifically O-18 labeled 1,2,4-trioxane-a simple chemical model system to probe the mechanisms of antimalarial activity of artemisinin (qinghaosu). J. Am. Chem. Soc. **114**, 8328-9.

Posner, G.H, Cumming, J.N., Ploypradith, P., and Chang, H.O. (1995). Evidence for Fe(IV)=O in the molecular mechanism of action of the trioxane antimalarial artemisinin. J. Am. Chem. Soc. **117**, 5885-6.

Olsen, A. and Milman G. (1978). Hypoxanthine phosphoribosyltransferase from Chinese Hamster brain and human erythrocytes. Methods in Enzymology, vol. LI. Academic Pree, Inc. pp 543-9.

Queen, S.A., van der Jart, D. and Reyes, P. (1988). Properties and substrate specificity of a purine phosphoribosyltransferase from human malaria parasite, *Plasmodium falciparum*. Mol. Biochem. Parasit. **33** 123-34.

Raevsky, O.A., Schaper, K.J., and Seydel, J.K (1995). H-bond contribution to octanol-water partition coefficients of polar compounds. Quant. Struct. Act. Relat. **14**, 433-6.

Raman, J., Ashok, C.S., Subbayya, S.I., Anand, R.P., Selvi, S.T., and Balaram, H. (2005). Plasmodium falciparum hypoxanthine guanine phosphoribosyltransferase. Stability studies on the product-activated enzyme. FEBS J. **272**(8), 1900-11.

Rao, Y.K., Fang, S. and Tzeng, Y. (2004). Differential effects of synthesized 2'-oxygenated chalcone derivatives: modulation of human cell cycle phase distribution. Bioorg. Med. Chem. **12**, 2679-86.

Reed, M.B., Saliba, K.J., Kirk, K. and Cowman, A.F. (2000). Pgh1 modulates sensitivity and resistance to multiple antimalarials in *Plasmodium falciparum*. Nature **403**, 906-9.

Rockett, K.A., Playfair, J.H., Ashall, F., Targett, G.A, Angliker, H. and Shaw, E. (1990). Inhibition of intraerythrocytic development of Plasmodium falciparum by proteinase inhibitors. FEBS Lett. **259**(2), 257-9.

Rosenthal, P.J., Olson, J.E., Lee, G.K., Palmer, J.T., Klaus, J.L. and Rasnick, D. (1996). Antimalarial effects of vinyl sulfone cysteine proteinase inhibitors. Antimicrob. Agents Chemother. **40**(7), 1600-3.

Sachs, J. and Malaney, P. (2002). The economic and social burden of malaria. Nature **415**, 680 - 5.

Salerno, C. and Giacomello, A. (1979). Human hypoxanthine-guanine phosphoribosyltransferase. IMP-GMP exchange stoichiometry and steady state kinetics of the reaction. J. Biol. Chem. **254**(20), 10232-6.

Salerno, C. and Giacomello, A. (1980). Human hypoxanthine-guanine phosphoribosyltransferase. The role of magnesium in a phosphoribosylpyrophosphate-utilizing enzyme J. Biol. Chem. **256**(8), 3671-3.

Satyanarana, K., and Rao, M.N.A., (1993). Anti-inflammatory, analgesic and antipyretic activities of 3-[4-[3-(4-dimethylamininophenyl)-1-oxo]-2-propenyl]sydnone. Indian Drugs **30**, 313-8.

Sauve, A.A., Cahill, S.M., Zech, S.G., Basso, L.A., Lewandowcz, A., Santos., D.S., Grubmeyer, C., Evans, G.B., Furneaux, R.H., Tyler, P.C., McDermott, A., Girvin, M.E., and Schramm, M.L. (2003). Ionic states of substrates and transition state analogues at the catalytic sites of *N*-ribosyltransferases. Biochemistry **42**, 5694-705.

Schneider, E.L. and Marletta, M.A. (2005). Heme binding to the histidine-rich protein II from *Plasmodium falciparum* Biochemistry **44**, 979-86.

Schumacher, M.A., Carter, D., Ross, D.S., Ullman, B and Brennan, R.G. (1996). Crystal structures of Toxoplasma gondii HGXPRTase reveal the catalytic role of a long flexible loop. Nat. Struct. Biol. **3**(10), 881-7.

Seidman, C.E., Struhl, K., Sheen, J., and Jessen, T. (1997). Introduction of Plasmid DNA into cells: In Current Protocols in Molecular Biology. John Wiley & Sons, Inc. pp 181-7.

Shahabuddin, M., and Scaife, J. (1990). The gene for hypoxanthine phosphoribosyltransferase of *Plasmodium falciparum* complements a bacterial *HPT* mutation. Mol. Biochem. Parasitol. **41**, 281-8.

Shenai, B.R., Sijwali, P.S., Singh, A., and Rosenthal, P.J. (2000). Characterization of native and recombinant falcipain-2, a principle trophozoite cysteine protease and essential hemoglobinase of *Plasmodium falciparum.* J. Biol. Chem. **275**, 29000-10.

Sherman, I.W. (1979). Biochemistry of *Plasmodium* (malarial parasites). Microbial. Rev. **43**, 453-95.

Shi, W., Ting, L.M., Kicska, G.A., Lewandowicz, A., Tyler, P.C., Evans, G.B., Furneaux, R.H., Kim, K., Almo, S.C. and Shramm, V.L. (2004). *Plasmodium falciparum* purine nucleoside phosphorylase. J. Biol. Chem. **279**(18), 18103-6.

Shi, W., Li, C.M., Tyler, P.C. Furneaux, R.H., Grubmeyer, C., Schramm, V.L. and Almo, S.C. (1999a). The 2.0 A structure of human hypoxanthine-guanine phosphoribosyltransferase in complex with a transition-state analog inhibitor. Nat. Struct. Biol. **6**(6), 588-93.

Shi, W.S., Li, C.M., Tyler, P.C., Furneaux, R.H., Cahill, S.M., Girvin, M.E., Grubmeyer, C., Shramm, V.L. and Almo, S.C. (1999b). The 2.0 Å structure of malarial purine phosphoribosyltransferase in complex with a transition-state analogue inhibitor. Biochemistry **38** (31), 9872-80.

Shi, W., Munagala, N.R., Wang, C.C., Li, C.M., Tyler, P.C., Furneaux, R.H., Grubmeyer, C., Schramm, V.L., and Almo, S.C. (2000). Crystal structures of *Giardia lamblia* guanine phosphoribosyltransferase at 1.75 Å. Biochemistry. **39**(23), 6781-90.

Shibata, S. (1994). Anti-tumorigenic chalcones. Stem cells **12**, 44-52.

Silfen, J., Yanai, P., and Cabantchik, Z.I. (1988). Bioflavonoid effects on in vitro cultures of Plasmodium falciparum. Inhibition of permeation pathways induced in the host cell membrane by the intraerythrocytic parasite. Biochem. Pharmacol. **37**(22), 4269-76.

Sijwali, P.S., Shenai, B.R., Gut, J., Singh, A., and Rosenthal, P.J. (2001). Expression and characterization of the *Plasmodium falciparum* haemoglobinase falcipain-3. Biochem. J. **360**(Pt 2), 481-9.

Sinha, S.C., and Smith, J.L. (2001). The PRT protein family. Curr. Opin. Struct. Biol. **11**(6), 733-9.

Sirawaraporn, W., Sirawaraporn, R., Cowman, A.F., Yuthavong, Y., and Santi, D.V. (1990). Heterologous expression of active thymidylate synthase-dihydrofolate reductase from *Plasmodium falciparum*. Biochemistry. **29**(48), 10779-85.

Skinner-Adams, T.S., McCarthy, J.S., Gardner, D.L., Hilton, P.M., and Andrews K.T. (2004). Antiretrovirals as antimalarial agents. J. Infect. Diseas. **190**, 1998-2000.

Slater, AFG., Swiggard, WJ., Orton, BR., Flitter, WD., Goldberg, DE., Cerami, A., and Henderson, CB. (1991). An iron-carboxylate bond links heme units of malaria pigments. Proc. Natl. Acad. Sci. U.S.A. **88**, 325-29.

Staines, H.M., Ellory, J.C., and Chibale, K. (2005). The New Permeability Pathways : Targets and selective routes for the development of new antimalarial agents. Comb. Chem. High Throughput Screen. **8**, 81-8.

Star, A.E., and Mabry, T.J. (1971). Flavonoids frond exudates from two Jaimacan ferns, *Pityrogramma tartarea* and *P. calomelanos.* Phytochemistry **10**, 2812-17.

Stevens, R.V., Chapman, K.T. and Weller, H.N. (1980). Convenient and inexpensive procedure for oxidation of secondary alcohols to ketones. J. Org. Chem. **45**, 2030-2.

Stevens, J.F., Taylor, A.W., Nickerson, G.B., Ivancic, M., Henning, J., Haunold, A., and Deiner, M.L. (2000). Prenylflavonoid variation inhumulus lupulus: distribution and taxonomic

significance of xanthogalenol and 4'-*O*-methylxanthogalenol and 4'-*O*-methylxanthohumol. Phytochemistry 53, 759-79.

Storts, D.R. and Bhattacharjee, J.K. (1987). Purification and properties of saccharopine dehydrogenase (glutamate forming) in the Saccharomyces cerevisiae lysine biosynthetic pathway. J. Bacteriol. **169**(1), 416-8.

Sullivan, D.J., Gluzman, I.Y., and Goldberg, D.E. (1996). *Plasmodium* hemozoin formation mediated by histidine-rich protein. Science **271**, 219-21.

Tao, W., Grubmeyer, C. and Blanchard, J.S. (1996). Transition state structure of *Salmonella typhimurium* orotate phosphoribosyltransferase. Biochemistry **35**, 14-21.

Ting, L.M., Shi, W., Lewandowicz, A., Singh, V., Mwakingwe, A., Birck, M.R., Ringia, E.A., Bench, G., Madrid, D.C., Tyler, P.C., Evans, G.B., Furneaux, R.H., Shramm, V.L., and Kim, K. (2005). Targeting a novel Plasmodium falciparum purine recycling pathway with specific immucillins. J. Biol. Chem., **280**(10), 9547-54.

Tuttle, J.V., and Krenitsky, T.A. (1984). Effects of acyclovir and its metabolites on purine nucleoside phosphorylase. J. Biol. Chem. **259**(7), 4065-9.

Triglia, T., and Cowman, A.F. (1994). Primary structure and expression of the dihydropteroate synthetase gene of *Plasmodium falciparum*. Proc. Natl. Acad. Sci. U. S. A. **91**(15), 7149-53.

Triglia, T. Menting, J.G.T., Wilson, C. and Cowman, A.F. (1997). Mutations in dihydropteroate synthase are responsible for sulfone and sulfonamide resistance in Plasmodium falciparum. Proc. Natl. Acad. Sci. U. S. A. **94**(25), 13944-9.

Ullman, B. and Carter, D. (1995). Hypoxanthine-guanine phosphoribosyltranferase as a therapeutic target in protozoal infections. Infections. Infect. Agents Dis. **4**, 29-40.

Urbatsch I.L., al-Shawi M.K., and Senior A.E. (1994). Characterization of the ATPase activity of purified Chinese hamster P-glycoprotein. Biochemistry. **33**(23), 7069-76

Vennerstrom, J.L, Arbe-Barnes, S., Brun, R., Charman, S.A., Chiu, F.C., Chollet, J., Dong, Y., Dorn, A., Hunziker, D., Matile, H., McIntosh, K., Padmanilayam, M., Santo Tomas, J., Scheurer, C., Scorneaux, B., Tang, Y., Urwyler, H., Wittlin, S., and Charman, W.N. (2004). Identification of an antimalarial synthetic trioxolane drug development candidate. Nature, **430**, 900-4

Vos, S., de Jersey, J., and Martin, J.L. (1997). Crystal structure of *Escherichia coli* xanthine phosphoribosyltransferase. Biochemistry **36**, 29 – 40

de Wet, H., McIntosh, D.B., Conseil, G., Baubichon-Cortay, H., Krell, T., Jault, J.M., Daskiewicz, J.B., Barron, D., and Di Pietro A. (2001). Sequence requirements of the ATP-binding site within the C-terminal nucleotide-binding domain of mouse P-glycoprotein: structure-activity relationships for flavonoid binding. Biochemistry **40** (34), 10382-91.

Wiser, M.F. (2003). Mechanisms of Drug Action and Resistance (focus on anti-malarials). http://www.tulane.edu/~wiser/protozoology/notes/drus.html

Woerdenbebag, H.J., Moskal, T.A., Pras, N., Mallingre, T.M., el-Faraly, F.S., Kampinga, H.H., and Konings, A.W. (1993). Cytotoxicity of artemisinin-related endoperoxides to Enhrlich ascites tumor cells. J. Nat. Prod. **56**, 849-56.

World Health Organisation (2003). http://rbm.who.int/wmr2005/html/map1.htm

World Health Organization/UNICEF, 2003
http://www.who.int/malaria/amd2003/amr2003/ch1.htm

Wu, X., Wilairat, P. and Go, M.L. (2002). Antimalarial activity of ferrocenyl chalcones. Bioorg. Med. Chem. Lett. **12**, 2299-302.

Xu,Y., Eads, Sacchettini, JC., and Grubmeyer, C. (1997). Kinetic mechanism of human hypoxanthine-guanine phosphoribosyltransferase: Rapid phosphoribosyl transfer chemistry. Biochemistry **36**(12), 3700-12.

Xu, Y., and Grubmeyer, C. (1998). Catalysis in human hypoxanthine-guanine phosphoribosyltransferase: Asp 137 acts as a general acid/base. Biochemistry. **37**(12), 4114-24

Yuthavong, Y., Yuvaniyama, J., Chitnumsub, P., Vanichtanakul, J., Chusacultanachai, S., Tarnchompoo, B., Vilaivan, T. and Kamchonwongpaisan, S. (2005). Malarial (*Plasmodium falciparum*) dihydrofolate reductase-thymidylate synthase: structural basis for antifolate resistance and development of effective inhibitors. Parasitology. **130**(Pt 3), 249-59.

Yuvaniyama, J., Chitnumsub P., Kamchonwongpaisan, S., Vanichtanankul, J., Sirawaraporn, W., Taylor, P., Walkinshaw, M.D., and Yuthavong, Y. (2003). Insights into antifolate resistance from malarial DHFR-TS structures. Nat. Struct. Biol. **10**(5), 357-65.